Response of Blade-Row to Upstream Vortical Disturbance in Relative Motion

by

Shin-Juh Chen

B.S., Aeronautical Engineering
Rensselaer Polytechnic Institute, 1992

SUBMITTED TO THE DEPARTMENT OF
AERONAUTICS AND ASTRONAUTICS
IN PARTIAL FULFILLMENT OF THE
REQUIREMENTS FOR THE DEGREE OF

Master of Science

in

Aeronautics and Astronautics

at the

Massachusetts Institute of Technology

June 1995

Signature of Author _____
Department of Aeronautics and Astronautics
March 16, 1995

Certified by _____
Dr. Choon S. Tan
Thesis Supervisor

Accepted by _____
Professor Harold Y. Wachman
Chairman, Department Graduate Committee

Response of Blade-Row to Upstream Vortical Disturbances in Relative Motion

by

Shin-Juh Chen

Submitted to the Department of Aeronautics and Astronautics
on March 16, 1995 in partial fulfillment of
the requirements for the Degree of
Master of Science in Aeronautics and Astronautics

Abstract

The flowfield associated with the interaction of stator blade row with inlet vortical disturbances due to upstream moving wakes is calculated. Clebsch's transformation is used to write the velocity field as the sum of an irrotational and a rotational part. The disturbance flow is assumed to be small compared to the steady background flowfield in the absence of the unsteady inlet disturbances. This assumption allowed the governing flow equations to be linearized about the steady background flow. The linearization led to simplified linearized equations that govern the unsteady disturbance flowfield. These linearized equations are spatially and temporally discretized using finite volume methods and four-stage Runge-Kutta time-integration. Numerical calculations of unsteady disturbance flow are carried out in a two- and three-dimensional rectilinear stator blade passages with the prescription of upstream moving wakes along the inlet boundary. These numerical computations served to illustrate the use of the approach taken in this thesis for calculating the unsteady disturbance flow in stator blade passages in the presence of upstream moving wakes.

Thesis advisor: Dr. Choon S. Tan
Title: Principal Research Engineer

Acknowledgements

This thesis is dedicated to my parents, sisters and special friends who have always been there to support me in many ways. Thank you for your supports. Without my parents' help in funding my education in times of need, I would not have been able to carry the research to its completion; their financial support is greatly and most appreciated.

Special thanks to Professor Edward M. Greitzer for convincing me to understake this research task at the time when I was not sure what research topic to pursue for my Master thesis. My experience in this research have been most rewarding.

In this regard, I would like to also thank my thesis advior, Dr. Choon S. Tan, for giving me the opportunity to challenge myself academically and learn about an exciting field of research that was unfamiliar to me at the beginning, and for his guidance throughout the course of this work. Many thanks to Dr. Tan for also providing the eight months of research assistanship that was vital in temporarily alleviating the financial burdens on my parents' shoulders. I would like to also thank Sir William R. Hawthorne for stimulating my interests in the theory of "Secondary Flow," and for his help to understanding the theory.

Finally, thanks to all current and past members of the Gas Turbine Laboratory who have occasionally helped me, and to all other people who have somewhat contributed to my experience at MIT.

Funding for this research was provided by the NASA Lewis Research Center under contract No. NAG3-1176 and under the technical monitoring of Dr. John Adamczyk. Additional funds for supporting my education were provided by my parents. These supports are greatly acknowledged.

Contents

Nomenclature

A	Face area of cell volume
A_x , A_y , A_z	Face areas of three-dimensional cell in the x-, y-, z-direction
BT, TP	Bottom and top face of a cell
C_p	Pressure coefficient of unsteady flow
$\overline{C}_p$	Pressure coefficient of steady background flow
$D_{\frac{\delta^*}{2}}$, $D_{-\frac{\delta^*}{2}}$	Velocity distributions from wake's center to upper and lower wake's regions.
$D^{(2)}$	Second-order smoothing term
$D^{(4)}$	Fourth-order smoothing term
F, G, H	Fluxes in Cartesian coordinates in x-, y-, z-direction, respectively
FT, RT, BK, LT	Front, right, and back face or vertex, respectively
J	Jacobian in generalized coordinates transformation
L	Span of blade
L_1	Distance between the cell center and the center of its right face or vertex
L_2	Distance between the cell center and the center of its left face or vertex
P, $\overline{P}$, $\tilde{P}$	Static pressure of unsteady flow, background flow, and disturbance flow
P_t , $\overline{P}_t$, $\tilde{P}_t$	Total pressure of unsteady flow, background flow, and disturbance flow
P_w	Wake's spatial periodicity
$R(\Theta)$	Residual of Θ in the convective equation solver
S	Blade spacing (pitch)
t, T	Time

T_o	Period of simulation
U	Rotor velocity in stator frame of reference
u, v, w	Velocity components of unsteady flow
$\overline{u}, \overline{v}, \overline{w}$	Velocity components of steady background flow
$\tilde{u}, \tilde{v}, \tilde{w}$	Velocity component of unsteady disturbance flow
U_t, U_n	Wall velocity in wall coordinates (t,n)
U_w	Wake's x-component of velocity
V	Volume of a three-dimensional cell
$\vec{V}, \overline{\vec{V}}, \tilde{\vec{V}}$	Velocity vector of unsteady flow, background flow, and disturbance flow
x, y, z	Position in Cartesian coordinates
x_ξ, y_ξ, z_ξ	(x, y, z) coordinates derivatives with respect to ξ
x_η, y_η, z_η	(x, y, z) coordinates derivatives with respect to η
$x_\varsigma, y_\varsigma, z_\varsigma$	(x, y, z) coordinates derivatives with respect to ς

Greek Symbols

α	Ratio of distances defined as $L_1 \,/\, (L_1 + L_2)$
$\alpha_1, \alpha_2, \alpha_3$	Constant coefficients for the 1st, 2nd, 3rd step of time-integration
β	Shear defect
$\varepsilon_f^{(4)}$	Fourth-order switch for face f
$\vec{\chi}$	Position vector in Cartesian coordinates
$\Delta\xi, \Delta\eta, \Delta\varsigma$	Grid spacings in rectangular grid for the generalized coordinates system
δ^*	Wake thickness (in percent of blade spacing)
$\delta_f(\ )$	First difference of the quantity inside ( ) across face f
$\Delta x, \Delta y$	Lengths of cell vertex in x- and y-direction
∇	Gradient operator
Δt	Time increment (step) in numerical solvers

Δt_n	Local time-step in n-direction (n=x, y, z) in a cell
$\Delta\overline{x}$, $\Delta\overline{y}$, $\Delta\overline{z}$	Mean distances across a cell in x-, y-, and z-direction
E []	Integer part of the quantity inside [ ]
ϕ, $\overline{\phi}$, $\tilde{\phi}$	Velocity potential of unsteady flow, background flow, and disturbance flow
κ	Relaxation factor in Poisson equation solver
λ^*	Courant number
λ	Scalar quantity
Θ^n	Arbitrary variable at time-step n
μ	Scalar quantity
ν_2, ν_4	Smoothing coefficients in artificial smoothing
Θ	Arbitrary variable
θ^*	Velocity defect in wake
θ_{wall}	Wall surface angle
ρ	Density of fluid
σ, $\overline{\sigma}$, $\tilde{\sigma}$	Scalar quantity of unsteady flow, background flow, and disturbance flow
Ω	Area of a two-dimensional cell
τ, $\overline{\tau}$, $\tilde{\tau}$	Drift time of unsteady flow, background flow, and disturbance flow
$\vec{\omega}$, $\overline{\vec{\omega}}$, $\tilde{\vec{\omega}}$	Vorticity vector of unsteady flow, background flow, and disturbance flow
ξ, η, ς	Generalized coordinates system in rectangular grid

Subscripts

$[\ ]_\infty$	Freestream condition

List of Figures

All figures are attached at the end of the thesis. The numbers on the left margin denote the figure numbers and those on the right margin denote the page numbers.

List of Tables

Chapter 1

Introduction

1.1 Problem Statement

Turbomachinery blades can encounter induced and/or forced vibrations due to unsteady aerodynamic forces associated with blade row interactions. Structural failure of blades can occur when the frequencies of these vibrations are close to the structure's natural frequency.

In this study a stator blade row interacting with upstream moving wake is investigated. Flow calculations are conducted with wakes moving relative to stator blade passages. Theses moving wakes are shed from upstream rotor blades. The computations are done on two- and three-dimensional rectilinear blade geometry.

The background (mean) flow is defined as the flow in stator in the absence of inlet moving wakes. This flow is steady, and assumed to be inviscid, incompressible and irrotational. The unsteady flow is the flow in stator in the presence of inlet moving wakes. Thus, the disturbance flow is the flow obtained from substracting the steady flow from the unsteady flow, and it is unsteady. For this study, the disturbance flow is assumed to be small compared to the steady mean flow.

1.2 Literature Review

For the past decade or so, published papers on unsteady flow in turbomachinary blades are extensive. A review of the relevant papers pertaining to wake interacting with upstream rotor or stator blades are mentioned in here. Hodson [1984], Hall [1987, 1989], Verdon [1990] and Giles [1987, 1991], Valkov [1992] investigated these interactions in blade passages. Hall and Verdon linearized the governing fluid equations with the assumption that the unsteady disturbance flow is small relative to the mean flow; they also employed the splitting of the

velocity field into an irrotational and a rotational part. Hodson, Giles and Valkov solved the unsteady flow problem using unsteady flow equations.

1.3 Technical Objective

The overall technical objective is to examine unsteady flow phenomena in stator blade passages subjected to upstream moving wakes.

1.4 Technical Approaches

Clebsch's transformation is used to represent the velocity as the sum of an irrotational and a rotational part. With the disturbance flow asssumed to be small compared to the steady background flow, the governing flow equations can therefore be linearized about the steady mean flow.

1.5 Thesis Organization

This thesis is organized as follow. Chapter 2 discusses the theoretical approach to solve the problem of interest. Clebsch's formulation of the velocity equation and linearization of the governing flow equations are presented. The relevant equations for solving the disturbance flowfield are derived. The analytical formulae for prescribing inlet moving wakes is also described in this chapter.

Chapter 3 presents the numerical procedures for solving the linearized equations derived in Chapter 2. The procedures include those for solving the convective and Poisson equation with the appropriate boundary conditions. In addition, equations for solving the flow variables such as disturbance flowfields and vorticity fields are derived. The equations for obtaining static pressure coefficients on blade surfaces are also derived.

Chapter 4 discusses the numerical results obtained for the two- and three-dimensional blade geometry.

The results are summarized in Chapter 5.

Chapter 2

Problem of Study

The use of the Clebsch's transformation and the linearization of the governing disturbance flow equations are presented here. The analytical formulae for prescribing inlet moving wakes are also described.

2.1 Problem Definition

Clebsch's transformation [Rowe 1966, Hawthorne 1967 and 1977, Tan 1991 and 1992] is utilized to represent the unsteady velocity vector as the sum of an irrotational and a rotational part, written as

$$\vec{V} = \nabla\phi + \sigma\nabla\tau\,, \tag{2.1}$$

where σ and τ are scalar quantities. On the RHS (right hand side) of equation (2.1), the first term is the irrotational part, and the second term is the rotational part.

With the assumption that the disturbance flow is small compared to the background flow, the disturbance flow is linearized about the background flow. The unsteady velocity vector, the unsteady velocity potential, and the above two scalar quantities are rewritten as the sum of a mean and a disturbance part.

$$\vec{V} = \bar{\vec{V}} + \tilde{\vec{V}} \tag{2.2a}$$

$$\phi = \bar{\phi} + \tilde{\phi} \tag{2.2b}$$

$$\sigma = \bar{\sigma} + \tilde{\sigma} \tag{2.2c}$$

$$\tau = \bar{\tau} + \tilde{\tau} \tag{2.2d}$$

The unsteady, incompressible Euler's equation with no body forces can be written in rotational form [Fox and McDonald, 1985] as

$$-\frac{\partial \vec{V}}{\partial t} + \left(\vec{V} \times \vec{\omega}\right) = \nabla\left(\frac{P_t}{\rho}\right). \tag{2.3}$$

The unsteady total pressure can also be rewritten as the sum of a mean part and a disturbance part as

$$\frac{P_t}{\rho} = \frac{\bar{P}_t}{\rho} + \frac{\tilde{P}_t}{\rho}. \tag{2.4}$$

The unsteady vorticity vector, $\vec{\omega}$, is defined as

$$\vec{\omega} = \nabla \times \vec{V}. \tag{2.5}$$

Upon expanding equation (2.5) and rewriting in terms of ($\bar{\phi}$, $\tilde{\phi}$, $\bar{\sigma}$, $\tilde{\sigma}$, $\bar{\tau}$, $\tilde{\tau}$) using equations (2.2) and (2.1), we obtain

$$\vec{\omega} = \nabla \times \left(\nabla\bar{\phi} + \nabla\tilde{\phi} + \bar{\sigma}\nabla\bar{\tau} + \bar{\sigma}\nabla\tilde{\tau} + \tilde{\sigma}\nabla\bar{\tau} + \tilde{\sigma}\nabla\tilde{\tau}\right). \tag{2.6}$$

Noting that for any potential ϕ,

$$\nabla \times \nabla\phi \equiv 0\,, \tag{2.7}$$

for any scalar μ and λ,

$$\nabla \times \left(\lambda\nabla\mu\right) = \nabla\lambda \times \nabla\mu\,, \tag{2.8}$$

and eliminating the last term, which is a second-order term, on the RHS of equation (2.6), the vorticity equation becomes

$$\vec{\omega} = \left(\nabla\bar{\sigma} \times \nabla\bar{\tau}\right) + \left(\nabla\bar{\sigma} \times \nabla\tilde{\tau}\right) + \left(\nabla\tilde{\sigma} \times \nabla\bar{\tau}\right). \tag{2.9}$$

The terms in the Euler's equation (2.3) can now be fully expanded in terms of ($\overline{\vec{V}}$, $\tilde{\vec{V}}$, $\overline{\phi}$, $\tilde{\phi}$, $\overline{\sigma}$, $\tilde{\sigma}$, $\overline{\tau}$, $\tilde{\tau}$). The first term on the LHS (left hand side) of equation (2.3) is expanded by using equations (2.1) and (2.2) to give

$$\frac{\partial \vec{V}}{\partial t} = \frac{\partial}{\partial t}\left(\nabla\overline{\phi} + \nabla\tilde{\phi} + \overline{\sigma}\nabla\overline{\tau} + \overline{\sigma}\nabla\tilde{\tau} + \tilde{\sigma}\nabla\overline{\tau} + \tilde{\sigma}\nabla\tilde{\tau}\right). \tag{2.10}$$

Since the background flow is steady, the first and third term on the RHS of the equation are discarded. These two terms do not vary with time, t. The last term on the RHS is also discarded since it is a second-order term. With these, equation (2.10) is reduced to

$$\frac{\partial \vec{V}}{\partial t} = \frac{\partial}{\partial t}\left(\nabla\tilde{\phi} + \overline{\sigma}\nabla\tilde{\tau} + \tilde{\sigma}\nabla\overline{\tau}\right) \tag{2.11}$$

The last two terms on the RHS of equation (2.11) can be further expanded using the following relation for any scalar μ and λ,

$$\frac{\partial}{\partial t}(\lambda\nabla\mu) = \nabla\left(\lambda\frac{\partial\mu}{\partial t}\right) + \nabla\mu\frac{\partial\lambda}{\partial t} - \nabla\lambda\frac{\partial\mu}{\partial t}, \tag{2.12}$$

which gives

$$\frac{\partial \vec{V}}{\partial t} = \nabla\frac{\partial\tilde{\phi}}{\partial t} + \nabla\left(\overline{\sigma}\frac{\partial\tilde{\tau}}{\partial t}\right) + \nabla\tilde{\tau}\frac{\partial\overline{\sigma}}{\partial t} - \nabla\overline{\sigma}\frac{\partial\tilde{\tau}}{\partial t} + \nabla\left(\tilde{\sigma}\frac{\partial\overline{\tau}}{\partial t}\right) + \nabla\overline{\tau}\frac{\partial\tilde{\sigma}}{\partial t} - \nabla\tilde{\sigma}\frac{\partial\overline{\tau}}{\partial t}. \tag{2.13}$$

With the assumption that the mean flow is steady, the scalar quantities ($\overline{\sigma}$, $\overline{\tau}$) do not vary with time. The derivatives of these quantities with respect to time are set to zero. Equation (2.13) is further reduced to

$$\frac{\partial \vec{V}}{\partial t} = \nabla\frac{\partial\tilde{\phi}}{\partial t} + \nabla\left(\overline{\sigma}\frac{\partial\tilde{\tau}}{\partial t}\right) - \nabla\overline{\sigma}\frac{\partial\tilde{\tau}}{\partial t} + \nabla\overline{\tau}\frac{\partial\tilde{\sigma}}{\partial t} \tag{2.14}$$

Using equations (2.2a) and (2.9), the second term on the LHS of Euler's equation (2.3) becomes

$$\vec{V} \times \vec{\omega} = \left(\bar{\vec{V}} + \tilde{\vec{V}}\right) \times \left[(\nabla\bar{\sigma} \times \nabla\bar{\tau}) + (\nabla\bar{\sigma} \times \nabla\tilde{\tau}) + (\nabla\tilde{\sigma} \times \nabla\bar{\tau})\right]. \quad (2.15)$$

Expansion of equation (2.15) leads to

$$\begin{aligned}\vec{V} \times \vec{\omega} = {} & \left(\bar{\vec{V}} \bullet \nabla\bar{\tau}\right)\nabla\bar{\sigma} - \left(\bar{\vec{V}} \bullet \nabla\bar{\sigma}\right)\nabla\bar{\tau} + \left(\tilde{\vec{V}} \bullet \nabla\bar{\tau}\right)\nabla\bar{\sigma} - \left(\tilde{\vec{V}} \bullet \nabla\bar{\sigma}\right)\nabla\bar{\tau} \\ & + \left(\bar{\vec{V}} \bullet \nabla\tilde{\tau}\right)\nabla\bar{\sigma} - \left(\bar{\vec{V}} \bullet \nabla\bar{\sigma}\right)\nabla\tilde{\tau} + \left(\tilde{\vec{V}} \bullet \nabla\tilde{\tau}\right)\nabla\bar{\sigma} - \left(\tilde{\vec{V}} \bullet \nabla\bar{\sigma}\right)\nabla\tilde{\tau} \\ & + \left(\bar{\vec{V}} \bullet \nabla\bar{\tau}\right)\nabla\tilde{\sigma} - \left(\bar{\vec{V}} \bullet \nabla\tilde{\sigma}\right)\nabla\bar{\tau} + \left(\tilde{\vec{V}} \bullet \nabla\bar{\tau}\right)\nabla\tilde{\sigma} - \left(\tilde{\vec{V}} \bullet \nabla\tilde{\sigma}\right)\nabla\bar{\tau}\end{aligned} \quad (2.16)$$

Upon neglecting second-order terms, equation (2.16) is reduced to

$$\begin{aligned}\vec{V} \times \vec{\omega} = {} & \left(\bar{\vec{V}} \bullet \nabla\bar{\tau}\right)\nabla\bar{\sigma} - \left(\bar{\vec{V}} \bullet \nabla\bar{\sigma}\right)\nabla\bar{\tau} + \left(\tilde{\vec{V}} \bullet \nabla\bar{\tau}\right)\nabla\bar{\sigma} - \left(\tilde{\vec{V}} \bullet \nabla\bar{\sigma}\right)\nabla\bar{\tau} \\ & + \left(\bar{\vec{V}} \bullet \nabla\tilde{\tau}\right)\nabla\bar{\sigma} - \left(\bar{\vec{V}} \bullet \nabla\bar{\sigma}\right)\nabla\tilde{\tau} + \left(\bar{\vec{V}} \bullet \nabla\bar{\tau}\right)\nabla\tilde{\sigma} - \left(\bar{\vec{V}} \bullet \nabla\tilde{\sigma}\right)\nabla\bar{\tau}\end{aligned} \quad (2.17)$$

Rewriting the Euler's equation (2.3) by using equations (2.4), (2.14) and (2.17), we obtain

$$\begin{aligned}& \frac{\partial\tilde{\tau}}{\partial t}\nabla\bar{\sigma} - \frac{\partial\tilde{\sigma}}{\partial t}\nabla\bar{\tau} \\ & + \left(\bar{\vec{V}} \bullet \nabla\bar{\tau}\right)\nabla\bar{\sigma} + \left(\tilde{\vec{V}} \bullet \nabla\bar{\tau}\right)\nabla\bar{\sigma} + \left(\bar{\vec{V}} \bullet \nabla\tilde{\tau}\right)\nabla\bar{\sigma} \\ & - \left(\bar{\vec{V}} \bullet \nabla\bar{\sigma}\right)\nabla\bar{\tau} - \left(\tilde{\vec{V}} \bullet \nabla\bar{\sigma}\right)\nabla\bar{\tau} - \left(\bar{\vec{V}} \bullet \nabla\tilde{\sigma}\right)\nabla\bar{\tau} \\ & - \left(\bar{\vec{V}} \bullet \nabla\bar{\sigma}\right)\nabla\tilde{\tau} + \left(\bar{\vec{V}} \bullet \nabla\bar{\tau}\right)\nabla\tilde{\sigma} \\ & = \nabla\left(\frac{\bar{P}_t}{\rho} + \frac{\tilde{P}_t}{\rho} + \frac{\partial\tilde{\phi}}{\partial t} + \bar{\sigma}\frac{\partial\tilde{\tau}}{\partial t}\right)\end{aligned} \quad (2.18)$$

Following Lamb's discussion on the Clebsch's transformation [Lamb, 1932], the RHS terms in equation (2.18) can be assigned as follows:

$$\bar{\sigma} = \frac{\bar{P}_t}{\rho} \quad (2.19a)$$

$$\tilde{\sigma} = \frac{\tilde{P}_t}{\rho} + \frac{\partial\tilde{\phi}}{\partial t} + \bar{\sigma}\frac{\partial\tilde{\tau}}{\partial t}. \quad (2.19b)$$

From equation (2.19a) the scalar quantity, $\bar{\sigma}$, represents the mean total pressure. Substituting equation (2.19) into equation (2.18) and re-arranging terms, the Euler's equation in terms of the Clebsch's variables is written as

$$\left[\left(\bar{\bar{V}} \bullet \nabla\bar{\tau}\right) + \left(\tilde{\bar{V}} \bullet \nabla\bar{\tau}\right) + \left(\bar{\bar{V}} \bullet \nabla\tilde{\tau}\right) + \frac{\partial\tilde{\tau}}{\partial t} - 1\right]\nabla\bar{\sigma}$$
$$-\left[\left(\bar{\bar{V}} \bullet \nabla\bar{\sigma}\right) + \left(\tilde{\bar{V}} \bullet \nabla\bar{\sigma}\right) + \left(\bar{\bar{V}} \bullet \nabla\tilde{\sigma}\right) + \frac{\partial\tilde{\sigma}}{\partial t}\right]\nabla\bar{\tau}$$
$$-\left(\bar{\bar{V}} \bullet \nabla\bar{\sigma}\right)\nabla\tilde{\tau} + \left[\left(\bar{\bar{V}} \bullet \nabla\bar{\tau}\right) - 1\right]\nabla\tilde{\sigma} = 0. \qquad (2.20)$$

The linearized equations describing the convection of ($\bar{\sigma}$, $\tilde{\sigma}$, $\bar{\tau}$, $\tilde{\tau}$) are obtained from equation (2.20). The last two terms on the LHS of equation (2.20) give the convective equations for $\bar{\sigma}$ and $\bar{\tau}$:

$$\left(\bar{\bar{V}} \bullet \nabla\right)\bar{\sigma} = 0 \qquad (2.21)$$

$$\left(\bar{\bar{V}} \bullet \nabla\right)\bar{\tau} - 1 = 0 \qquad (2.22)$$

Using equations (2.21), (2.22) and the remaining terms in equation (2.20), two additional equations can be obtained; these are the convetive equations for $\tilde{\sigma}$ and $\tilde{\tau}$:

$$\frac{\partial\tilde{\tau}}{\partial t} + \left(\bar{\bar{V}} \bullet \nabla\right)\tilde{\tau} + \left(\tilde{\bar{V}} \bullet \nabla\right)\bar{\tau} = 0 \qquad (2.23)$$

$$\frac{\partial\tilde{\sigma}}{\partial t} + \left(\bar{\bar{V}} \bullet \nabla\right)\tilde{\sigma} + \left(\tilde{\bar{V}} \bullet \nabla\right)\bar{\sigma} = 0 \qquad (2.24)$$

With the assumption that the mean flow is steady, inviscid and irrotational, the mean total pressure is uniform throughout the flowfield [Kuethe and Chow, 1986]. Thus, the gradient of the mean total pressure is zero; that is

$$\nabla\bar{\sigma} = 0. \qquad (2.25)$$

This assumption allows the linearized Euler equation (2.20) to be considerably simplified to

$$-\left[\frac{\partial\tilde{\sigma}}{\partial t} + \left(\bar{\bar{V}} \bullet \nabla\tilde{\sigma}\right)\right]\nabla\bar{\tau} + \left[\left(\bar{\bar{V}} \bullet \nabla\bar{\tau}\right) - 1\right]\nabla\tilde{\sigma} = 0 \tag{2.26}$$

Then, from equation (2.26) the equations describing the convection of $\tilde{\sigma}$ and $\bar{\tau}$ are

$$\left(\bar{\bar{V}} \bullet \nabla\right)\bar{\tau} - 1 = 0 \tag{2.27}$$

$$\frac{\partial\tilde{\sigma}}{\partial t} + \left(\bar{\bar{V}} \bullet \nabla\right)\tilde{\sigma} = 0. \tag{2.28}$$

The scalar quantity, $\bar{\tau}$, is the classical fluid particle drift time [Lighthill, 1956, and Hawthorne, 1966]. The scalar quantity, $\tilde{\sigma}$, is now represented by the sum of the disturbance total pressure and the temporal variation of the disturbance potential. This is written as

$$\tilde{\sigma} = \frac{\tilde{P}_t}{\rho} + \frac{\partial\tilde{\phi}}{\partial t} \tag{2.29}$$

For computational purposes, the temporal variation of the scalar quantity, $\bar{\tau}$, is added to equation (2.27) and time-stepping is applied for obtaining the steady solution. Thus, equation (2.27) can be rewritten as

$$\frac{\partial\bar{\tau}}{\partial t} + \left(\bar{\bar{V}} \bullet \nabla\right)\bar{\tau} = 1. \tag{2.30}$$

To rewrite equations (2.28) and (2.30) in a more compact form, a convective operator D/Dt is defined as

$$\frac{D}{Dt} = \frac{\partial}{\partial t} + \left(\bar{\bar{V}} \bullet \nabla\right) \tag{2.31}$$

Then, equations (2.28) and (2.30) become

$$\frac{D\bar{\tau}}{Dt} = 1 \tag{2.32}$$

$$\frac{D\tilde{\sigma}}{Dt} = 0 . \tag{2.33}$$

Using equation (2.25), the vorticity equation (2.9) now contains only the contribution from the disturbance flow; that is

$$\tilde{\vec{\omega}} = \nabla\tilde{\sigma} \times \nabla\bar{\tau} \tag{2.34}$$

The equations describing the mean and disturbance velocity potential are obtained as follow. Upon substituting equation (2.2) into equation (2.1), discarding second-order terms, and collecting terms for the steady mean and unsteady disturbance potential, we have

$$\nabla\bar{\phi} = \bar{\vec{V}} - \bar{\sigma}\nabla\bar{\tau} \tag{2.35}$$

$$\nabla\tilde{\phi} = \tilde{\vec{V}} - \left(\bar{\sigma}\nabla\tilde{\tau} + \tilde{\sigma}\nabla\bar{\tau}\right) \tag{2.36}$$

Upon taking the divergence of equations (2.35) and (2.36) and using the conservation of mass, the above two equations are reduced to

$$\nabla^2\bar{\phi} = -\nabla \cdot \left(\bar{\sigma}\nabla\bar{\tau}\right) \tag{2.37}$$

$$\nabla^2\tilde{\phi} = -\nabla \cdot \left(\bar{\sigma}\nabla\tilde{\tau} + \tilde{\sigma}\nabla\bar{\tau}\right) \tag{2.38}$$

However, note that the first term on the RHS of equation (2.38) can be absorbed into the term on the LHS without any loss of generality; this gives

$$\nabla^2\tilde{\phi} = -\nabla \cdot \left(\tilde{\sigma}\nabla\bar{\tau}\right) \tag{2.39}$$

Finally, the remaining tasks are to solve equations (2.32), (2.33) and (2.39) to obtain $(\bar{\tau}, \tilde{\sigma}, \tilde{\phi})$. Then, these quantities are substituted into

$$\tilde{\vec{V}} = \nabla\tilde{\phi} + \tilde{\sigma}\nabla\bar{\tau} \tag{2.40}$$

to obtain the resulting disturbance flowfield due to the inlet moving wakes. The numerical discretization of equations (2.32), (2.33), (2.39) and (2.40) are detailed in Chapter 3.

2.2 Formulations of Inlet Vortical Disturbances

The inlet moving wakes used in the two- and three-dimensional case studies are formulated in this section. For the two-dimensional case, the inlet moving wakes contain only the x-component of velocity, U_w. This velocity component varies with time and in the y-direction; that is $U_w = U_w(y,t)$. Dimensionless parameters for describing the inlet wakes are shown below. The wake thickness, δ^*, is defined as a percent of the blade spacing, S. This thickness is described as the distance between two locations where U_w is at its minimum. The velocity defect is defined as the maximum value of U_w.

U	2.0	Rotor Velocity
S	0.40	Blade Spacing
δ^*	10%	Wake Thickness
θ^*	0.05	Velocity Defect

Table 1: Wake parameters for two-dimensional pase.

The prescribed wake moves along the y-axis. The lower corner of the inlet boundary is defined as the reference point, y_{ref}, for the wake's movement along the y-axis. The position of the wake's center (at any time t) along the y-axis is determined from

$$y_w(t) = U\,t. \tag{2.41}$$

The spatial periodicity, P_w, of the wake is obtained from

$$P_w = \frac{y_w}{S} - E\left[\frac{y_w}{S}\right], \tag{2.42}$$

where $E[\ ]$ is the integer part of the quantity inside the brackets. The locations of two wakes' centers in the spatial periodicity needs to be determined. The location of the lower and upper wake's center are found from

$$y_l = S\,P_w; \qquad y_u = S\left(1 + P_w\right). \tag{2.43}$$

The wake regions for the lower and upper wake are determined from

$$y_{u_{min}} = y_u - \frac{\delta^*}{2}; \qquad y_{u_{max}} = y_u + \frac{\delta^*}{2} \tag{2.44a}$$

$$y_{l_{min}} = y_l - \frac{\delta^*}{2}; \qquad y_{l_{max}} = y_l + \frac{\delta^*}{2} \tag{2.44b}$$

For each wake, the velocity distribution between the wake's center and the locations $(\frac{\delta^*}{2}, -\frac{\delta^*}{2})$ are described by

$$D_{\frac{\delta^*}{2}} = \sin\left(\frac{\pi}{\delta^*}\left|y_{pos} - y_u\right|\right) \tag{2.45a}$$

$$D_{-\frac{\delta^*}{2}} = \sin\left(\frac{\pi}{\delta^*}\left|y_{pos} - y_l\right|\right), \tag{2.45b}$$

where

$$y_{pos} = y_{(IMIN,j)} - y_{ref} \tag{2.46}$$

is the distance along the inlet boundary between the y-location of interest, $y_{(IMIN,j)}$, and the reference y-location denoted as y_{ref}.

When y_{pos} is within the bounds set by equation (2.44a), the x-component of wake's velocity is

$$U_w(y,t) = \theta^*\left(D_{\frac{\delta^*}{2}} - 1\right). \tag{2.47a}$$

However, when y_{pos} is within the bounds set by equation (2.44b), the x-component of the wake's velocity is

$$U_w(y,t) = \theta^*\left(D_{\frac{\delta^*}{2}} - 1\right). \tag{2.47b}$$

For all other values of y_{pos} not located within the bounds of equations (2.44a) and (2.44b), the x-component of the wake's velocity is set to zero.

For the three-dimensional case, the wake has only the x-component of velocity. This velocity component has both a variation in the y- and z-direction and in time; that is $U_w = U_w(y,z,t)$. The dimensionless wake parameters used for the three-dimensional case are shown below. The procedures for obtaining the wake's velocity along the inlet boundary are as follow. First, compute the wake's velocity along the y-direction at z=0 using the equations established for the two-dimensional case. These equations are (2.47a) and (2.47b) with the bounds given by equations (2.44a) and (2.44b). Then, impose a z-variation of the wake along the span of the blade, L.

U	2.0	Rotor Velocity
S	0.40	Blade Spacing
δ^*	15%	Wake Thickness
θ^*	0.05	Velocity Defect
L	1.0	Span of Blade
β	-0.02	Shear Defect

Table 2: Wake parameters for three-dimensional case.

To include the z-variation of the wake's x-component of velocity, a shear defect is added to the already determined wake structure for the two-dimensional case. At each z-location of interest, $z_{(IMIN,j,k)}$, along the inlet boundary, the x-component of velocity is defined by

$$U_w(y,z,t) = \{U_w(y,t)\}_{2-D\ case} + \frac{\beta}{L} z_{pos}, \tag{2.48}$$

where

$$z_{pos} = z_{(IMIN,j,k)} - z_{ref}\,. \tag{2.49}$$

Refering to Figure 8, z_{ref} is any z-location along the bottom side of the inlet boundary. Since each blade span from z=0 to z=1, z_{ref} is set zero.

Chapter 3

Numerical Formulations of the Problem

The locations of flow variables in the computational domain are discussed. The numerical techniques for solving the convective and Poisson equation are presented. Numerical procedures for obtaining the disturbance flowfields, disturbance vorticity fields, and pressure coefficients are also shown in this chapter.

3.1 Cell Locations of Flow Variables

In the three-dimensional case, the steady background velocity components $(\overline{u}, \overline{v}, \overline{w})$ and the cell's geometries (x, y, z) are defined at cell nodes. The x- and y-component of the velocity is from a two-dimensional velocity field. The z-component of the velocity is set to zero throughout the flowfield. The two- and three-dimensional coordinates systems used in this study are shown in Figures 1 and 6, repectively. The two-dimensional velocity field is obtained from Valkov [1992] which were generated using the PCPANNEL code by McFarland [1984].

The cell-centered values of the velocity flowfield and cell geometries are obtained using an averaging of the eight nodal values of each cell in the three-dimensional case and the four nodal values of each cell in the two-dimensional case. The variables of interest $\left(\overline{\tau}, \tilde{\sigma}, \tilde{\phi}, \tilde{\tilde{\omega}}\right)$ and the disturbance flowfield $(\tilde{u}, \tilde{v}, \tilde{w})$ are also defined at cell centers.

The mean and unsteady pressure coefficients $\left(\overline{C}_p, C_p\right)$ are defined at wall surfaces. These coefficients are obtained from extrapolating the centre values of cells along the wall surfaces to the appropriate wall locations.

3.2 Convective Equation

The equations describing the convection of $(\tilde{\sigma}, \bar{\tau})$ were derived in Chapter 2. In this section, the numerical formulations of these equations are discussed. The spatial discretization of the three- and two-dimensional convective equations is detailed in Appendix II-A and I-A, respectively. These numerical formulations involve the computation of facial fluxes, the steps of time-integration, the inclusion of artifical smoothing, and the specification of boundary conditions.

3.2.1 Fluxes

Referring to Appendix I-A and II-B, the spatially discretized convetive equation requires the computation of the fluxes denoted by F, H, G (x-, y-, and z-direction, respectively). These fluxes are defined at cell centers. The fluxes at cell faces (three-dimensional case) or vertices (two-dimensional case) are computed from an area-weighted averaging [Turkel, 1985] of two fluxes on either side of the face or vertex. In the three-dimensional case, for example, the right facial fluxes are (see Figure 7 for the notations of the cell faces)

$$F_{RT} = \alpha F_{i+1,j,k} + (1 - \alpha)F_{i,j,k} \tag{3.1}$$

$$G_{RT} = \alpha G_{i+1,j,k} + (1 - \alpha)G_{i,j,k} \tag{3.2}$$

$$H_{RT} = \alpha H_{i+1,j,k} + (1 - \alpha)H_{i,j,k} \tag{3.3}$$

where

$$\alpha = \frac{L_1}{L_1 + L_2}. \tag{3.4}$$

L_1 is defined as the distance between the cell center at (i, j, k) and the center of its right face. L_2 is defined as the distance between the cell center at (i+1, j, k) and the center of its left face.

However, in the two-dimensional case, referring to Figure 2 for the notations of the cell faces, L_1 is defined as the distance between the cell center at (i, j) and the center of its right vertex, and L_2 is defined as the distance between the cell center at (i+1, j) and the center of its left vertex. The subscripts (i, j, k) and (i+1, j, k) in equations (3.1) and (3.2) are replaced by (i, j) and (i+1, j), respectively. Obviously, the third component of flux in equation (3.3) is discarded for the two-dimensional case.

3.2.2 Time-Integration

The time-integration employed for the temporal discretization of the convective equation is the four-stage Runge-kutta scheme [Jameson, 1981]. The following stages must be performed at each (i, j, k) lcoation for the three-dimensional case or at each (i, j) location for the two-dimensional case in order to update an arbitrary variable denoted by Θ. The current time-step is denoted by the superscript (n), and the next time-step is denoted by the superscript (n+1).

$$
\begin{aligned}
\Theta^0 &= \Theta^n \\
\Theta^1 &= \Theta^0 - \alpha_1 \left(\frac{\lambda^* \Delta t}{V} \right) \left[R\left(\Theta^0\right) \right] \\
\Theta^2 &= \Theta^0 - \alpha_2 \left(\frac{\lambda^* \Delta t}{V} \right) \left[R\left(\Theta^1\right) \right] \\
\Theta^3 &= \Theta^0 - \alpha_3 \left(\frac{\lambda^* \Delta t}{V} \right) \left[R\left(\Theta^2\right) \right] \\
\Theta^4 &= \Theta^0 - \left(\frac{\lambda^* \Delta t}{V} \right) \left[R\left(\Theta^3\right) \right] \\
\Theta^{n+1} &= \Theta^4 ,
\end{aligned}
\tag{3.5}
$$

where V is the cell volume, Δt is the global time-step, and λ^* is the Courant number [Jameson, 1981] set by stability analysis to be $2\sqrt{2}$. The coefficients α_1, α_2, and α_3 are chosen to be 1/4, 1/3, and 1/2, respectively [Allmaras, 1985]. In the two-dimensional case, the cell volume, V, in equation (3.5) needs to be replaced by the cell area, Ω.

For the three-dimensional case, at each (i, j, k) location, the residual, $R(\Theta)$ is defined as

$$
R(\Theta) = \sum_{f=FT}^{TP} \left[F(\Theta)\, A_x + G(\Theta)\, A_y + H(\Theta)\, A_z \right]_f - W(\Theta) + Q \tag{3.6}
$$

The artificial viscosity or smoothing, $W(\Theta)$, is discussed in the next section. The facial areas $\left(A_x , A_y , A_z \right)$ are defined in Appendix II-C.

For the two-dimensional case, at each (i, j) location, the residual is reduced to

$$R(\Theta) = \sum_{f=BT}^{LT} \left[F(\Theta)\,\Delta y - G(\Theta)\,\Delta x \right]_f - W(\Theta) + Q \tag{3.7}$$

The terms Δx and Δy are defined in Appendix I-C. For both the two- and three-dimensional case, Q=1 when solving for $\bar{\tau}$, and Q=0 when solving for $\tilde{\sigma}$.

3.2.3 Artificial smoothing

The artificial smoothing term [Allmaras, 1985], $W(\Theta)$, in the three-dimensional case is defined as

$$W(\Theta) = \nu_2 D^{(2)} - D^{(4)}, \tag{3.8}$$

where $D^{(2)}$ and $D^{(4)}$ are the second-order and fourth-order smoothing terms, respectively. ν_2 is a defined constant coefficient. Throughout this study, inviscid flow solutions are of concern; so, $D^{(2)}$ term is ignored since no shock is present in the solutions. The fourth-order smoothing, $D^{(4)}$, is defined as

$$D^{(4)} = \sum_{f=FT}^{TP} \varepsilon_f^{(4)} \left(\frac{V}{\Delta t} \right)_f \delta_f \left[\left(\frac{\Delta t}{V} \right) \sum_{f'=FT}^{TP} \left(\frac{V}{\Delta t} \right)_{f'} \delta_{f'}(\Theta) \right], \tag{3.9}$$

where $\delta_f(\lambda)$ is the first difference of the quantity λ (an arbitrary variable) across a face (denoted by f).

$$\delta_f(\lambda) = \lambda_+ - \lambda_- \tag{3.10}$$

This is the smoothing flux across the face. It is evaluated at faces so that the smoothing is conservative. Its value at a particular face is taken as an average of the two cells on either side of the face. The term $\varepsilon_f^{(4)}$ is a switch, for example (for the right face),

$$\varepsilon_{RT}^{(4)} = \max\{0, \nu_4\}, \tag{3.11}$$

where ν_4 is a user-controllable value set between 0.001 and 0.01. In the three-dimensional case study, ν_4 is set to 0.005.

The evaluation of $W(\Theta)$ in equation (3.7) is only performed at the first stage (n=0) of the time-integration and frozen throughout the remaining stages of integration. This is to render the calculation of the smoothing terms less computationally-intensive. Using equation (3.11) we take the switch, $\varepsilon_f^{(4)}$, out of the summation in equation (3.9). The fourth-order smoothing term then gives

$$D^{(4)} = \nu_4 \sum_{f=FT}^{TP} \left(\frac{V}{\Delta t}\right)_f \delta_f \left[\left(\frac{\Delta t}{V}\right) \sum_{f'=FT}^{TP} \left(\frac{V}{\Delta t}\right)_{f'} \delta_{f'}(T) \right]. \tag{3.12}$$

The terms $\left(\frac{V}{\Delta t}\right)_f$ and $\left(\frac{V}{\Delta t}\right)_{f'}$ are evaluated as averages of the values in the two cells at either side of the face of interest (denoted by f or f').

In the two-dimensional case, the artificial viscocity is also computed from equation (3.12), but V must be replaced by Ω, and the summation is around four vertices (RT to LT) of each cell. The smoothing constant, ν_4 is set to 0.009. The smoothing flux, defined in equation (3.10), is now calculated across vertices of the two-dimensional cells. The averagings in equation (3.12) are also performed across vertices.

Since the solutions need to be time-accurate, no local time-stepping can be applied. A chosen global time step, Δt, is utilized throughout. The maximum global time step can be easily obtained by first computing the local time steps for each cell and then choose the maximum value. The maximum global time step can also be determined by trial-and-error or more precisely by solving an eigenvalue problem. The local time steps are determined by:

$$\Delta t_x = \frac{\Delta \bar{x}}{\bar{u}} ; \quad \Delta t_y = \frac{\Delta \bar{y}}{\bar{v}} ; \quad \Delta t_z = \frac{\Delta \bar{z}}{\bar{w}} \tag{3.13}$$

Note that the local time-steps approach infinity as $(\bar{u}, \bar{v}, \bar{w})$ approach zero. In this study, Δt is set to 1/1000 in the two-dimensional case and 1/100 in the three-dimensional case. The choice of time step is dictated by the Courant-Friedrichs-Lewy (CFL) condition. This is the conditional stability requirement set on the time step and the spacings of the mesh [Anderson, 1984].

3.2.4 Boundary Conditions

The necessary boundary conditions for solving the convective equation are detailed below for both the two- and three-dimensional case.

3.2.4.1 Two-dimensional case

The computational domain is set to be a passage between two stator blade surfaces. Referring to Figure 4, the lower and upper boundary are composed of wall surfaces (blades) and periodic boundary surfaces. The inlet boundary is the left side of the domain, and the outlet boundary is the right side of the domain.

The leftmost cells are used to implement the inlet boundary condition, and the rightmost cells are used to implement the outlet boundary condition. Dummy cells are defined along wall surfaces as a computational convenience to implement wall conditions. Upper and lower periodic extension of the blade passage along the y-axis allows the implementation of the periodic boundary conditions.

In solving the convective equation (I.A.1) with Q=1, an inlet initial condition needs to be prescribed at the inlet of the computational domain. Note that Θ needs to be replaced by $\overline{\tau}$. For the study of the two-dimensional problem, the inlet condition is set to be uniform along the inlet column of the computational domain.

$$\Theta_{INLET} = \Theta_{IMIN,j} = CONSTANT \tag{3.14}$$

However, in solving the convective equation with Q=0, the inlet boundary condition is set by

$$\Theta_{INLET} = \Theta_{IMIN,j} = \left(\overline{u}\,\tilde{u} + \overline{v}\,\tilde{v}\right)_{IMIN,j} \tag{3.15}$$

Note that Θ needs to be replaced by $\tilde{\sigma}$. This inlet condition varies at each time-step since the disturbance velocity components $(\tilde{u}, \tilde{v})$ are involved in equation (3.15).

The outlet boundary condition is obtained from extrapolating the values of the interior cells of the computational domain to the outlet boundary cells, using

$$\Theta_{OUTLET} = \Theta_{IMAX,j} = 2\,\Theta_{IMAX-1,j} - \Theta_{IMAX-2,j} \tag{3.16}$$

The periodic boundary conditions are defined for the lower and upper boundary of the domain as

$$\begin{aligned} \Theta_{\text{lower periodic}} &= \Theta_{i,JMIN-1} = \Theta_{i,JMAX} \\ \Theta_{\text{upper periodic}} &= \Theta_{i,JMAX+1} = \Theta_{i,JMIN} \end{aligned} \tag{3.17}$$

The wall boundary conditions are defined for the lower and upper boundary of the domain as

$$\begin{aligned} \Theta_{\text{lower wall}} &= \Theta_{i,JMIN-1} = \Theta_{i,JMIN} \\ \Theta_{\text{upper wall}} &= \Theta_{i,JMAX+1} = \Theta_{i,JMAX} \end{aligned} \tag{3.18}$$

To insure that there are no fluxes through wall surfaces, the steady background velocity components along the wall surfaces are reflected about the walls and then assigned to the dummy cells. This will enforce the no flux condition across wall surfaces.

The velocity components for the dummy cells along the wall surfaces are determined as follow. The wall angle is first determined by

$$\theta_{\text{wall}} = \tan^{-1}\left(\frac{\Delta y}{\Delta x}\right), \tag{3.19}$$

where $(\Delta x, \Delta y)$ are obtained from the wall face. The velocity components in the wall surface coordinates (the t-axis is pointing toward the right and tangent to the wall, and the n-axis is normal to and pointing away from the wall surface) are

$$\begin{aligned} U_t &= \bar{u} \cos\theta_{\text{wall}} + \bar{v} \sin\theta_{\text{wall}} \\ U_n &= -\bar{u} \sin\theta_{\text{wall}} + \bar{v} \cos\theta_{\text{wall}} \end{aligned} \tag{3.20}$$

Again, in the wall surface coordinates, the normal component of the velocity, U_n, is reflected from the wall surface to give

$$U_{n'} = -U_n \tag{3.21}$$

Now, with the two components of velocity from first equation of (3.20) and equation (3.21), we must transform these two components back into the x-y coordinates of the computational domain using

$$\begin{aligned} u' &= U_t \cos\theta_{\text{wall}} - U_{n'} \sin\theta_{\text{wall}} \\ v' &= U_t \sin\theta_{\text{wall}} + U_{n'} \cos\theta_{\text{wall}}. \end{aligned} \tag{3.22}$$

These velocity components from equation (3.22) are assigned to dummy cells along the wall surfaces. On the periodic boundaries, the steady background velocity components are defined by equation (3.17) and replacing Θ with $\bar{u}$ and $\bar{v}$.

3.2.4.2 Three-dimensional case

The computational domain is set to be a passage between two stator blade surfaces. Referring to Figure 8, the lower and upper boundary are composed of flat walls. The front and back boundary are composed of wall surfaces (blades) and periodic boundaries. The left boundary is the inlet boundary, and the right boundary is the outlet boundary.

The column of cells lying along the inlet boundary are used to implement the inlet boundary condition, and those lying along the outlet boundary are used for implementing the outlet boundary condition. Dummy cells are defined along wall surfaces for allowing the implementation of wall boundary conditions. Periodic extension of the blade passage along the y-axis allows the periodic boundary conditions to be implemented.

In solving the three-dimensional convective equation (II.A.3), the inlet boundary condition only needs to be prescribed. When solving for $\bar{\tau}$ (Q=1), the inlet condition is set to be uniform throughout the inlet boundary. Note that Θ needs to be replaced by $\bar{\tau}$.

$$\Theta_{INLET} = \Theta_{IMIN,j,k} = CONSTANT \tag{3.23}$$

When solving for $\tilde{\sigma}$ (Q=0), the inlet boundary condition is set by

$$\Theta_{INLET} = \Theta_{IMIN,j,k} = (\bar{u}\tilde{u} + \bar{v}\tilde{v} + \bar{w}\tilde{w})_{IMIN,j,k}, \tag{3.24}$$

and we need to replace Θ with $\tilde{\sigma}$. The disturbance velocity components $(\tilde{u}, \tilde{v}, \tilde{w})$ are prescribed at the inlet; they are from the inlet moving wakes. The inlet boundary condition varies at each time-step since unsteady velocity components are involved.

The outlet boundary condition is obtained from an extrapolation of the values at the interior cells of the computational domain to the outlet boundary cells, using

$$\Theta_{OUTLET} = \Theta_{IMAX,j,k} = 2\,\Theta_{IMAX-1,j,k} - \Theta_{IMAX-2,j,k} \tag{3.25}$$

The periodic boundary conditions of the front and back periodic boundaries are defined by

$$\Theta_{\text{front periodic}} = \Theta_{i,JMIN-1,k} = \Theta_{i,JMAX,k}$$
$$\Theta_{\text{back periodic}} = \Theta_{i,JMAX+1,k} = \Theta_{i,JMIN,k} \tag{3.26}$$

The wall boundary conditions of the front, back, top, and bottom computational boundaries are set by

$$\Theta_{\text{front wall}} = \Theta_{i,JMIN-1,k} = \Theta_{i,JMAX,k}$$
$$\Theta_{\text{back wall}} = \Theta_{i,JMAX+1,k} = \Theta_{i,JMIN,k}$$
$$\Theta_{\text{top wall}} = \Theta_{i,j,KMAX+1} = \Theta_{i,j,KMIN}$$
$$\Theta_{\text{bottom wall}} = \Theta_{i,j,KMIN-1} = \Theta_{i,j,KMAX} \tag{3.27}$$

To insure that there is no flow across wall surfaces, the net flux across the wall surfaces must be zero. Dummy cells are setup along walls surfaces for computational convenience. These dummy cells contain velocity components that will insure the condition of no net flux across wall surfaces. The procedures for computing these velocity components are detailed in section (3.2.4.1). The derivations in that section are still useful because there is no z-component of velocity, and the wall surfaces are still only two-dimensional geometries.

3.3 Poisson Equation

The spatial discretization of the three- and two-dimensional Poisson equation is discussed in Appendix II-B and I-B, respectively. This Poisson equation was derived in Chapter 2. To solve the discretized equation for the disturbance velocity potential, an iterative method called successive-over-relaxation (SOR) is used. This method is discussed in the first section. The second section discusses the necessary boundary conditions for solving the Poisson equation.

3.3.1 Successive-over-relaxation

The method of SOR is an iterative method, and it is a slight modification of the Gauss-Seidel method [Chapra and Canale, 1988]. A relaxation factor, κ, is included to enhance convergence. The relaxation factor is set between 1.0 and 2.0; the exact number is set by looking at the eigenvalue problem of interest. In this study, this factor is set to 1.20 by trial-and-error.

In the two-dimensional case, there are nine cells contributing to the cell at each (i, j) location. Their influence is only geometrical as it is shown in Appendix I-B. All the $COEF_n$ (n=1 to 9) contain only cell metrics.

$$\tilde{\phi}^{*}_{i,j} =$$
$$COEF_1\,\tilde{\phi}_{i+1,j-1} + COEF_2\,\tilde{\phi}_{i,j-1} + COEF_3\,\tilde{\phi}_{i-1,j-1} + COEF_4\,\tilde{\phi}_{i+1,j} +$$
$$COEF_6\,\tilde{\phi}_{i-1,j} + COEF_7\,\tilde{\phi}_{i+1,j+1} + COEF_8\,\tilde{\phi}_{i,j+1} + COEF_9\,\tilde{\phi}_{i-1,j+1} \tag{3.28}$$

The new estimate, without any relaxation, is computed from

$$\tilde{\phi}^{TEMP}_{i,j} = -\frac{1}{COEF_5}\left(\tilde{\phi}^{*}_{i,j} + d\tilde{\phi}^{BC}_{i,j} + Q_{i,j}\right), \tag{3.29}$$

where $Q_{i,j}$ is the value of the source terms in (I.B.9) . For a cell vertex that is of the Neumann type boundary condition, the derivatives in (I.B.4) corresponding to that vertex are not spatially discretized. These non-discretized derivatives are contained in $d\tilde{\phi}^{BC}_{i,j}$. The difference between the new estimate and the old value is determined from

$$DIFF = \tilde{\phi}^{TEMP}_{i,j} - \tilde{\phi}_{i,j} \tag{3.30}$$

The difference given by equation (3.30) is multiplied by the relaxation factor, κ, which intends to improve the new estimate, and is added to the old value to obtain the final estimate.

$$\tilde{\phi}^{new}_{i,j} = \tilde{\phi}^{old}_{i,j} + \kappa\, DIFF \tag{3.31}$$

Once computed, the final estimate immediately replaces the old one.

In the three-dimensional case, there are nineteen cells contributing to the cell at each (i, j, k) location. All the $COEF_n$ (n=1 to 19) contain only cell metrics, and they are derived in Appendix II-B. Equation (3.28) is replaced by the more complicated equation,

$$\tilde{\phi}^{*}_{i,j,k} = COEF_1\,\tilde{\phi}_{i,j-1,k-1} + COEF_2\,\tilde{\phi}_{i+1,j-1,k} + COEF_3\,\tilde{\phi}_{i,j-1,k+1} +$$
$$COEF_4\,\tilde{\phi}_{i-1,j-1,k} + COEF_5\,\tilde{\phi}_{i,j-1,k} + COEF_6\,\tilde{\phi}_{i,j,k-1} +$$
$$COEF_7\,\tilde{\phi}_{i+1,j,k-1} + COEF_8\,\tilde{\phi}_{i+1,j,k} + COEF_9\,\tilde{\phi}_{i+1,j,k+1} +$$

$$COEF_{10}\,\tilde{\phi}_{i,j,k+1} + COEF_{11}\,\tilde{\phi}_{i-1,j,k+1} + COEF_{12}\,\tilde{\phi}_{i-1,j,k} +$$
$$COEF_{13}\,\tilde{\phi}_{i-1,j,k-1} + COEF_{15}\,\tilde{\phi}_{i,j+1,k-1} + COEF_{16}\,\tilde{\phi}_{i+1,j+1,k} +$$
$$COEF_{17}\,\tilde{\phi}_{i,j+1,k+1} + COEF_{18}\,\tilde{\phi}_{i-1,j+1,k} + COEF_{19}\,\tilde{\phi}_{i,j+1,k} \quad (3.32)$$

The subscripts (i, j) in equations (3.29), (3.30) and (3.31) are replaced by (i, j, k). $COEF_5$ is replaced by $COEF_{14}$ in equation (3.29). The term $d\tilde{\phi}^{BC}_{i,j,k}$ (defined similarly as for the two-dimensional case) is the value of the non-discretized terms in (II.B.3a), and $Q_{i,j,k}$ is the value of the source terms in (II.B.3b).

3.3.2 Boundary conditions

To solve the Poisson equation, all boundary conditions must be defined. Boundary conditions can either be of the Neumann or Dirichlet type. Neumann type boundary conditions are implemented on computational boundary surfaces. Dirichlet type boundary conditions are implemented at centers of cells defined for implementing boundary conditions.

From the discretization of the three-dimensional Poisson equation in (II.B.3), the Neumann boundary conditions can be easily substituted into (II.B.3). Depending on which face of the cell lies the Neumann boundary condition, the derivatives in (II.B.3) for that face are not decomposed any further. Similarly for the two-dimensional Poisson equation shown in (I.B.4).

At the start of the iterative process, all $\tilde{\phi}$'s in the computational domain are set to zero. Then, the Neumann boundary conditions on the relevant cells' faces, f, are set by:

$$\left(\frac{\partial\tilde{\phi}}{\partial x}\right)_f = \left(\tilde{u} - \tilde{\sigma}\,\frac{\partial\bar{\tau}}{\partial x}\right)_f$$
$$\left(\frac{\partial\tilde{\phi}}{\partial y}\right)_f = \left(\tilde{v} - \tilde{\sigma}\,\frac{\partial\bar{\tau}}{\partial y}\right)_f \quad (3.33)$$
$$\left(\frac{\partial\tilde{\phi}}{\partial z}\right)_f = \left(\tilde{w} - \tilde{\sigma}\,\frac{\partial\bar{\tau}}{\partial z}\right)_f$$

The derivatives in equation (3.33) are decomposed using simple finite-differencing along the cells' faces. All facial values are taken as the average of the values on the two cells on either side of the face of interest.

In the three-dimensional case, $\tilde{\phi}$'s at both the inlet and outlet boundary cells are not included in the iterative process. Extrapolations are used to determine the inlet and outlet cells' values after each time-step.

$$\begin{aligned}\tilde{\phi}_{INLET} &= \tilde{\phi}_{IMIN,j,k} = 2\,\tilde{\phi}_{IMIN+1,j,k} - \tilde{\phi}_{IMIN+2,j,k} \\ \tilde{\phi}_{OUTLET} &= \tilde{\phi}_{IMAX,j,k} = 2\,\tilde{\phi}_{IMAX-1,j,k} - \tilde{\phi}_{IMAX-2,j,k}\end{aligned} \tag{3.34}$$

The wall boundary cells for the hypothetical cells' values along the front, back, top, and bottom wall surfaces are set by

$$\begin{aligned}\tilde{\phi}_{\text{front wall}} &= \tilde{\phi}_{i,JMIN-1,k} = \tilde{\phi}_{i,JMIN,k} \\ \tilde{\phi}_{\text{back wall}} &= \tilde{\phi}_{i,JMAX+1,k} = \tilde{\phi}_{i,JMAX,k} \\ \tilde{\phi}_{\text{top wall}} &= \tilde{\phi}_{i,j,KMAX+1} = \tilde{\phi}_{i,j,KMAX} \\ \tilde{\phi}_{\text{bottom wall}} &= \tilde{\phi}_{i,j,KMIN-1} = \tilde{\phi}_{i,j,KMIN}\,.\end{aligned} \tag{3.35}$$

The periodic boundary cells' values for the front and back boundaries are set by

$$\begin{aligned}\tilde{\phi}_{\text{front periodic}} &= \tilde{\phi}_{i,JMIN-1,k} = \tilde{\phi}_{i,JMAX,k} \\ \tilde{\phi}_{\text{back periodic}} &= \tilde{\phi}_{i,JMAX+1,k} = \tilde{\phi}_{i,JMIN,k}\,.\end{aligned} \tag{3.36}$$

In the two-dimensional case, $\tilde{\phi}$'s in the inlet and outlet boundary cells are not included in the iterative process. At each time-step, extrapolation is used to determine the values of $\tilde{\phi}$'s at these cells' locations.

$$\begin{aligned}\tilde{\phi}_{INLET} &= \tilde{\phi}_{IMIN,j} = 2\tilde{\phi}_{IMIN+1,j} - \tilde{\phi}_{IMIN+2,j} \\ \tilde{\phi}_{OUTLET} &= \tilde{\phi}_{IMAX,j} = 2\tilde{\phi}_{IMAX-1,j} - \tilde{\phi}_{IMAX-2,j}\end{aligned} \tag{3.37}$$

The hypothetical cell's values along the lower and upper wall surfaces are set by

$$\begin{aligned}\tilde{\phi}_{\text{lower wall}} &= \tilde{\phi}_{i,JMIN-1} = \tilde{\phi}_{i,JMIN} \\ \tilde{\phi}_{\text{upper wall}} &= \tilde{\phi}_{i,JMAX+1} = \tilde{\phi}_{i,JMAX}\end{aligned} \tag{3.38}$$

The periodic boundary cells are set by

$$\tilde{\phi}_{\text{lower periodic}} = \tilde{\phi}_{i,JMIN-1} = \tilde{\phi}_{i,JMAX}$$
$$\tilde{\phi}_{\text{upper periodic}} = \tilde{\phi}_{i,JMAX+1} = \tilde{\phi}_{i,JMIN} \tag{3.39}$$

Neumann boundary conditions for the appropriate cells' vertices are also obtained from equation (3.33). The last equation in equation (3.33) is discarded.

3.4 Disturbance Flowfield

The disturbance flowfield is utilized to visualize the propagation of the inlet vortical disturbances. The disturbance flow equation is obtained from equation (2.40). Decompose equation (2.40) into components in Cartesian coordinates.

$$\tilde{u} = \frac{\partial\tilde{\phi}}{\partial x} + \tilde{\sigma}\frac{\partial\bar{\tau}}{\partial x}; \qquad \tilde{v} = \frac{\partial\tilde{\phi}}{\partial y} + \tilde{\sigma}\frac{\partial\bar{\tau}}{\partial y}; \qquad \tilde{w} = \frac{\partial\tilde{\phi}}{\partial z} + \tilde{\sigma}\frac{\partial\bar{\tau}}{\partial z} \tag{3.40}$$

The derivatives in equation (3.40) are decomposed using generalized coordinates transformation [Anderson, Tannehill and Pletcher, 1984]. The formulations of these transformations in two and three dimensions are shown in Appendix III.

To insure that there is no net flux across wall surfaces, the disturbance velocity components must also be defined on hypothetical cells along wall surfaces. The procedures for determining these velocity components on the hypothetical cells are the same as for the steady velocity components. The formulations outlined in section (3.2.4.1) apply to both the two- and three-dimensional case. Note that in the three-dimensional case, the wall surfaces are still two-dimensional geometries.

3.5 Disturbance Vorticity

Disturbance vorticity fields are determined to enhance the understanding of vorticity convection through blade passages. The disturbance vorticity equation was derived in Chapter 2. Rewriting equation (2.28) in Cartesian components form, we obtain

$$\begin{aligned}
\tilde{\omega}_x &= \frac{\partial\tilde{\sigma}}{\partial y}\frac{\partial\bar{\tau}}{\partial z} - \frac{\partial\tilde{\sigma}}{\partial z}\frac{\partial\bar{\tau}}{\partial y} \\
\tilde{\omega}_z &= \frac{\partial\tilde{\sigma}}{\partial z}\frac{\partial\bar{\tau}}{\partial x} - \frac{\partial\tilde{\sigma}}{\partial x}\frac{\partial\bar{\tau}}{\partial z} \\
\tilde{\omega}_z &= \frac{\partial\tilde{\sigma}}{\partial x}\frac{\partial\bar{\tau}}{\partial y} - \frac{\partial\tilde{\sigma}}{\partial y}\frac{\partial\bar{\tau}}{\partial x}.
\end{aligned} \tag{3.41}$$

In the two-dimensional case, only the z-component of the disturbance vorticity is of interest. The derivatives involved in equation (3.41) are again decomposed using generalized coordinates transformation; refer to Appendix III.

3.6 Pressure Coefficients

The steady static pressure coefficient (in the absence of wakes) can be derived from the Bernouilli equation [Fox and McDonald, 1985]:

$$\bar{P}_\infty + \frac{1}{2}\rho_\infty\left(\bar{u}_\infty^2 + \bar{v}_\infty^2 + \bar{w}_\infty^2\right) = \bar{P} + \frac{1}{2}\rho\left(\bar{u}^2 + \bar{v}^2 + \bar{w}^2\right) \tag{3.42}$$

The steady static pressure coefficient is defined as

$$\bar{C}_p = \frac{\bar{P} - \bar{P}_\infty}{q_\infty}, \tag{3.43}$$

where

$$q_\infty = \frac{1}{2}\rho_\infty\left(\bar{u}_\infty^2 + \bar{v}_\infty^2 + \bar{w}_\infty^2\right). \tag{3.44}$$

Note that the density, ρ, is constant everywhere in the flowfield since the background flow is assumed incompressible. Equations (3.42) and (3.44) are substituted into equation (3.43); we obtain the equation for the steady static pressure coefficient:

$$\bar{C}_p = 1 - \frac{\bar{u}^2 + \bar{v}^2 + \bar{w}^2}{\bar{u}_\infty^2 + \bar{v}_\infty^2 + \bar{w}_\infty^2} \tag{3.45}$$

The unsteady static pressure coefficient can be derived using the unsteady Bernouilli equation:

$$\bar{P}_\infty + \frac{1}{2}\rho_\infty\left(\bar{u}_\infty^2 + \bar{v}_\infty^2 + \bar{w}_\infty^2\right) =$$
$$\bar{P} + \tilde{P} + \frac{1}{2}\rho\left[\left(\bar{u} + \tilde{u}\right)^2 + \left(\bar{v} + \tilde{v}\right)^2 + \left(\bar{w} + \tilde{w}\right)^2 + \frac{\partial\tilde{\phi}}{\partial t}\right] \tag{3.46}$$

Neglecting second-order terms, and rewriting equation (3.46) in the form of equation (3.43), we obtain

$$C_p = 1 - \frac{\left(\bar{u}^2 + \bar{v}^2 + \bar{w}^2\right) + 2\left(\bar{u}\tilde{u} + \bar{v}\tilde{v} + \bar{w}\tilde{w}\right) + \frac{\partial\tilde{\phi}}{\partial t}}{\bar{u}_\infty^2 + \bar{v}_\infty^2 + \bar{w}_\infty^2} \tag{3.47}$$

For the two-dimensional case, all the z-components of velocities are discarded in equations (3.45) and (3.47).

3.7 Numerical Procedures for Solving the Problem

The procedures leading to the computation of the disturbance flowfields, disturbance vorticity fields, and pressure coefficients are detailed in this section. The disturbance flowfields are determined from the following steps:

(1) Solve the first convective equation (2.32), $\frac{D\bar{\tau}}{Dt} = 1$, for the drift times, $\bar{\tau}$. This equation is solved only once for a given background flowfield. Time-stepping is applied until a steady solution is obtained. The drift times are convected by the background flow.

Then, at each time-step the following calculations are performed:

(2) Prescribe inlet moving wakes at the inflow boundary.

(3) Solve the second convective equation (2.33), $\frac{D\tilde{\sigma}}{Dt} = 0$, for the disturbance variable $\tilde{\sigma}$. This disturbance variable is convected by the background flow.

(4) Solve the Poisson equation (2.39), $\nabla^2\tilde{\phi} = -\nabla \bullet (\tilde{\sigma}\nabla\bar{\tau})$, for the disturbance velocity potential, $\tilde{\phi}$ using the values of $\tilde{\sigma}$ from (3) and $\bar{\tau}$ from (1).

(5) Solve the disturbance velocity equation (2.40), $\tilde{\vec{V}} = \nabla\tilde{\phi} + \tilde{\sigma}\nabla\bar{\tau}$, for the disturbance flowfields. All unknowns are already determined from steps (1), (3) and (4).

(6) Repeat steps (2) through (5) until a periodic solution for the disturbance flowfield is attained.

Disturbance vorticity fields are easily obtained using equation (2.34) and solutions from steps (1) and (3). Unsteady pressure coefficients on the blade surfaces are obtained using equation (3.47) and solutions from steps (4) and (5).

Chapter 4

Numerical Results

Numerical results for the two- and three-dimensional rectilinear blade passages will be presented here to illustrate the utility of the approach. Calculations based on the numerical schemes of Chapter 3 are carried out for inlet moving wakes interacting with the two- and three-dimensional rectilinear blade passages.

4.1 Two-Dimensional Blade Passage

For each Eppler blade passage, there are 90 by 59 grid nodes. This blade geometry is chosen because of the available steady flowfield which were provided by Valkov [1992]. Figure 9 shows the two-dimensional grid for the Eppler blade passages. The numerical computations are performed on a single blade passage with periodic boundaries that simulate the spatial periodicity of the blades. The computational grid is generated using a simple algebraic method.

The steady background flowfield used in the convection of ($\tilde{\sigma}$, $\bar{\tau}$) is shown in Figure 10. For a given steady background flow, the steady drift times, $\bar{\tau}$, are computed only once. Figure 11 shows the drift times through the two-dimensional blade passages. Drift times are necessary for computing the disturbance flow variables as noted in the theoretical formulations presented in Chapter 2. The sources of the oscillatory behavior in the drift times in the neighborhood of the blade trailing edges are as yet undetermined at this time.

Upon prescribing the inlet moving wakes, the disturbance flowfields, the disturbance vorticity contours, and the static pressure coefficients (from unsteady flow) on blade surfaces are computed for one full period, T_o, of simulation. Results are collected at every one-fifth of the period. One full period is defined as the time between the passage of two consecutive wakes.

The convection of inlet moving wakes through the blade passages are shown in Figures 12a to 12e. The figures show that the wakes are purely convected through the passages. In

addition, Figures 13a to 13e show that the vorticity in the wakes is also convected downstream. As the wakes convect downstream, the vorticiy in the wakes remains within the wake regions. The wakes are simply intercepted at the leading edges as they pass along the blades. These results agree qualitatively well with those obtained by Valkov [1992]. The diffusion of vorticity fields seen in Figures 13a to 13e is to be expected. The diffusion is due to the use of artificial smoothing in the convective solvers. In addition, the noises seen in the vorticity contours from three-quarter of blade chord to the outlet boundary may be attributed to the oscillatory behavior of the drift times seen in Figure 11.

The effects of the moving wakes on the static pressure distribution are shown in Figures 15a to 15e. The differences betweeen the steady (shown in Figure 14) and the unsteady static pressure coefficients are due to the presence of moving wakes along the blade surfaces.

However, the two-dimensional results show two problems. The first problem deals with overshoots of disturbance flowfields. In Figures 12a to 12e of the disturbance flowfields, the velocity vectors overshoot at the leading and trailing edges. The overshoots are most apparent near the trailing edges on Figures 12a and 12e. This behavior is also observed in Figures 15a to 15e of the unsteady static pressure coefficients. The overshoots near regions of trailing edges may be due to the Kutta condition not been satisfied exactly at the trailing edges. In this study, the Kutta condition is imposed by enforcing the pressures of the suction and pressure side at the trailing edge to be the same. At the leading edges, the reason is probably due the lack of grid resolution.

The second problem deals with the velocity vectors not been tangent to the blade surfaces, especially at leading edge. This problem is attributed to the use of first-order approximation in extrapolating computed flow variables from the centers of the cells along the blade surfaces to the cell nodes on the blade surfaces.

Besides these two problems, the two-dimensional numerical study has elucidated the use of Clebsch's tranformation for small unsteady disturbance flowfield.

4.2 Three-Dimensional Blade Passage

For each Eppler blade passage, there are 33 x 17 x 13 grid nodes. Figure 16 shows a cross-section of the grid in the x-y plane at any z location along the span. Similar to the two-dimensional case, the numerical computations are only performed through a single blade passage. Periodic boundaries are used to impose the spatial periodicity of the blade passages. The computational grid is first generated using a two-dimensional grid in the x-y plane. Then, the grids are extended from z=0 to z=1.

The three-dimensional steady background flowfield in the x-y plane is shown in Figure 10. In this study, the background flowfield does not have the z-component of velocity. Due to the two-dimensional flowfield and the use of flat endwalls at z=0 and z=1, any two-dimensional cut in the x-y plane is essentially a two-dimensional solution of a two-dimensional blade passage. The background flowfield is used for the convection of ($\tilde{\sigma}$, $\bar{\tau}$). The steady drift times (at any x-y plane) used in solving the disturbance flow variables are shown in Figure 17. No oscillatory behavior is observed in these drifts times. The discrepancy between these drift times for the coarse grid (in x-y plane) and those of the two-dimensional case (in high resolution grid) is odd and unexplainable at this time. One would expect a high resolution grid to yied better results than a coarse grid, but the solutions appear to show otherwise.

In this simulation, disturbance vorticity contours are only collected at every one-half of the period of simulation. To describe the convection of inlet moving wakes through the passages, the x-, y- and z-component of vorticity fields are computed. Figures 18a to 18e show the convection of the z-component of vorticity along the x-y plane at time T. These plots show the vorticity fields at every quarter of the span. At time T + 0.5To, the vorticity contours are shown in Figures 19a to 19e.

The convection of the y-component of vorticity is not shown in here because of their relative small value. The y-components are due to the spanwise linear variation of the inlet wakes. Since the spanwise variation is small (compared to the pitchwise variation), the values of vorticity are an order of magnitude smaller than those of the z-components.

The x-component of vorticity are not shown in here since their values are extremely small (it is two-order of magnitudes smaller than those of the z-components).

All these plots (Figures 18 and 19) show that vorticity is contained within the wake regions as the wakes convect downstream of the passages. In addition, these wakes are purely convected. These behaviors correspond to those obtained in the two-dimensional case. Furthermore, The diffusion of vorticity fields is more easily observed here than in the two-dimensional case. The use of extermely coarse grids have mainly led to excessive diffusion of vorticity. In addition, the use of artificial smoothing in the convective solvers has also contributed to some of the diffusion.

The effects of the moving wakes on the blade surfaces for every one-half of the period of simulation are shown in Figures 21 and 22. These plots show the unsteady static pressure coefficients at any location along the span of a blade. The differences between the unsteady and steady (Figures 20) static pressure coefficients are due the presence of moving wakes along the blade surfaces.

A time, T, of the simulation, the presence of all wakes on the pressure side of the blades are not seen in Figure 21. Only the wake located at the leading edge is seen on the plot. This is

A time, T, of the simulation, the presence of all wakes on the pressure side of the blades are not seen in Figure 21. Only the wake located at the leading edge is seen on the plot. This is due to the excessive diffusion of vorticity in the wakes along the pressure sides of the blades as the wakes convect downstream. However, at time T + 0.5To (Figure 22), all wakes are seen on both the pressure and suction side of the blades, because the diffusion of vorticity is not as severe here along the blade chord. The diffusion is due to the use of relatively coarse grids.

Note also that there is a sharp peak near the trailing edge on the plots of unsteady static pressure coefficients. Again, this peak may be associated with the fact that the Kutta condition is not satisfied exactly at the trailing edges.

In conclusion, the three-dimensional numerical study has demonstrated the use of the approach taken in this thesis.

Chapter 5

Summary

An approach based on the Clebsch's transformation of the inviscid flow equations is used to calculate the unsteady flowfield associated with the wake-stator interaction. In this application, the unsteady disturbance flow is assumed to be small compared to the steady background flow; this allowed the governing equations for the Clebsch's variables to be linearized about the steady mean flow. These linearized equations are spatially and temporally discretized using finite volume methods and four-stage Runge-Kutta time integration. Since these fully-discretized equations are of the convective and Poisson type equation, known numerical techniques can be applied to solve them. Computed results for the interaction of a stator blade with upstream moving wakes are presented to illustrate the use of the approach presented in this thesis.

Bibliography

Anderson D. A., Tannehill J. C. and Pletcher R. H., (1984). *Computational Fluid Mechanics and Heat Transfer*. Series in Computationa Methods in Mechanics and Thermal Sciences, Hemisphere Publishing Corporation.

Allmaras S. R., (1985). Embedded Mesh Solutions of the 2-D Euler Equation using a Cell-Centered Finite Volume Scheme. Master of Science thesis, Massachusetts Institute of Technology.

Chapra S. C and Canale R. P., (1988). *Numerical Methods For Engineers*. 2nd edition, McGraw-Hill, Inc.

Fletcher C. A. J., (1991). *Computational Techniques for Fluid Dynamics*.. 2nd edition, Springer-Verlarg.

Fox R. W. and McDonald A. T., (1985). *Introduction to Fluid Mechanics*. 3rd edition, John Wiley & Sons, Inc.

Giles M. B., (1987). Calculation of Unsteady Wake/Rotor Interaction. *Journal of Propulsion and Power*, Vol. 4, No. 4, July-August 1988.

Giles M. B., (1991). UNSFLOW: A Numerical Method for the Calculation of Unsteady Flow in Turbomachinery. *Gas Turbine Laboratory Report* No. 205, Massachusetts Institute of Technology.

Goldstein M. E., (1978). Unsteady Vortical and Entropic Distortions of Potential Flows Round Arbitrary Obstacles. *Journal of Fluid Mechanics*, Vol. 89(3), pp. 433-468.

Hall K. C., (1987). A Linearized Euler Analysis of Unsteady Flows in Turbomachinery. *Gas Turbine Report* No. 190. Massachusetts Institute of Technology.

Hall K. C., (1989). Gust Response Analysis for Cascades Operating in Nonuniform Mean Flows. Presented at the Gas Turbine Laboratory, Massachusetts Institute of Technology, December 12.

Hawthorne W. R., (1966). On the Theory of Shear Flow. *Gas Turbine Laboratory Report* No. 88, Massachusetts Institute of Technology.

Hawthorne W. R., (1967). The Applicability of Secondary Flow Analyses to the Solution of Internal Flow Problems. *Fluid Mechanics of Internal Flow*, pp. 239-269

Hawthorne W. R., (1977). Extension of Hawthorne-Clebsch Transformation to Unsteady Flows. Private Notes, September 9.

Hodson H. P., (1984). An Inviscid Blade-to-Blade Prediction of a Wake-Generated Unsteady Flow. ASME Paper 84-GT-43.

Jameson A., Schmidt, W. and Turkel, E., (1981). Numerical Solution of the Euler Equations by Finite Volume Methods Using Runge Kutta Time Stepping Schemes. AIAA 81-1259.

Kuethe A. M. and Chow C. Y., (1986). *Foundations of Aerodynamics*, 4th edition, John Wiley & Sons.

Lamb H., (1932). *Hydrodynamics*. 6th edition, Cambridge Universtiy Press.

Lighthill M. J., (1956). Drift, *Journal of Fluid Mechanics*, Vol. 1, pp. 31-53; note also Corrigenda to Drift. *Journal of Fluid Mechanics*, (1957), Vol. 2, pp. 311-312.

McFarland E. R., (1984). A Rapid Blade-To-Blade Solution for Use in Turbomachinery Design. ASME *Journal of Engineering for Gas Turbines and Power*, Vol. 106(2), pp. 376-382.

Rowe M., (1966). Some Secondary Flow Problems in Fluid Dynamics. Doctor of Philosophy Dissertation, University of Cambridge, England.

Tan C. S., (1991). Unsteady Three-Dimensional Flow in Marine Propellers. Presented at the Gas Turbine Laboratory, Massachusetts Institute of Technology, April 30.

Tan C. S., (1992). Clebsch's Transformation for Unsteady FLows. Private Notes.

Turkel E., Yaniv S. and Landau U., (1985). Accuracy of Schemes for the Euler Equations with Non-Uniform Meshes. NASA Contractor Report 85-59.

Valkov T. V., (1992). Control of the Unsteady Flow in a Stator Blade Row Interacting with Upstream Moving Wakes. Master of Science thesis, Massachusetts Institute of Technology.

Verdon J. M. and Hall K. C., (1990). Development of a Linearized Unsteady Aerodynamic Analysis for Cascade Gust Response Predictions. NASA Contractor Report 4308.

Appendix I

Finite Volume Discretization of the Two-Dimensional Problem

Appendix I-A

Convective Equation

The two-dimensional convective equation, derived in Chapter 2, in Cartesian coordinates is written for an arbitrary variable, Θ, as

$$\frac{\partial \Theta}{\partial t} + \bar{u}\frac{\partial \Theta}{\partial x} + \bar{v}\frac{\partial \Theta}{\partial y} = Q \qquad \text{(I.A.1)}$$

Rewriting equation (I.A.1) in the conservative form and using the conservation of mass, we obtain

$$\frac{\partial \Theta}{\partial t} + \frac{\partial F}{\partial x} + \frac{\partial G}{\partial y} = Q, \qquad \text{(I.A.2)}$$

$$F = \bar{u}\,\Theta \qquad\qquad G = \bar{v}\,\Theta . \qquad \text{(I.A.3)}$$

The convective equation is used to solve $\bar{\tau}$ and $\tilde{\sigma}$, with Q=1 and Q=0, respectively. Applying Green's theorem to equation (I.A.2) or integrating around a control volume [Fletcher, 1991], we obtain for each (i, j) location

$$\int_{ABCD} 1\left(\frac{\partial \Theta}{\partial t} + \frac{\partial F}{\partial x} + \frac{\partial G}{\partial y}\right) dx\, dy = \frac{Q}{\Omega_{ABCD}} \qquad \text{(I.A.4)}$$

An approximation to equation (I.A.4) is given by

$$\frac{d\Theta}{dt} + \frac{1}{\Omega_{ABCD}} \sum_{f=BT}^{LT} \left(F\,\Delta y - G\,\Delta x\right)_f = \frac{Q}{\Omega_{ABCD}} \qquad \text{(I.A.5)}$$

The computations of Δx, Δy and Ω are detailed in Appendix I-C.

Appendix I-B

Poisson Equation

The two-dimensional Poisson equation, derived in Chapter 2, in Cartesian coordinates is written as

$$\frac{\partial^2\tilde{\phi}}{\partial x^2} + \frac{\partial^2\tilde{\phi}}{\partial y^2} = -\left[\frac{\partial}{\partial x}\left(\tilde{\sigma}\frac{\partial\tilde{\tau}}{\partial x}\right) + \frac{\partial}{\partial y}\left(\tilde{\sigma}\frac{\partial\tilde{\tau}}{\partial y}\right)\right] \tag{I.B.1}$$

Integrating the LHS of equation (I.B.1) over the area of the cell ABCD [Fletcher, 1991],

$$\int_{ABCD} 1\left(\frac{\partial^2\tilde{\phi}}{\partial x^2} + \frac{\partial^2\tilde{\phi}}{\partial y^2}\right)dx\,dy = \int_{ABCD} \vec{H}\bullet\vec{n}\,ds \tag{I.B.2}$$

$$\vec{H}\bullet\vec{n}\,ds = \frac{\partial\tilde{\phi}}{\partial x}dy - \frac{\partial\tilde{\phi}}{\partial y}dx \tag{I.B.3}$$

Expanding equation (I.B.2) further using equation (I.B.3), we obtain

$$\begin{aligned}
&\left[\frac{\partial\tilde{\phi}}{\partial x}\right]_{i,j-\frac{1}{2}}\Delta y_{BT} - \left[\frac{\partial\tilde{\phi}}{\partial y}\right]_{i,j-\frac{1}{2}}\Delta x_{BT} \\
&+\left[\frac{\partial\tilde{\phi}}{\partial x}\right]_{i+\frac{1}{2},j}\Delta y_{RT} - \left[\frac{\partial\tilde{\phi}}{\partial y}\right]_{i+\frac{1}{2},j}\Delta x_{RT} \\
&+\left[\frac{\partial\tilde{\phi}}{\partial x}\right]_{i,j+\frac{1}{2}}\Delta y_{TP} - \left[\frac{\partial\tilde{\phi}}{\partial y}\right]_{i,j+\frac{1}{2}}\Delta x_{TP}
\end{aligned}$$

$$+\left[\frac{\partial\tilde{\phi}}{\partial x}\right]_{i-\frac{1}{2},j}\Delta y_{LT} - \left[\frac{\partial\tilde{\phi}}{\partial y}\right]_{i-\frac{1}{2},j}\Delta x_{LT} \qquad \text{(I.B.4)}$$

The derivatives in equations (I.B.4) are evaluated along the vertices of each cell. An hypothetical cell is used to enclose each vertex. The derivatives at each cell vertex are evaluated by integrating along the vertices of the hypothetical cell. For example, for the bottom cell vertex (referring to Figure 5 for notations),

$$\left(\frac{\partial\tilde{\phi}}{\partial x}\right)_{i,j-\frac{1}{2}} = \left(\frac{1}{\Omega_{A'B'C'D'}}\right)\iint\left(\frac{\partial\tilde{\phi}}{\partial x}\right)dx\,dy = \left(\frac{1}{\Omega_{A'B'C'D'}}\right)\int\tilde{\phi}\,dy,$$
$$\left(\frac{\partial\tilde{\phi}}{\partial y}\right)_{i,j-\frac{1}{2}} = \left(\frac{1}{\Omega_{A'B'C'D'}}\right)\iint\left(\frac{\partial\tilde{\phi}}{\partial y}\right)dx\,dy = -\left(\frac{1}{\Omega_{A'B'C'D'}}\right)\int\tilde{\phi}\,dx,$$

(I.B.5)

and

$$\int_{A'B'C'D'}\tilde{\phi}\,dy \approx \tilde{\phi}_{i,j-1}\Delta y_{BT}^{BT} + \tilde{\phi}_{B}\Delta y_{BT}^{RT} + \tilde{\phi}_{i,j}\Delta y_{BT}^{TP} + \tilde{\phi}_{A}\Delta y_{BT}^{LT}$$
$$\int_{A'B'C'D'}\tilde{\phi}\,dx \approx \tilde{\phi}_{i,j-1}\Delta x_{BT}^{BT} + \tilde{\phi}_{B}\Delta x_{BT}^{RT} + \tilde{\phi}_{i,j}\Delta x_{BT}^{TP} + \tilde{\phi}_{A}\Delta x_{BT}^{LT}$$

(I.B.6)

The computation of the geometrical data such as Δx, Δy, and Ω, are detailed in Appendix I-C. All the other derivatives in equations (I.B.4) are decomposed similarly at the remaining cell vertices.

The components of $\tilde{\phi}$ located on cell's nodes are decomposed using an averaging of the values in the four surrounding cells. There are four such nodal components for each cell. These components are

$$\tilde{\phi}_A = \frac{1}{4}\left(\tilde{\phi}_{i,j} + \tilde{\phi}_{i-1,j} + \tilde{\phi}_{i,j-1} + \tilde{\phi}_{i-1,j-1}\right)$$
$$\tilde{\phi}_B = \frac{1}{4}\left(\tilde{\phi}_{i,j} + \tilde{\phi}_{i+1,j} + \tilde{\phi}_{i,j-1} + \tilde{\phi}_{i+1,j-1}\right)$$
$$\tilde{\phi}_C = \frac{1}{4}\left(\tilde{\phi}_{i,j} + \tilde{\phi}_{i+1,j} + \tilde{\phi}_{i,j+1} + \tilde{\phi}_{i+1,j+1}\right)$$

$$\tilde{\phi}_D = \frac{1}{4}\left(\tilde{\phi}_{i,j} + \tilde{\phi}_{i-1,j} + \tilde{\phi}_{i,j+1} + \tilde{\phi}_{i-1,j+1}\right) \qquad \text{(I.B.7)}$$

By substituting equations (I.B.7) into equations (I.B.6) and collecting all terms with similar $\tilde{\phi}$'s, we obtain 9 types of $\tilde{\phi}$'s multiplied by some geometrical coefficients, $COEF_n$ (n=1 to 9), for each (i, j) location. These are:

(i+1, j-1)

$$COEF_1 = \frac{1}{4\,\Omega_{BT}}\left(\Delta y_{BT}\,\Delta y_{BT}^{RT} + \Delta x_{BT}\,\Delta x_{BT}^{RT}\right) + \frac{1}{4\,\Omega_{RT}}\left(\Delta y_{RT}\,\Delta y_{RT}^{BT} + \Delta x_{RT}\,\Delta x_{RT}^{BT}\right)$$

(i, j-1)

$$COEF_2 = \frac{1}{\Omega_{BT}}\left[\begin{array}{l}\Delta y_{BT}\left(\Delta y_{BT}^{BT} + \frac{1}{4}\Delta y_{RT}^{BT} + \frac{1}{4}\Delta y_{LT}^{BT}\right) + \\ \Delta x_{BT}\left(\Delta x_{BT}^{BT} + \frac{1}{4}\Delta x_{RT}^{BT} + \frac{1}{4}\Delta x_{LT}^{BT}\right)\end{array}\right] + \frac{1}{4\,\Omega_{RT}}\left(\Delta y_{RT}\,\Delta y_{RT}^{BT} + \Delta x_{RT}\,\Delta x_{RT}^{BT}\right) + \frac{1}{4\,\Omega_{LT}}\left(\Delta y_{LT}\,\Delta y_{LT}^{BT} + \Delta x_{LT}\,\Delta x_{LT}^{BT}\right)$$

(i-1, j-1)

$$COEF_3 = \frac{1}{4\,\Omega_{BT}}\left(\Delta y_{BT}\,\Delta y_{BT}^{LT} + \Delta x_{BT}\,\Delta x_{BT}^{LT}\right) + \frac{1}{4\,\Omega_{LT}}\left(\Delta y_{LT}\,\Delta y_{LT}^{BT} + \Delta x_{LT}\,\Delta x_{LT}^{BT}\right)$$

(i+1, j)

$$COEF_4 = \frac{1}{4\,\Omega_{BT}}\left(\Delta y_{BT}\,\Delta y_{BT}^{RT} + \Delta x_{BT}\,\Delta x_{BT}^{RT}\right) + \frac{1}{4\,\Omega_{TP}}\left(\Delta y_{TP}\,\Delta y_{TP}^{RT} + \Delta x_{TP}\,\Delta x_{TP}^{RT}\right) + \frac{\Delta y_{RT}}{\Omega_{RT}}\left(\frac{1}{4}\Delta y_{RT}^{BT} + \Delta y_{RT}^{RT} + \frac{1}{4}\Delta y_{RT}^{TP}\right) + \frac{\Delta x_{RT}}{\Omega_{RT}}\left(\frac{1}{4}\Delta x_{RT}^{BT} + \Delta x_{RT}^{RT} + \frac{1}{4}\Delta x_{RT}^{TP}\right)$$

(i,j)

$$COEF_5 = \frac{\Delta y_{BT}}{\Omega_{BT}}\left(\frac{1}{4}\Delta y_{BT}^{RT} + \Delta y_{BT}^{TP} + \frac{1}{4}\Delta y_{BT}^{LT}\right) +$$

$$\frac{\Delta x_{BT}}{\Omega_{BT}}\left(\frac{1}{4}\Delta x_{BT}^{RT} + \Delta x_{BT}^{TP} + \frac{1}{4}\Delta x_{BT}^{LT}\right) +$$

$$\frac{\Delta y_{RT}}{\Omega_{RT}}\left(\frac{1}{4}\Delta y_{RT}^{BT} + \frac{1}{4}\Delta y_{RT}^{TP} + \Delta y_{RT}^{LT}\right) + \frac{\Delta x_{RT}}{\Omega_{RT}}\left(\frac{1}{4}\Delta x_{RT}^{BT} + \frac{1}{4}\Delta x_{RT}^{TP} + \Delta x_{RT}^{LT}\right) +$$

$$\frac{\Delta y_{TP}}{\Omega_{TP}}\left(\Delta y_{TP}^{BT} + \frac{1}{4}\Delta y_{TP}^{RT} + \frac{1}{4}\Delta y_{TP}^{LT}\right) + \frac{\Delta x_{RT}}{\Omega_{TP}}\left(\Delta x_{TP}^{BT} + \frac{1}{4}\Delta x_{TP}^{RT} + \frac{1}{4}\Delta x_{TP}^{LT}\right) +$$

$$\frac{\Delta y_{LT}}{\Omega_{LT}}\left(\Delta y_{LT}^{BT} + \frac{1}{4}\Delta y_{LT}^{RT} + \frac{1}{4}\Delta y_{LT}^{TP}\right) + \frac{\Delta x_{RT}}{\Omega_{LT}}\left(\Delta x_{LT}^{BT} + \frac{1}{4}\Delta x_{LT}^{RT} + \frac{1}{4}\Delta x_{LT}^{TP}\right)$$

(i-1, j)

$$COEF_6 = \frac{1}{4\,\Omega_{BT}}\left(\Delta y_{BT}\,\Delta y_{BT}^{LT} + \Delta x_{BT}\,\Delta x_{BT}^{LT}\right) +$$

$$\frac{1}{4\,\Omega_{TP}}\left(\Delta y_{TP}\,\Delta y_{TP}^{LT} + \Delta x_{TP}\,\Delta x_{TP}^{LT}\right) +$$

$$\frac{\Delta y_{LT}}{4\,\Omega_{LT}}\left(\frac{1}{4}\Delta y_{LT}^{BT} + \frac{1}{4}\Delta y_{LT}^{TP} + \Delta y_{LT}^{LT}\right) + \frac{\Delta x_{LT}}{4\,\Omega_{LT}}\left(\frac{1}{4}\Delta x_{LT}^{BT} + \frac{1}{4}\Delta x_{LT}^{TP} + \Delta x_{LT}^{LT}\right)$$

(i+1, j+1)

$$COEF_7 = \frac{1}{4\,\Omega_{RT}}\left(\Delta y_{RT}\,\Delta y_{RT}^{TP} + \Delta x_{RT}\,\Delta x_{RT}^{TP}\right) +$$

$$\frac{1}{4\,\Omega_{TP}}\left(\Delta y_{TP}\,\Delta y_{TP}^{RT} + \Delta x_{TP}\,\Delta x_{TP}^{RT}\right)$$

(i, j+1)

$$COEF_8 = \frac{1}{4\,\Omega_{RT}}\left(\Delta y_{RT}\,\Delta y_{RT}^{TP} + \Delta x_{RT}\,\Delta x_{RT}^{TP}\right) +$$

$$\frac{1}{4\,\Omega_{LT}}\left(\Delta y_{LT}\,\Delta y_{LT}^{TP} + \Delta x_{LT}\,\Delta x_{LT}^{TP}\right) +$$

$$\frac{\Delta y_{TP}}{\Omega_{TP}}\left(\frac{1}{4}\Delta y_{TP}^{RT} + \Delta y_{TP}^{TP} + \frac{1}{4}\Delta y_{TP}^{LT}\right) + \frac{\Delta x_{TP}}{\Omega_{TP}}\left(\frac{1}{4}\Delta x_{TP}^{RT} + \Delta x_{TP}^{TP} + \frac{1}{4}\Delta x_{TP}^{LT}\right)$$

(i-1, j+1)

$$COEF_9 = \frac{1}{4\,\Omega_{TP}}\left(\Delta y_{TP}\,\Delta y_{TP}^{LT} + \Delta x_{TP}\,\Delta x_{TP}^{LT}\right) +$$

$$\frac{1}{4\,\Omega_{LT}}\left(\Delta y_{LT}\,\Delta y_{LT}^{TP} + \Delta x_{LT}\,\Delta x_{LT}^{TP}\right) \qquad \text{(I.B.8)}$$

Integrating the source terms on the RHS of equation (I.B.1) over the area of the cell ABCD, we obtain

$$\tilde{\sigma}_{AB}\left(\left[\frac{\partial\bar{\tau}}{\partial x}\right]_{i,j-\frac{1}{2}}\Delta y_{BT}-\left[\frac{\partial\bar{\tau}}{\partial y}\right]_{i,j-\frac{1}{2}}\Delta x_{BT}\right)$$
$$+\tilde{\sigma}_{BC}\left(\left[\frac{\partial\bar{\tau}}{\partial x}\right]_{i+\frac{1}{2},j}\Delta y_{RT}-\left[\frac{\partial\bar{\tau}}{\partial y}\right]_{i+\frac{1}{2},j}\Delta x_{RT}\right)$$
$$+\tilde{\sigma}_{CD}\left(\left[\frac{\partial\bar{\tau}}{\partial x}\right]_{i,j+\frac{1}{2}}\Delta y_{TP}-\left[\frac{\partial\bar{\tau}}{\partial y}\right]_{i,j+\frac{1}{2}}\Delta x_{TP}\right)$$
$$+\tilde{\sigma}_{DA}\left(\left[\frac{\partial\bar{\tau}}{\partial x}\right]_{i-\frac{1}{2},j}\Delta y_{LT}-\left[\frac{\partial\bar{\tau}}{\partial y}\right]_{i-\frac{1}{2},j}\Delta x_{LT}\right) \qquad \text{(I.B.9)}$$

The derivatives in equations (I.B.9) are decomposed similarly as equations (I.B.5). For example, consider the bottom cell vertex, we have

$$\left(\frac{\partial\bar{\tau}}{\partial x}\right)_{i,j-\frac{1}{2}}=\left(\frac{1}{\Omega_{A'B'C'D'}}\right)\iint\left(\frac{\partial\bar{\tau}}{\partial x}\right)dx\,dy=\left(\frac{1}{\Omega_{A'B'C'D'}}\right)\int\bar{\tau}\,dy\,,$$
$$\left(\frac{\partial\bar{\tau}}{\partial y}\right)_{i,j-\frac{1}{2}}=\left(\frac{1}{\Omega_{A'B'C'D'}}\right)\iint\left(\frac{\partial\bar{\tau}}{\partial y}\right)dx\,dy=-\left(\frac{1}{\Omega_{A'B'C'D'}}\right)\int\bar{\tau}\,dx\,, \qquad \text{(I.B.10)}$$

and

$$\int_{A'B'C'D'}\bar{\tau}\,dy\approx\bar{\tau}_{j,k-1}\Delta y_{BT}^{BT}+\bar{\tau}_{B}\Delta y_{BT}^{RT}+\bar{\tau}_{j,k}\Delta y_{BT}^{TP}+\bar{\tau}_{A}\Delta y_{BT}^{LT}$$
$$\int_{A'B'C'D'}\bar{\tau}\,dx\approx\bar{\tau}_{j,k-1}\Delta x_{BT}^{BT}+\bar{\tau}_{B}\Delta x_{BT}^{RT}+\bar{\tau}_{j,k}\Delta x_{BT}^{TP}+\bar{\tau}_{A}\Delta x_{BT}^{LT} \qquad \text{(I.B.11)}$$

Similar to equations (I.B.7), the components of $\bar{\tau}$ located on cell's nodes are decomposed using an averaging of 4 surrounding cells. The values of $\tilde{\sigma}$ located on the cell vertices are obtained from averaging the values of the two cells on either side of each vertex. These are:

$$\begin{aligned}
\tilde{\sigma}_{AB} &= \frac{1}{2}\left(\tilde{\sigma}_{i,j} + \tilde{\sigma}_{i,j-1}\right) \\
\tilde{\sigma}_{BC} &= \frac{1}{2}\left(\tilde{\sigma}_{i,j} + \tilde{\sigma}_{i+1,j}\right) \\
\tilde{\sigma}_{CD} &= \frac{1}{2}\left(\tilde{\sigma}_{i,j} + \tilde{\sigma}_{i,j+1}\right) \\
\tilde{\sigma}_{DA} &= \frac{1}{2}\left(\tilde{\sigma}_{i,j} + \tilde{\sigma}_{i-1,j}\right)
\end{aligned} \qquad \text{(I.B.12)}$$

Appendix I-C

Cell Metrics

I.C.1 Cell Vertices

Referring to Figure 2, the definitions of the subscripts or/and superscripts in the variables Δx, Δy, and Ω are as follow:

$$\begin{aligned} &BT = \text{BOTTOM VERTEX} = AB \\ &RT = \text{RIGHT VERTEX} = BC \\ &TP = \text{TOP VERTEX} = CD \\ &LT = \text{LEFT VERTEX} = DA \end{aligned} \tag{I.C.1}$$

When the variables Δx and Δy contain only a subscript, this subscript refers to the vertex of the cell in question. For example, the variables with subscript BT means that variable's value on the bottom vertex. When the variables contain one subscript and a superscript, this means that the subscript defines the vertex enclosed by an hypothetical cell, and the superscript defines the vertex of that hypothetical cell referred by the subscript.

The variable Ω containing only a subscript refers to the hypothetical area enclosing that specified cell vertex. For example, the variable with subscript BT means the hypothetical area enclosing the bottom vertex.

The hypothetical cell is defined by four nodes computed from two cells that shared the vertex of interest. For example, the hypothetical cell (A'B'C'D') enclosing the bottom vertex of the cell (ABCD) located at (i,j) have the following nodes location:

$$x_{A'} = \frac{1}{2}\left(\left[x_A\right]_{i,j-1} + \left[x_A\right]_{i,j}\right)$$
$$x_{B'} = \frac{1}{2}\left(\left[x_B\right]_{i,j-1} + \left[x_B\right]_{i,j}\right)$$

$$x_{C'} = \frac{1}{2}\left(\left[x_B\right]_{i,j} + \left[x_C\right]_{i,j}\right)$$
$$x_{D'} = \frac{1}{2}\left(\left[x_A\right]_{i,j} + \left[x_D\right]_{i,j}\right), \qquad \text{(I.C.2)}$$

and similarly for the y's variables and for the other remaining hypothetical cells enclosing the remaining vertices. Figure 3 shows the notations for the two-dimensional neighboring cells.

The variables Δx, and Δy , with subscripts, for each (i, j) location are defined in the counter-clockwise direction as

$$\begin{aligned} \Delta x_{BT} &= x_B - x_A & \Delta y_{BT} &= y_B - y_A \\ \Delta x_{RT} &= x_C - x_B & \Delta y_{RT} &= y_C - y_B \\ \Delta x_{TP} &= x_D - x_C & \Delta y_{TP} &= y_D - y_C \\ \Delta x_{LT} &= x_A - x_D & \Delta y_{LT} &= y_A - y_D. \end{aligned} \qquad \text{(I.C.3)}$$

The variables Δx, and Δy , with subscripts and superscripts, for each (i, j) location are defined for the bottom vertex as:

$$\begin{aligned} \Delta x_{BT}^{BT} &= x_{B'} - x_{A'} & \Delta y_{BT}^{BT} &= y_{B'} - y_{A'} \\ \Delta x_{BT}^{RT} &= x_{C'} - x_{B'} & \Delta y_{BT}^{RT} &= y_{C'} - y_{B'} \\ \Delta x_{BT}^{TP} &= x_{D'} - x_{C'} & \Delta y_{BT}^{TP} &= y_{D'} - y_{C'} \\ \Delta x_{BT}^{LT} &= x_{A'} - x_{D'} & \Delta y_{BT}^{LT} &= y_{A'} - y_{D'} \end{aligned} \qquad \text{(I.C.4)}$$

For other vertices, equations (I.C.2) must be redefined for each cell's vertex following the same procedure. Then, the subscripts in equations (I.C.4) are replaced by the appropriate cell vertex notation of interest (i.e. RT, TP and LT).

I.C.2 Cell Areas

The computation of each cell area at each (i, j) location is quite simple. For a general quadrilateral, the area can be computed form the vector products of the quadrilateral's diagonals [Fletcher, 1991] as

$$\Omega_{ABCD} = \frac{1}{2}\left|\vec{\chi}_{AC} + \vec{\chi}_{BD}\right|, \tag{I.C.5}$$

where

$$\begin{aligned} \vec{\chi}_{AC} &= \vec{\chi}_C - \vec{\chi}_A \\ \vec{\chi}_{BD} &= \vec{\chi}_D - \vec{\chi}_B \end{aligned} \tag{I.C.6}$$

and

$$\begin{aligned} \vec{\chi}_A &= x_A\hat{i} + y_A\hat{j} \qquad \vec{\chi}_B = x_B\hat{i} + y_B\hat{j} \\ \vec{\chi}_C &= x_C\hat{i} + y_C\hat{j} \qquad \vec{\chi}_D = x_D\hat{i} + y_D\hat{j} \end{aligned} \tag{I.C.7}$$

Then, we have

$$\Omega_{ABCD} = \frac{1}{2}\left[\left(x_C - x_A\right)\left(y_D - y_B\right) - \left(y_C - y_A\right)\left(x_D - x_B\right)\right] \tag{I.C.8}$$

which can be rewritten as

$$\Omega_{ABCD} = \left[\Delta x_{AC}\,\Delta y_{BD} - \Delta x_{BD}\,\Delta y_{AC}\right]. \tag{I.C.9}$$

The areas of the hypothetical cells enclosing the cell vertices are computed in the similar way; however, the x and y nodal values of the hypothetical cells must be defined as in equations (I.C.2).

Appendix II

Finite Volume Discretization of the Three-Dimensional Problem

Appendix II-A

Convective Equation

The three-dimensional convective equation, derived in Chapter 2, in Cartesian coordinates is written for an arbitrary variable, Θ, as

$$\frac{D\Theta}{Dt} = Q \tag{II.A.1}$$

$$\frac{D}{Dt} = \frac{\partial}{\partial t} + \bar{\vec{V}} \bullet \nabla \tag{II.A.2}$$

$$\frac{\partial \Theta}{\partial t} + \bar{u}\frac{\partial \Theta}{\partial x} + \bar{v}\frac{\partial \Theta}{\partial y} + \bar{w}\frac{\partial \Theta}{\partial z} = Q \tag{II.A.3}$$

Rewriting equation (II.A.3) in the conservative form and using the conversation of mass, we obtain

$$\frac{\partial \Theta}{\partial t} + \frac{\partial F}{\partial x} + \frac{\partial G}{\partial y} + \frac{\partial H}{\partial z} = Q \tag{II.A.4}$$

$$F = \bar{u}\Theta; \quad G = \bar{v}\Theta; \quad H = \bar{w}\Theta \tag{II.A.5}$$

The convective equation is used to solve $\bar{\tau}$ and $\tilde{\sigma}$, with Q=1 and Q=0, respectively. Applying Green's theorem to equation (II.A.4) or integrating around a control volume, we have for each (i,j,k) location:

$$\int_{CV} 1\left(\frac{\partial \Theta}{\partial t} + \frac{\partial F}{\partial x} + \frac{\partial G}{\partial y} + \frac{\partial H}{\partial z}\right) dx\, dy\, dz = \frac{Q}{V} \tag{II.A.6}$$

An approximation to equation (II.A.6) is:

$$\frac{d\Theta}{dt} + \frac{1}{V} \sum_{f=FT}^{TP} \left(F\, A_x + +G\, A_y + H\, A_z \right)_f = \frac{Q}{V} \qquad \text{(II.A.7)}$$

The computations of A_x, A_y, A_z and V at each (i, j, k) location are detailed in Appendix II-C.

Appendix II-B

Poisson Equation

The three-dimensional Poisson equation, derived in Chapter 2, is rewritten here in the expanded form using the Cartesian coordinates system as

$$\frac{\partial^2\tilde{\phi}}{\partial x^2} + \frac{\partial^2\tilde{\phi}}{\partial y^2} + \frac{\partial^2\tilde{\phi}}{\partial z^2} = -\left(\frac{\partial}{\partial x}\left(\tilde{\sigma}\,\frac{\partial\bar{\tau}}{\partial x}\right) + \frac{\partial}{\partial y}\left(\tilde{\sigma}\,\frac{\partial\bar{\tau}}{\partial y}\right) + \frac{\partial}{\partial z}\left(\tilde{\sigma}\,\frac{\partial\bar{\tau}}{\partial z}\right)\right) \tag{II.B.1}$$

The above equation is discretized using a three-dimensional control volume surrounding each computational node. A finite volume discretization is utilized to spatially discretize the equation. In finite volume form the LHS of the above equation is represented as:

$$\frac{1}{V}\int_{CV}\left(\frac{\partial^2\tilde{\phi}}{\partial x^2} + \frac{\partial^2\tilde{\phi}}{\partial y^2} + \frac{\partial^2\tilde{\phi}}{\partial z^2}\right) dV \tag{II.B.2a}$$

and the RHS is represented by:

$$-\int_{CV}\left(\frac{\partial}{\partial x}\left(\tilde{\sigma}\,\frac{\partial\bar{\tau}}{\partial x}\right) + \frac{\partial}{\partial y}\left(\tilde{\sigma}\,\frac{\partial\bar{\tau}}{\partial y}\right) + \frac{\partial}{\partial z}\left(\tilde{\sigma}\,\frac{\partial\bar{\tau}}{\partial z}\right)\right) dV \tag{II.B.2b}$$

Transforming the volume integral into an area integral along the control volume using Green's theorem, the LHS yields

$$\frac{1}{V}\sum_{f=FT}^{TP}\left(\frac{\partial\tilde{\phi}}{\partial x}A_x + \frac{\partial\tilde{\phi}}{\partial y}A_y + \frac{\partial\tilde{\phi}}{\partial z}A_z\right)_f , \tag{II.B.3a}$$

and the RHS yields

$$-\frac{1}{V}\sum_{f=FT}^{TP}\tilde{\sigma}_f\left(\frac{\partial\bar{\tau}}{\partial x}A_x+\frac{\partial\bar{\tau}}{\partial y}A_y+\frac{\partial\bar{\tau}}{\partial z}A_z\right)_f. \qquad \text{(II.B.3b)}$$

The derivatives on the LHS of equation (II.B.3a) are further decomposed. For each face, the derivatives are computed using an artificial volume enclosing that face. Consider the front face denoted by (f=FT), the derivatives are decomposed as:

$$\left(\frac{\partial\tilde{\phi}}{\partial x}\right)_f = \frac{1}{V_f}\oiint\tilde{\phi}\,dy\,dz$$

$$= \frac{1}{V_f}\left(\begin{matrix}\tilde{\phi}_{i,j-1,k}A_{f_x}^{FT}+\tilde{\phi}_{BC}A_{f_x}^{RT}+\tilde{\phi}_{i,j,k}A_{f_x}^{BK}+\\ \tilde{\phi}_{DA}A_{f_x}^{LT}+\tilde{\phi}_{AB}A_{f_x}^{BT}+\tilde{\phi}_{CD}A_{f_x}^{TP}\end{matrix}\right)$$

$$\left(\frac{\partial\tilde{\phi}}{\partial y}\right)_f = -\frac{1}{V_f}\oiint\tilde{\phi}\,dx\,dz$$

$$= -\frac{1}{V_f}\left(\begin{matrix}\tilde{\phi}_{i,j-1,k}A_{f_y}^{FT}+\tilde{\phi}_{BC}A_{f_y}^{RT}+\tilde{\phi}_{i,j,k}A_{f_y}^{BK}+\\ \tilde{\phi}_{DA}A_{f_y}^{LT}+\tilde{\phi}_{AB}A_{f_y}^{BT}+\tilde{\phi}_{CD}A_{f_y}^{TP}\end{matrix}\right)$$

$$\left(\frac{\partial\tilde{\phi}}{\partial z}\right)_f = -\frac{1}{V_f}\oiint\tilde{\phi}\,dx\,dy$$

$$= -\frac{1}{V_f}\left(\begin{matrix}\tilde{\phi}_{i,j-1,k}A_{f_z}^{FT}+\tilde{\phi}_{BC}A_{f_z}^{RT}+\tilde{\phi}_{i,j,k}A_{f_z}^{BK}+\\ \tilde{\phi}_{DA}A_{f_z}^{LT}+\tilde{\phi}_{AB}A_{f_z}^{BT}+\tilde{\phi}_{CD}A_{f_z}^{TP}\end{matrix}\right) \qquad \text{(II.B.4)}$$

For the remaining faces, the derivatives are decomposed in the similar fashion. The components of $\tilde{\phi}$ located on the cell vertices of the volume (there are a total of 12) are further decomposed using an averaging of the four cells surrounding each vertex. The first four components are:

$$\tilde{\phi}_{AB} = \frac{1}{4}\left(\tilde{\phi}_{i,j,k}+\tilde{\phi}_{i,j-1,k}+\tilde{\phi}_{i,j,k-1}+\tilde{\phi}_{i,j-1,k-1}\right)$$

$$\tilde{\phi}_{BC} = \frac{1}{4}\left(\tilde{\phi}_{i,j,k} + \tilde{\phi}_{i,j-1,k} + \tilde{\phi}_{i+1,j,k} + \tilde{\phi}_{i+1,j-1,k}\right)$$
$$\tilde{\phi}_{CD} = \frac{1}{4}\left(\tilde{\phi}_{i,j,k} + \tilde{\phi}_{i,j-1,k} + \tilde{\phi}_{i,j,k+1} + \tilde{\phi}_{i,j-1,k+1}\right)$$
$$\tilde{\phi}_{DA} = \frac{1}{4}\left(\tilde{\phi}_{i,j,k} + \tilde{\phi}_{i,j-1,k} + \tilde{\phi}_{i-1,j,k} + \tilde{\phi}_{i-1,j-1,k}\right) \qquad \text{(II.B.5)}$$

The remaining 8 components are decomposed in the similar fashion. The computations of cells' volumes and cell's face areas are detailed in Appendix II-C. Equations (II.B.5) are substituted into equations (II.B.4).

For each (i, j, k) location there are 18 neighboring cells influencing that location. The constant terms (a result of the spatial discretization) of 19 locations are reduced to the following:

(i,j-1,k-1)

$$COEF_1 = \frac{1}{4\,V_{FT}} \sum_{d=x,y,z}\left(A_{FT_d} A^{BT}_{FT_d}\right) + \frac{1}{4\,V_{BT}} \sum_{d=x,y,z}\left(A_{TP_d} A^{FT}_{BT_d}\right)$$

(i+1,j-1,k)

$$COEF_2 = \frac{1}{4\,V_{FT}} \sum_{d=x,y,z}\left(A_{FT_d} A^{RT}_{FT_d}\right) + \frac{1}{4\,V_{RT}} \sum_{d=x,y,z}\left(A_{RT_d} A^{TP}_{RT_d}\right)$$

(i,j-1,k+1)

$$COEF_3 = \frac{1}{4\,V_{FT}} \sum_{d=x,y,z}\left(A_{FT_d} A^{TP}_{FT_d}\right) + \frac{1}{4\,V_{TP}} \sum_{d=x,y,z}\left(A_{TP_d} A^{FT}_{TP_d}\right)$$

(i-1,j-1,k)

$$COEF_4 = \frac{1}{4\,V_{FT}} \sum_{d=x,y,z}\left(A_{FT_d} A^{LT}_{FT_d}\right) + \frac{1}{4\,V_{LT}} \sum_{d=x,y,z}\left(A_{LT_d} A^{FT}_{LT_d}\right)$$

(i,j-1,k)

$$COEF_5 = \frac{1}{V_{FT}} \sum_{d=x,y,z} A_{FT_d}\left(\begin{array}{l} A^{FT}_{FT_d} + \frac{1}{4} A^{RT}_{FT_d} + \frac{1}{4} A^{LT}_{FT_d} + \\ \frac{1}{4} A^{BT}_{FT_d} + \frac{1}{4} A^{TP}_{FT_d} \end{array}\right) +$$
$$\frac{1}{4\,V_{RT}} \sum_{d=x,y,z}\left(A_{RT_d} A^{FT}_{RT_d}\right) + \frac{1}{4\,V_{LT}} \sum_{d=x,y,z}\left(A_{LT_d} A^{FT}_{LT_d}\right) +$$

$$\frac{1}{4\,V_{BT}}\sum_{d=x,y,z}\left(A_{BT_d}A^{FT}_{BT_d}\right)+\frac{1}{4\,V_{TP}}\sum_{d=x,y,z}\left(A_{TP_d}A^{FT}_{TP_d}\right)$$

(i,j,k-1)

$$COEF_6=\frac{1}{V_{BT}}\sum_{d=x,y,z}A_{BT_d}\left(\begin{matrix}\frac{1}{4}A^{FT}_{BT_d}+\frac{1}{4}A^{RT}_{BT_d}+\frac{1}{4}A^{BK}_{BT_d}+\\ \frac{1}{4}A^{LT}_{BT_d}+A^{BT}_{BT_d}\end{matrix}\right)+$$
$$\frac{1}{4\,V_{FT}}\sum_{d=x,y,z}\left(A_{FT_d}A^{BT}_{FT_d}\right)+\frac{1}{4\,V_{RT}}\sum_{d=x,y,z}\left(A_{RT_d}A^{BT}_{RT_d}\right)+$$
$$\frac{1}{4\,V_{BK}}\sum_{d=x,y,z}\left(A_{BK_d}A^{BT}_{BK_d}\right)+\frac{1}{4\,V_{LT}}\sum_{d=x,y,z}\left(A_{LT_d}A^{BT}_{LT_d}\right)$$

(i+1,j,k-1)

$$COEF_7=\frac{1}{4\,V_{RT}}\sum_{d=x,y,z}\left(A_{RT_d}A^{BT}_{RT_d}\right)+\frac{1}{4\,V_{BT}}\sum_{d=x,y,z}\left(A_{BT_d}A^{RT}_{BT_d}\right)$$

(i+1,j,k)

$$COEF_8=\frac{1}{V_{RT}}\sum_{d=x,y,z}A_{RT_d}\left(\begin{matrix}\frac{1}{4}A^{FT}_{RT_d}+A^{RT}_{RT_d}+\frac{1}{4}A^{BK}_{RT_d}+\\ \frac{1}{4}A^{BT}_{RT_d}+\frac{1}{4}A^{TP}_{RT_d}\end{matrix}\right)+$$
$$\frac{1}{4\,V_{FT}}\sum_{d=x,y,z}\left(A_{FT_d}A^{RT}_{FT_d}\right)+\frac{1}{4\,V_{BK}}\sum_{d=x,y,z}\left(A_{BK_d}A^{RT}_{BK_d}\right)+$$
$$\frac{1}{4\,V_{BT}}\sum_{d=x,y,z}\left(A_{BT_d}A^{RT}_{BT_d}\right)+\frac{1}{4\,V_{TP}}\sum_{d=x,y,z}\left(A_{TP_d}A^{RT}_{TP_d}\right)$$

(i+1,j,k+1)

$$COEF_9=\frac{1}{4\,V_{RT}}\sum_{d=x,y,z}\left(A_{RT_d}A^{TP}_{RT_d}\right)+\frac{1}{4\,V_{TP}}\sum_{d=x,y,z}\left(A_{TP_d}A^{RT}_{TP_d}\right)$$

(i,j,k+1)

$$COEF_{10}=\frac{1}{V_{TP}}\sum_{d=x,y,z}A_{TP_d}\left(\begin{matrix}\frac{1}{4}A^{FT}_{TP_d}+\frac{1}{4}A^{RT}_{TP_d}+\frac{1}{4}A^{BK}_{TP_d}+\\ \frac{1}{4}A^{LT}_{TP_d}+A^{TP}_{TP_d}\end{matrix}\right)+$$

$$\frac{1}{4\,V_{FT}}\sum_{d=x,y,z}\left(A_{FT_d}A^{TP}_{FT_d}\right)+\frac{1}{4\,V_{RT}}\sum_{d=x,y,z}\left(A_{RT_d}A^{TP}_{RT_d}\right)+$$
$$\frac{1}{4\,V_{BK}}\sum_{d=x,y,z}\left(A_{BK_d}A^{TP}_{BK_d}\right)+\frac{1}{4\,V_{LT}}\sum_{d=x,y,z}\left(A_{LT_d}A^{TP}_{LT_d}\right)$$

(i-1,j,k+1)

$$COEF_{11}=\frac{1}{4\,V_{LT}}\sum_{d=x,y,z}\left(A_{LT_d}A^{TP}_{LT_d}\right)+\frac{1}{4\,V_{TP}}\sum_{d=x,y,z}\left(A_{TP_d}A^{LT}_{TP_d}\right)$$

(i-1,j,k)

$$COEF_{12}=\frac{1}{V_{LT}}\sum_{d=x,y,z}A_{LT_d}\left(\begin{array}{l}\frac{1}{4}A^{FT}_{LT_d}+\frac{1}{4}A^{BK}_{LT_d}+A^{LT}_{LT_d}+\\ \frac{1}{4}A^{BT}_{LT_d}+\frac{1}{4}A^{TP}_{LT_d}\end{array}\right)+$$
$$\frac{1}{4\,V_{FT}}\sum_{d=x,y,z}\left(A_{FT_d}A^{LT}_{FT_d}\right)+\frac{1}{4\,V_{BK}}\sum_{d=x,y,z}\left(A_{BK_d}A^{LT}_{BK_d}\right)+$$
$$\frac{1}{4\,V_{BT}}\sum_{d=x,y,z}\left(A_{BT_d}A^{LT}_{BT_d}\right)+\frac{1}{4\,V_{TP}}\sum_{d=x,y,z}\left(A_{TP_d}A^{LT}_{TP_d}\right)$$

(i-1,j,k-1)

$$COEF_{13}=\frac{1}{4\,V_{LT}}\sum_{d=x,y,z}\left(A_{LT_d}A^{BT}_{LT_d}\right)+\frac{1}{4\,V_{BT}}\sum_{d=x,y,z}\left(A_{BT_d}A^{LT}_{BT_d}\right)$$

(i,j,k)

$$COEF_{14}=$$
$$\frac{1}{V_{FT}}\sum_{d=x,y,z}A_{FT_d}\left(\frac{1}{4}A^{RT}_{FT_d}+A^{BK}_{FT_d}+\frac{1}{4}A^{LT}_{FT_d}+\frac{1}{4}A^{BT}_{FT_d}+\frac{1}{4}A^{TP}_{FT_d}\right)+$$
$$\frac{1}{V_{RT}}\sum_{d=x,y,z}A_{RT_d}\left(\frac{1}{4}A^{FT}_{RT_d}+\frac{1}{4}A^{BK}_{RT_d}+A^{LT}_{RT_d}+\frac{1}{4}A^{BT}_{RT_d}+\frac{1}{4}A^{TP}_{RT_d}\right)+$$
$$\frac{1}{V_{BK}}\sum_{d=x,y,z}A_{BK_d}\left(A^{FT}_{BK_d}+\frac{1}{4}A^{RT}_{BK_d}+\frac{1}{4}A^{LT}_{BK_d}+\frac{1}{4}A^{BT}_{BK_d}+\frac{1}{4}A^{TP}_{BK_d}\right)+$$
$$\frac{1}{V_{LT}}\sum_{d=x,y,z}A_{LT_d}\left(\frac{1}{4}A^{FT}_{LT_d}+A^{RT}_{LT_d}+\frac{1}{4}A^{BK}_{LT_d}+\frac{1}{4}A^{BT}_{LT_d}+\frac{1}{4}A^{TP}_{LT_d}\right)+$$
$$\frac{1}{V_{BT}}\sum_{d=x,y,z}A_{BT_d}\left(\frac{1}{4}A^{FT}_{BT_d}+\frac{1}{4}A^{RT}_{BT_d}+\frac{1}{4}A^{BK}_{BT_d}+\frac{1}{4}A^{LT}_{BT_d}+A^{TP}_{BT_d}\right)+$$

$$\frac{1}{V_{TP}} \sum_{d=x,y,z} A_{TP_d} \left(\frac{1}{4} A^{FT}_{TP_d} + \frac{1}{4} A^{RT}_{TP_d} + \frac{1}{4} A^{BK}_{TP_d} + \frac{1}{4} A^{LT}_{TP_d} + A^{BT}_{TP_d} \right)$$

(i,j+1,k-1)

$$COEF_{15} = \frac{1}{4\, V_{BK}} \sum_{d=x,y,z} \left(A_{BK_d} A^{BT}_{BK_d} \right) + \frac{1}{4\, V_{BT}} \sum_{d=x,y,z} \left(A_{BT_d} A^{BK}_{BT_d} \right)$$

(i+1,j+1,k)

$$COEF_{16} = \frac{1}{4\, V_{RT}} \sum_{d=x,y,z} \left(A_{RT_d} A^{BK}_{RT_d} \right) + \frac{1}{4\, V_{BK}} \sum_{d=x,y,z} \left(A_{BK_d} A^{RT}_{BK_d} \right)$$

(i,j+1,k+1)

$$COEF_{17} = \frac{1}{4\, V_{BK}} \sum_{d=x,y,z} \left(A_{BK_d} A^{TP}_{BK_d} \right) + \frac{1}{4\, V_{TP}} \sum_{d=x,y,z} \left(A_{TP_d} A^{BK}_{TP_d} \right)$$

(i-1,j+1,k)

$$COEF_{18} = \frac{1}{4\, V_{BK}} \sum_{d=x,y,z} \left(A_{BK_d} A^{LT}_{BK_d} \right) + \frac{1}{4\, V_{LT}} \sum_{d=x,y,z} \left(A_{LT_d} A^{BK}_{LT_d} \right)$$

(i,j+1,k)

$$COEF_{19} = \frac{1}{V_{BK}} \sum_{d=x,y,z} A_{BK_d} \left(\begin{array}{l} \frac{1}{4} A^{RT}_{BK_d} + A^{BK}_{BK_d} + \frac{1}{4} A^{LT}_{BK_d} + \\ \frac{1}{4} A^{BT}_{BK_d} + \frac{1}{4} A^{TP}_{BK_d} \end{array} \right) +$$
$$\frac{1}{4\, V_{RT}} \sum_{d=x,y,z} \left(A_{RT_d} A^{BK}_{RT_d} \right) + \frac{1}{4\, V_{LT}} \sum_{d=x,y,z} \left(A_{LT_d} A^{BK}_{LT_d} \right) +$$
$$\frac{1}{4\, V_{BT}} \sum_{d=x,y,z} \left(A_{BT_d} A^{BK}_{BT_d} \right) + \frac{1}{4\, V_{TP}} \sum_{d=x,y,z} \left(A_{TP_d} A^{BK}_{TP_d} \right)$$

(II.B.6)

The derivatives in equation (II.B.3b) are further decomposed similarly as in equation (II.B.3a) into the forms shown in equations (II.B.4). Consider the front face (f=FT) of a cell,

$$\left(\frac{\partial\bar{\tau}}{\partial x}\right)_f = \frac{1}{V_f}\oiint \bar{\tau}\, dy\, dz$$

$$= \frac{1}{V_f}\left(\begin{array}{l}\bar{\tau}_{i,j-1,k}A_{f_x}^{FT} + \bar{\tau}_{BC}A_{f_x}^{RT} + \bar{\tau}_{i,j,k}A_{f_x}^{BK} + \\ \bar{\tau}_{DA}A_{f_x}^{LT} + \bar{\tau}_{AB}A_{f_x}^{BT} + \bar{\tau}_{CD}A_{f_x}^{TP}\end{array}\right)$$

$$\left(\frac{\partial\bar{\tau}}{\partial y}\right)_f = -\frac{1}{V_f}\oiint \bar{\tau}\, dx\, dz$$

$$= -\frac{1}{V_f}\left(\begin{array}{l}\bar{\tau}_{i,j-1,k}A_{f_y}^{FT} + \bar{\tau}_{BC}A_{f_y}^{RT} + \bar{\tau}_{i,j,k}A_{f_y}^{BK} + \\ \bar{\tau}_{DA}A_{f_y}^{LT} + \bar{\tau}_{AB}A_{f_y}^{BT} + \bar{\tau}_{CD}A_{f_y}^{TP}\end{array}\right)$$

$$\left(\frac{\partial\bar{\tau}}{\partial z}\right)_f = -\frac{1}{V_f}\oiint \bar{\tau}\, dx\, dy$$

$$= -\frac{1}{V_f}\left(\begin{array}{l}\bar{\tau}_{i,j-1,k}A_{f_z}^{FT} + \bar{\tau}_{BC}A_{f_z}^{RT} + \bar{\tau}_{i,j,k}A_{f_z}^{BK} + \\ \bar{\tau}_{DA}A_{f_z}^{LT} + \bar{\tau}_{AB}A_{f_z}^{BT} + \bar{\tau}_{CD}A_{f_z}^{TP}\end{array}\right) \qquad \text{(II.B.7)}$$

Similar to equations (II.B.5), the components of $\bar{\tau}$ located on the cell vertices of the volume are also computed as averages of the four cells surrounding each vertex.

Appendix II-C

Cell Metrics

II.C.1 Face Areas

The definitions of subscripts and/or superscripts for the variables A (face area of volume) and V (volume) are as follow (referring to Figure 7 for the cell faces notations):

FT = FRONT FACE OF VOLUME = ABCD
RT = RIGHT FACE OF VOLUME = BFGC
BK = BACK FACE OF VOLUME = FEHG
LT = LEFT FACE OF VOLUME = EADH
BT = BOTTOM FACE OF VOLUME = AEFB
TP = TOP FACE OF VOLUME = CGHD (II.C.1)

The variable V with one subscript means the hypothetical volume enclosing the cell face specified by the subscript. For example, the variable with subscript BT means the hypothetical volume enclosing the bottom cell's face. The variable V with no subscripts and no supercripts means the volume enclosing the location (i, j, k) of interest.

The variable A with one subscript means the cell's face area of the face specified by the subscript. Note also that this variable has three components (x-,y-, and z-direction) for each cell's face. Each component is defined by a subscript below the subscript specifying the cell's face of interest. The variable A with one subscript and one superscript means that the subscript defines the cell's face enclosed by the hypothetical volume, and the superscript defines the hypothetical cell's face of interest. A subscript is also below the subscript of A that specifies the component of the area of interest.

An hypothetical cell volume is constructed using two volumes sharing the cell's face of interest. The 8 nodes of the hypothetical cell are each defined by an averaging of two nodes from the two original volumes.

For each cell's face we have three area projections in the x-, y-, and z-direction. The approximation for the cell's face areas are done using (consider the face ABCD)

$$\vec{\Omega}_{ABCD} = \frac{1}{2}\left|\vec{\chi}_{AC} \times \vec{\chi}_{BD}\right|, \tag{II.C.2}$$

where

$$\begin{aligned} \vec{\chi}_{AC} &= \vec{\chi}_C - \vec{\chi}_A \\ \vec{\chi}_{BD} &= \vec{\chi}_D - \vec{\chi}_B \end{aligned} \tag{II.C.3}$$

$$\begin{aligned} \vec{\chi}_A &= x_A\hat{i} + y_A\hat{j} + z_A\hat{k} \\ \vec{\chi}_B &= x_B\hat{i} + y_B\hat{j} + z_B\hat{k} \\ \vec{\chi}_C &= x_C\hat{i} + y_C\hat{j} + z_C\hat{k} \\ \vec{\chi}_D &= x_D\hat{i} + y_D\hat{j} + z_D\hat{k} \end{aligned} \tag{II.C.4}$$

After performing the cross product in equation (II.C.2) and assembling all terms of the same directional component, we obtain:

$$A_x = \frac{1}{2}\left[\begin{array}{l}\left(y_C z_D - z_C y_D\right) - \left(y_C z_B - z_C y_B\right) - \\ \left(y_A z_D - z_A y_D\right) + \left(y_A z_B - z_A y_B\right)\end{array}\right] \tag{II.C.5a}$$

$$A_y = \frac{1}{2}\left[\begin{array}{l}\left(z_C x_D - x_C z_D\right) - \left(z_C x_B - x_C z_B\right) - \\ \left(z_A x_D - x_A z_D\right) + \left(z_A x_B - x_A z_B\right)\end{array}\right] \tag{II.C.5b}$$

$$A_z = \frac{1}{2}\left[\begin{array}{l}\left(x_C y_D - y_C x_D\right) - \left(x_C y_B - y_C x_B\right) - \\ \left(x_A y_D - y_A x_D\right) + \left(x_A y_B - y_A x_B\right)\end{array}\right] \tag{II.C.5c}$$

II.C.2 Cell Volume

To compute the volume of an hexahedron, the hexahedron is decomposed twice into five tetrahedra: (1) four originating from cell node D and one form cell node F; (2) four originating

from cell node F and one from cell node D. The two volumes are averaged to determine the volume of an hexahedron [Fletcher, 1991]. Refer to Figure 7 for the cell nodes notations.

$$V_1 = V_{DABE} + V_{DBCG} + V_{DEGH} + V_{DBGE} + V_{FBEG} \quad \text{(II.C.6a)}$$

$$V_2 = V_{FACB} + V_{FAEH} + V_{FCHG} + V_{FAHC} + V_{DACH} \quad \text{(II.C.6b)}$$

$$V = \frac{1}{2}\left(V_1 + V_2\right) \quad \text{(II.C.7)}$$

Each of the components in equations (II.C.6a) and (II.C.6b) are computed as follow, for example, consider the term V_{FABC}:

$$V_{FABC} = \frac{1}{6}\vec{\chi}_{FA} \bullet \left(\vec{\chi}_{BC} \times \vec{\chi}_{CA}\right)$$

$$V_{FABC} = \frac{1}{6}\vec{\chi}_{FA} \bullet \vec{\Omega}_{ABC} \quad \text{(II.C.8)}$$

Decomposing equation (II.C.8) further, the volume a tetrahedron, FABC, becomes

$$\begin{aligned} V_{FABC} = {} & \frac{1}{6}\left(x_A - x_F\right)\left[\left(y_C - y_B\right)\left(z_A - z_C\right) - \left(z_C - z_B\right)\left(y_A - y_C\right)\right] \\ & + \frac{1}{6}\left(y_A - y_F\right)\left[\left(z_C - z_B\right)\left(x_A - x_C\right) - \left(x_C - x_B\right)\left(z_A - z_C\right)\right] \\ & + \frac{1}{6}\left(z_A - z_F\right)\left[\left(x_C - x_B\right)\left(y_A - y_C\right) - \left(y_C - y_B\right)\left(x_A - x_C\right)\right] \end{aligned} \quad \text{(II.C.9)}$$

The remaining nine volumes in equations (II.C.6a) and (II.C.6b) are defined in same way as outlined above.

Appendix III

Generalized Coordinates Transformation

The generalized coordinates transformation is taken from Anderson [1984], and it is summarized below.

III.A Two-Dimensional Transformation

The computational grid is transformed into a rectangular grid on which derivatives are computed. The derivatives are written in terms of the coordinates of the rectangular grid as:

$$\frac{\partial}{\partial x} = \xi_x \frac{\partial}{\partial \xi} + \eta_x \frac{\partial}{\partial \eta}; \qquad \frac{\partial}{\partial y} = \xi_y \frac{\partial}{\partial \xi} + \eta_y \frac{\partial}{\partial \eta} \tag{III.1}$$

where,

$$\xi_x = \frac{1}{J} y_\eta; \qquad \xi_y = -\frac{1}{J} x_\eta; \qquad \eta_x = -\frac{1}{J} y_\xi; \qquad \eta_y = \frac{1}{J} x_\xi \tag{III.2}$$

The equations (III.1) are then transformed back into the x-y coordinates system of the computational grid using equations (III.2). This yields

$$\frac{\partial}{\partial x} = \frac{1}{J}\left(y_\eta \frac{\partial}{\partial \xi} - y_\xi \frac{\partial}{\partial \eta}\right); \qquad \frac{\partial}{\partial y} = \frac{1}{J}\left(-x_\eta \frac{\partial}{\partial \xi} + x_\xi \frac{\partial}{\partial \eta}\right) \tag{III.3}$$

where,

$$x_\xi = \frac{x_{i,+1,j} - x_{i-1,j}}{2\,\Delta\xi}\,; \qquad x_\eta = \frac{x_{i,j+1} - x_{i,j-1}}{2\,\Delta\eta}$$
$$y_\xi = \frac{y_{i+1,j} - y_{i-1,j}}{2\,\Delta\xi}\,; \qquad y_\eta = \frac{y_{i,j+1} - y_{j,k-1}}{2\,\Delta\eta} \tag{III.4}$$

$$\Delta\xi = \frac{1}{\text{INODES} - 1}\,; \qquad \Delta\eta = \frac{1}{\text{JNODES} - 1} \tag{III.5}$$

The Jacobian is defined from

$$J = x_\xi\, y_\eta - y_\xi\, x_\eta \tag{III.6}$$

III.B Three-Dimensional Transformation

The computational domain is again transformed into a rectangular grid on which the derivatives are determined. The derivatives are written in terms of the coordinates of the rectangular grid as

$$\begin{aligned}
\frac{\partial}{\partial x} &= \xi_x \frac{\partial}{\partial \xi} + \eta_x \frac{\partial}{\partial \eta} + \zeta_x \frac{\partial}{\partial \zeta} \\
\frac{\partial}{\partial y} &= \xi_y \frac{\partial}{\partial \xi} + \eta_y \frac{\partial}{\partial \eta} + \zeta_y \frac{\partial}{\partial \zeta} \\
\frac{\partial}{\partial z} &= \xi_z \frac{\partial}{\partial \xi} + \eta_z \frac{\partial}{\partial \eta} + \zeta_z \frac{\partial}{\partial \zeta}\,,
\end{aligned} \tag{III.7}$$

where

$$\begin{aligned}
\xi_x &= J\left(y_\eta z_\zeta - y_\zeta z_\eta\right);\ \xi_y = -J\left(x_\eta z_\zeta - x_\zeta z_\eta\right);\ \xi_z = J\left(x_\eta y_\zeta - x_\zeta y_\eta\right) \\
\eta_x &= -J\left(y_\xi z_\zeta - y_\zeta z_\xi\right);\ \eta_y = J\left(x_\xi z_\zeta - x_\zeta z_\xi\right);\ \eta_z = -J\left(x_\xi y_\zeta - x_\zeta y_\xi\right) \\
\zeta_x &= J\left(y_\xi z_\eta - y_\eta z_\xi\right);\ \zeta_y = -J\left(x_\xi z_\eta - x_\eta z_\xi\right);\ \zeta_z = J\left(x_\xi y_\eta - x_\eta y_\xi\right).
\end{aligned} \tag{III.8}$$

Then, the results are transformed back into the x-y coordinates system of the computational grid by substituting equations (III.8) into equations (III.7), where

$$x_\xi = \frac{x_{i+1,j,k} - x_{i-1,j,k}}{\Delta\xi}$$
$$x_\eta = \frac{x_{i,j+1,k} - x_{i,j-1,k}}{\Delta\eta}$$
$$x_\zeta = \frac{x_{i,j,k+1} - x_{i,j,k-1}}{\Delta\zeta} \qquad \text{(III.9)}$$

and similarly for the derivatives $(y_\xi , y_\eta , y_\zeta)$ and $(z_\xi , z_\eta , z_\zeta)$. Futhermore, the Jacobian is determined from

$$J = \frac{1}{\left[x_\xi \left(y_\eta z_\zeta - y_\zeta z_\eta \right) - x_\eta \left(y_\xi z_\zeta - y_\zeta z_\xi \right) + x_\zeta \left(y_\xi z_\eta - y_\eta z_\xi \right) \right]}, \qquad \text{(III.10)}$$

In equations (III.9), use

$$\Delta\xi = \frac{1}{\text{INODES} - 1}; \qquad \Delta\eta = \frac{1}{\text{JNODES} - 1}; \qquad \Delta\zeta = \frac{1}{\text{KNODES} - 1}. \qquad \text{(III.11)}$$

Figures

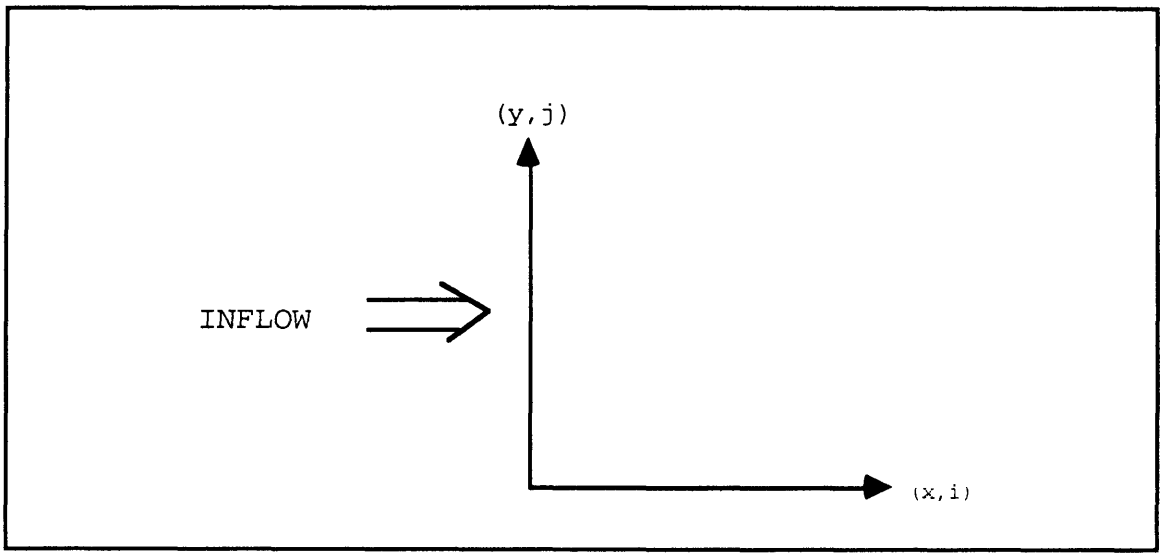

Figure 1: Two-dimensional axis-coordinates

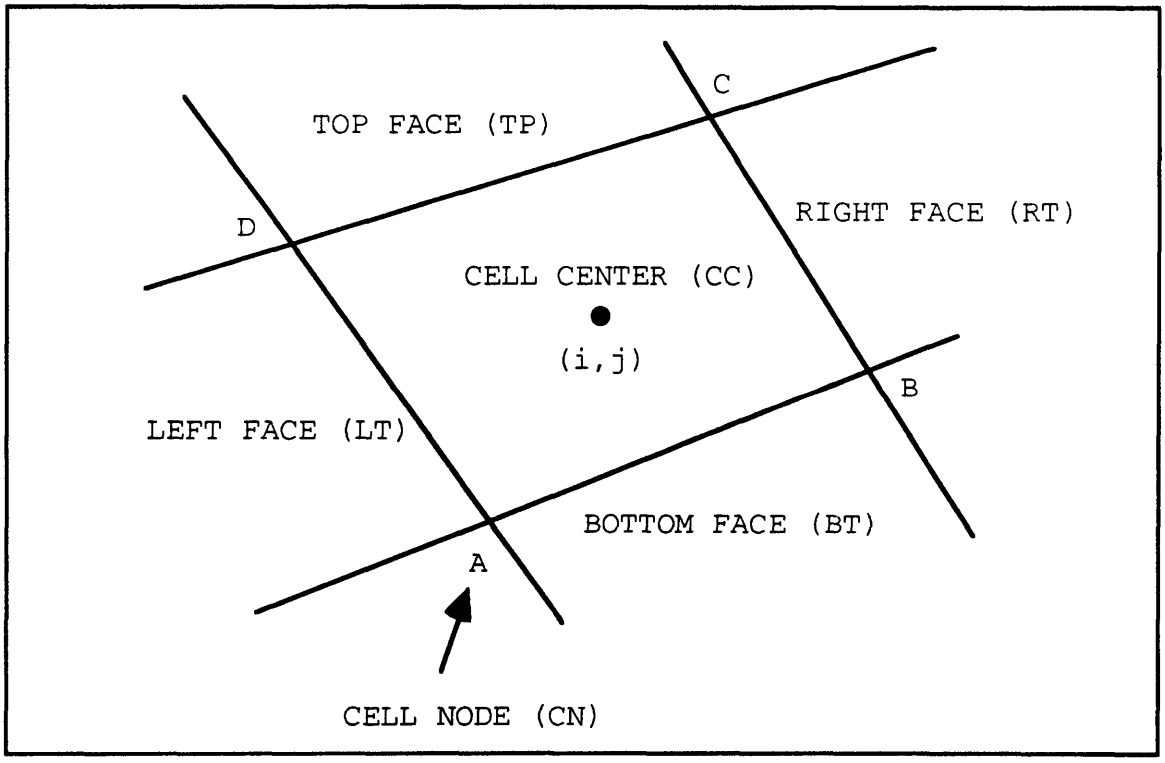

Figure 2: Two-dimensional cell notation

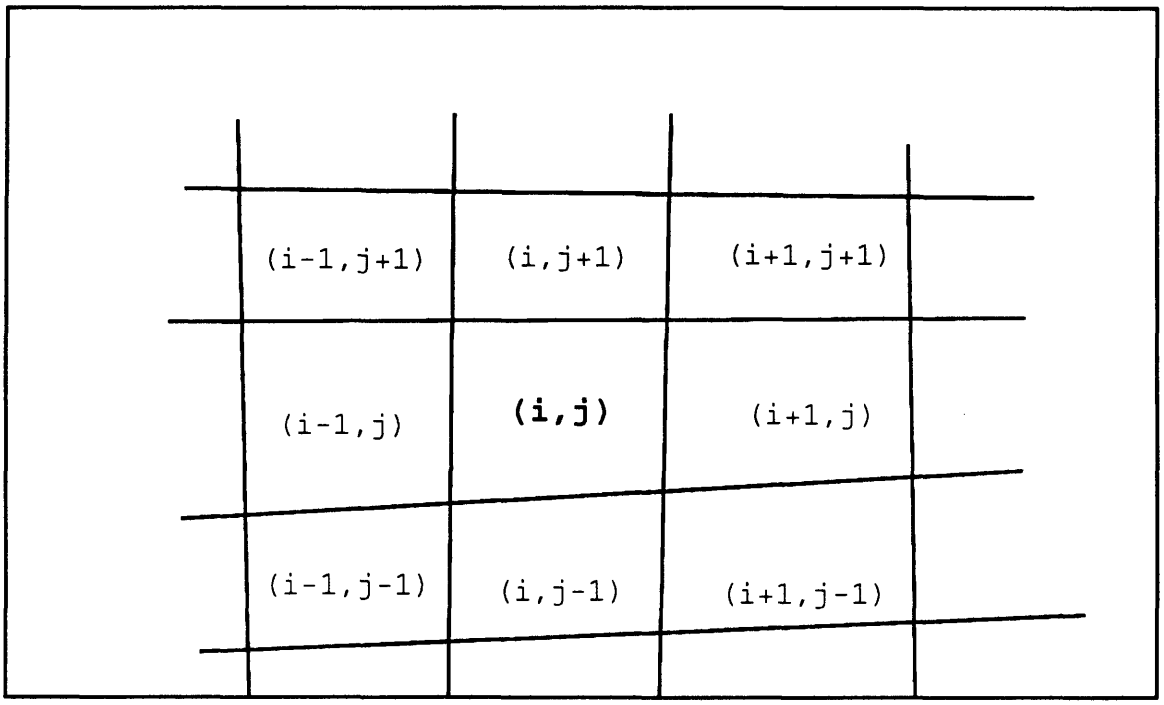

Figure 3: Two-dimensional neighboring cells notation

(SPACE LEFT BLANK)

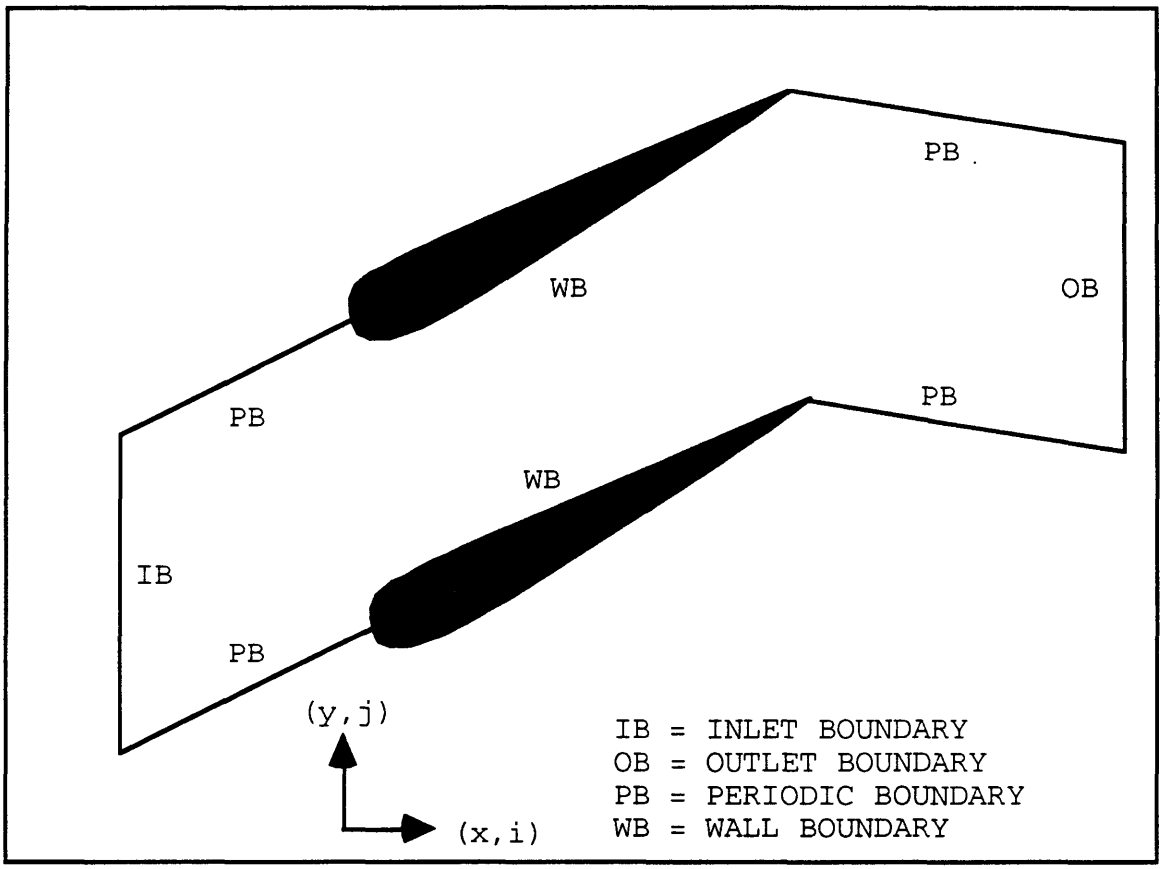

Figure 4: Two-dimensional computational boundaries

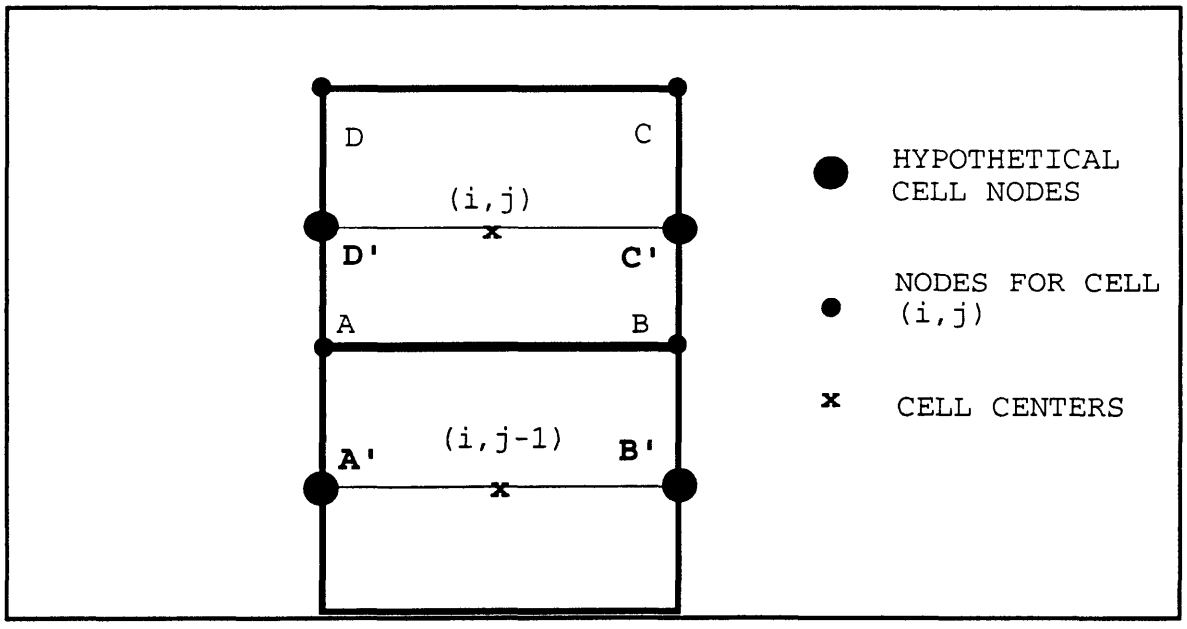

Figure 5: Defintion of a two-dimensional hypothetical cell

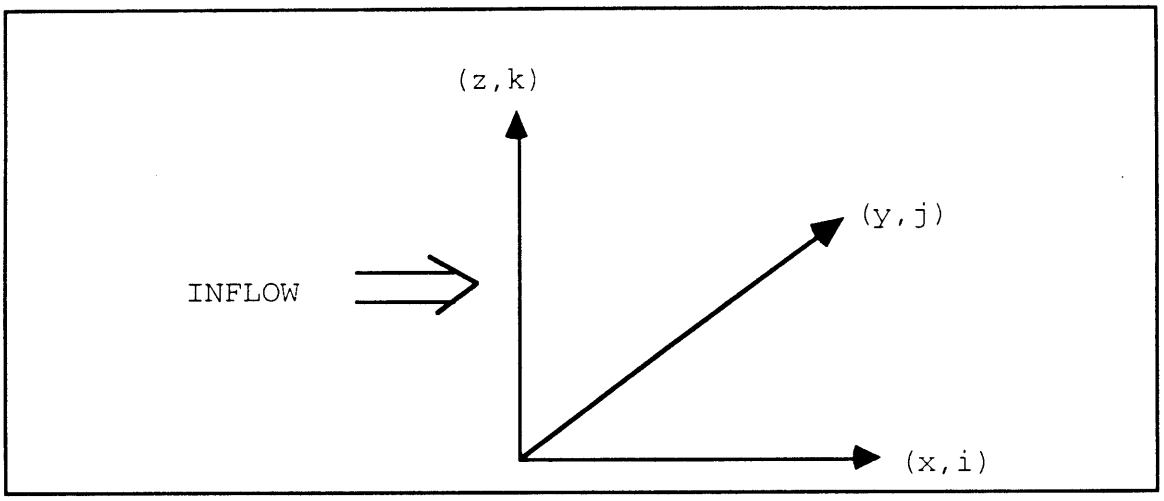

Figure 6: Three-dimensional axis-coordinates

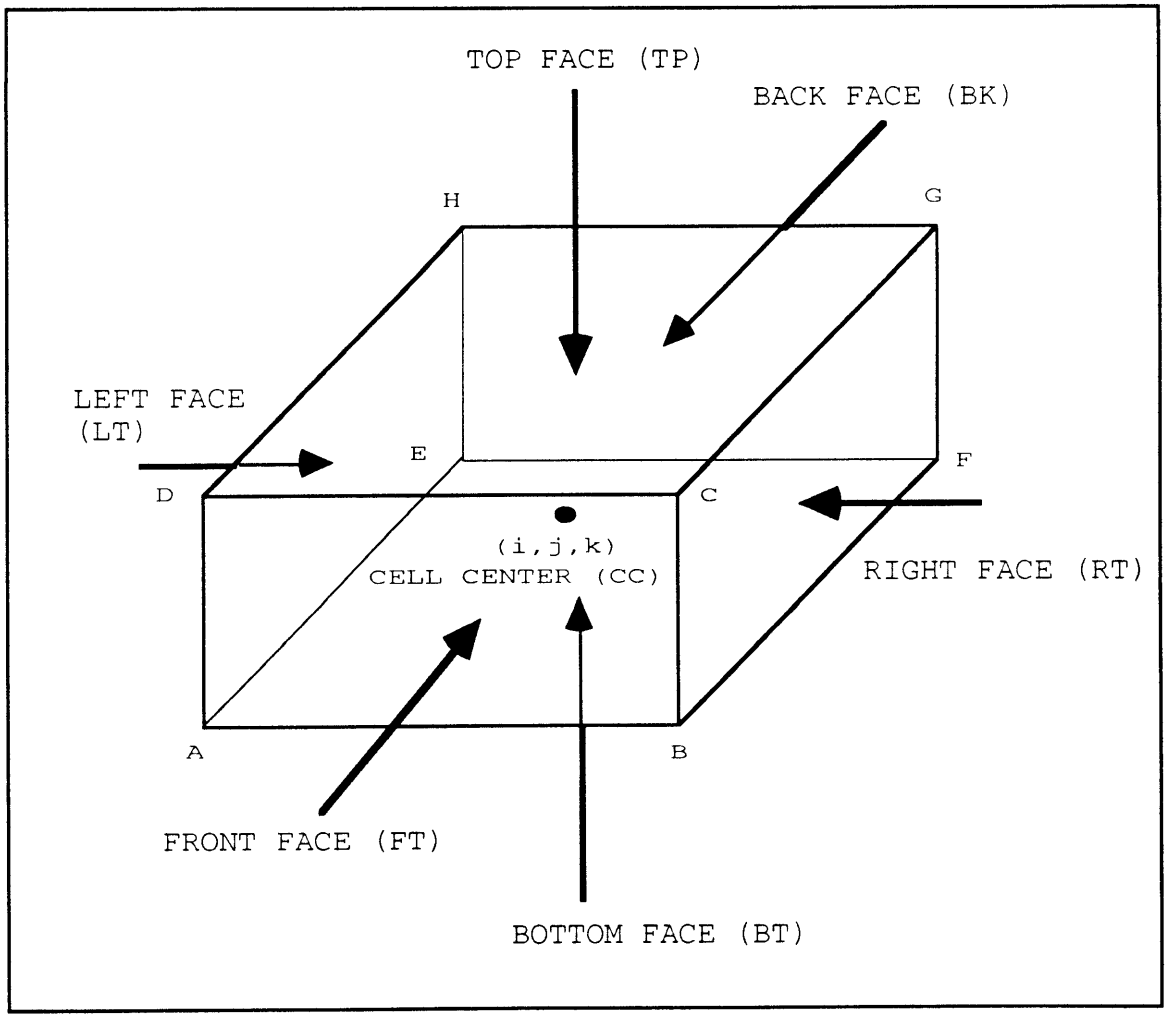

Figure 7: Three-dimensional cell notation

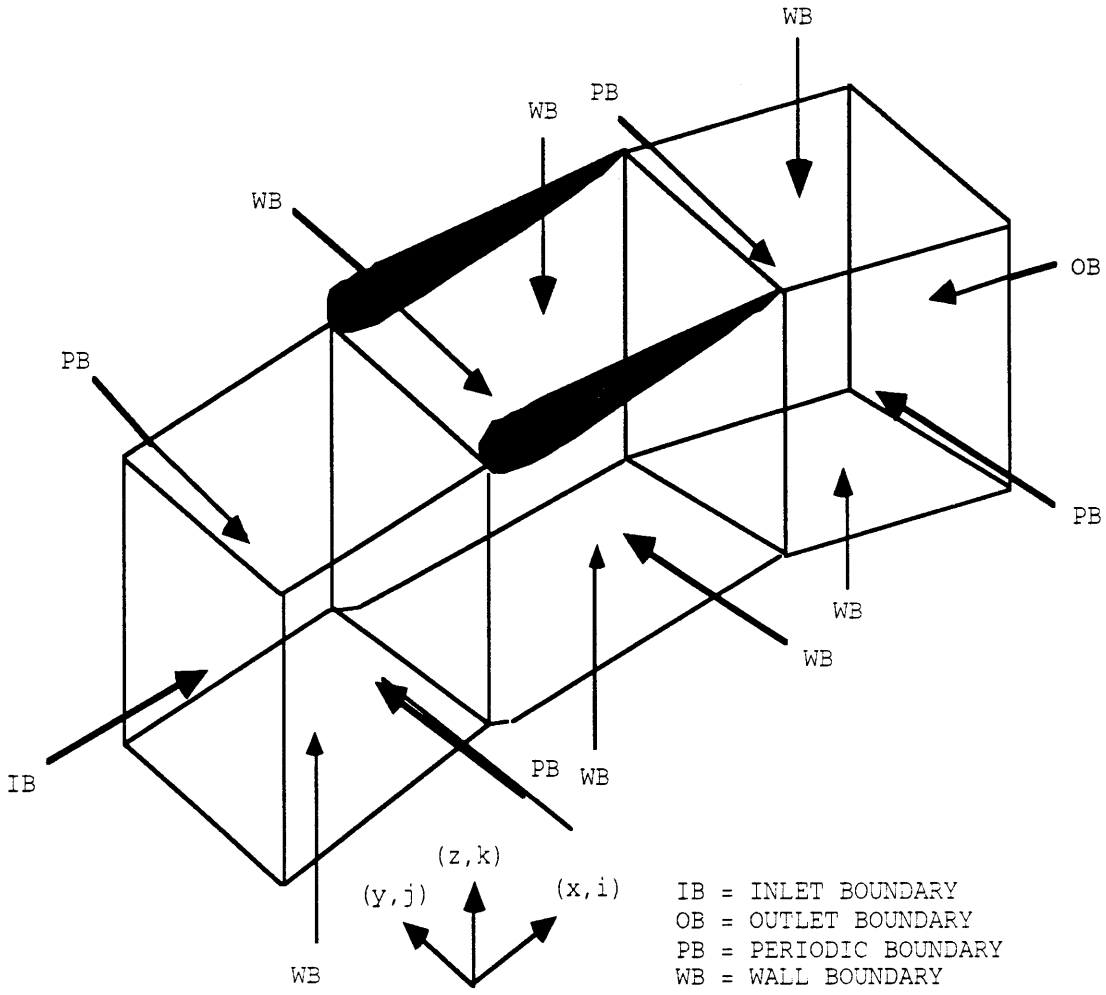
WB
PB
WB
WB
OB
PB
PB
WB
WB
IB
PB
WB
(z,k)
(y,j)
(x,i)
WB
IB = INLET BOUNDARY
OB = OUTLET BOUNDARY
PB = PERIODIC BOUNDARY
WB = WALL BOUNDARY

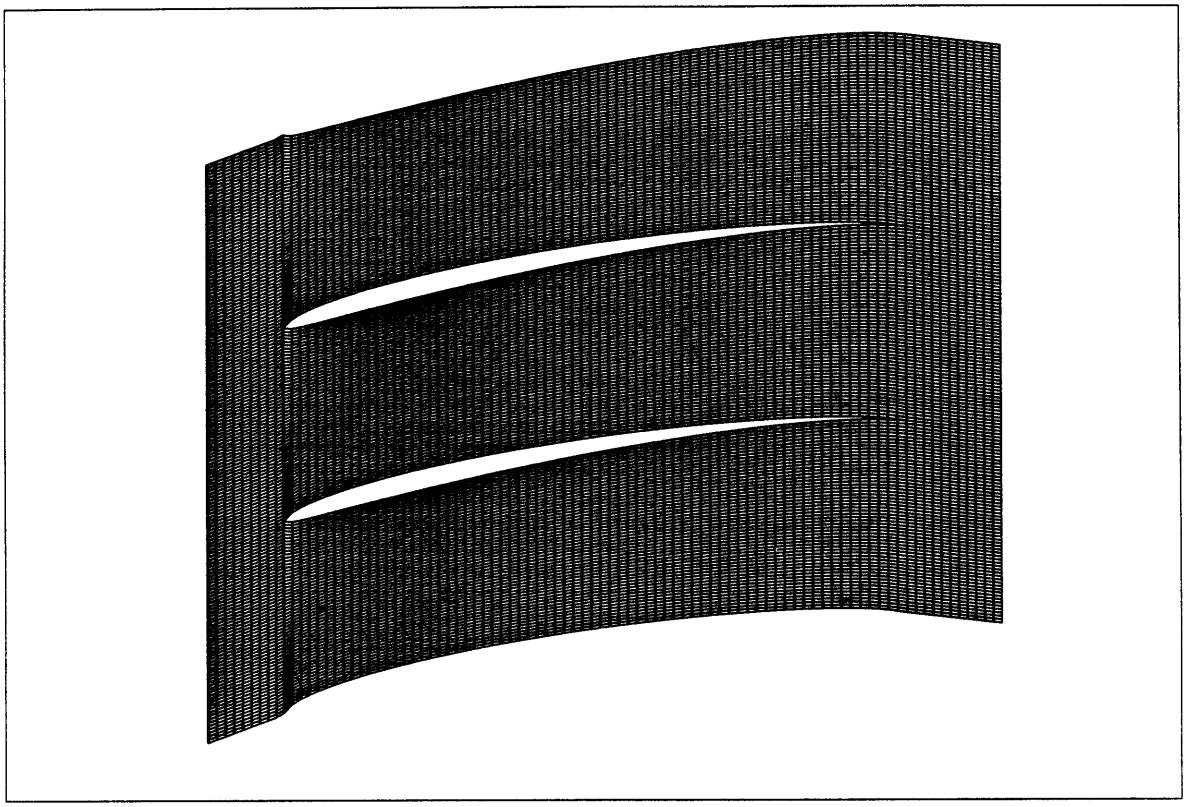

Figure 9: Eppler blade passages

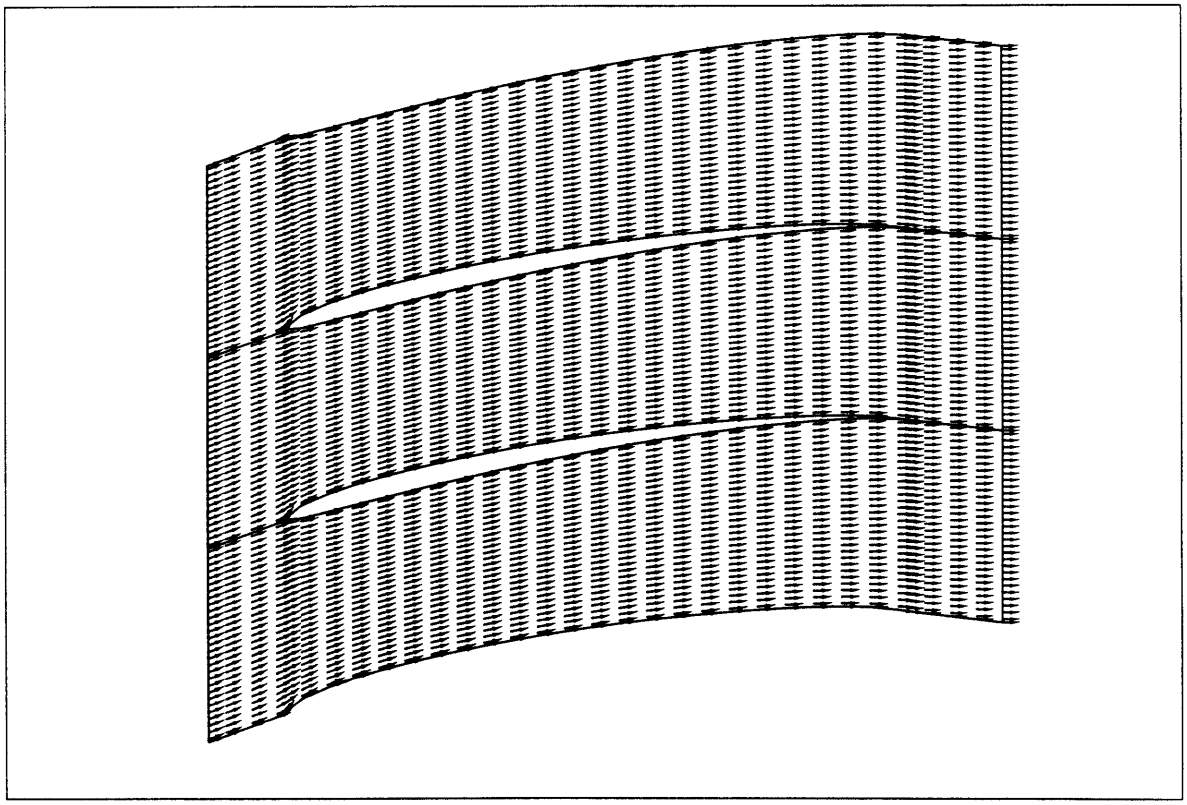

Figure 10: Steady background flowfield

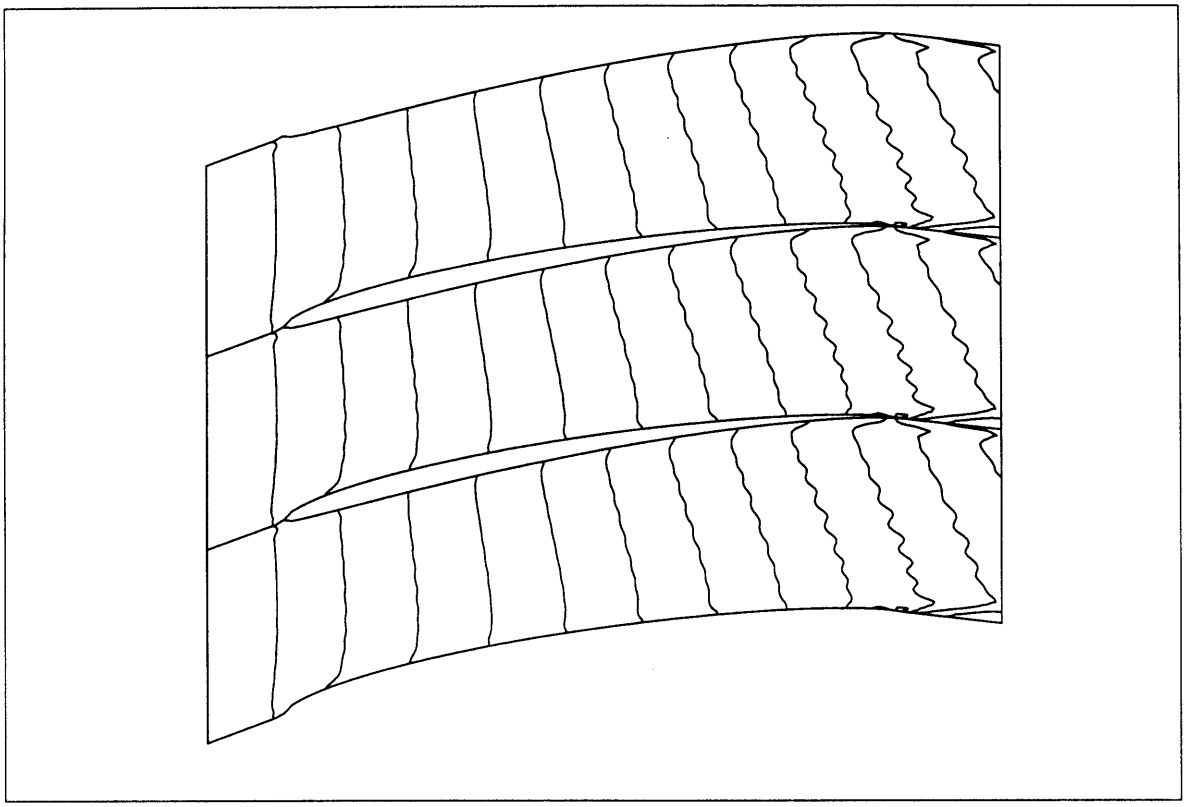

Figure 11: Drift times based on steady background flowfield

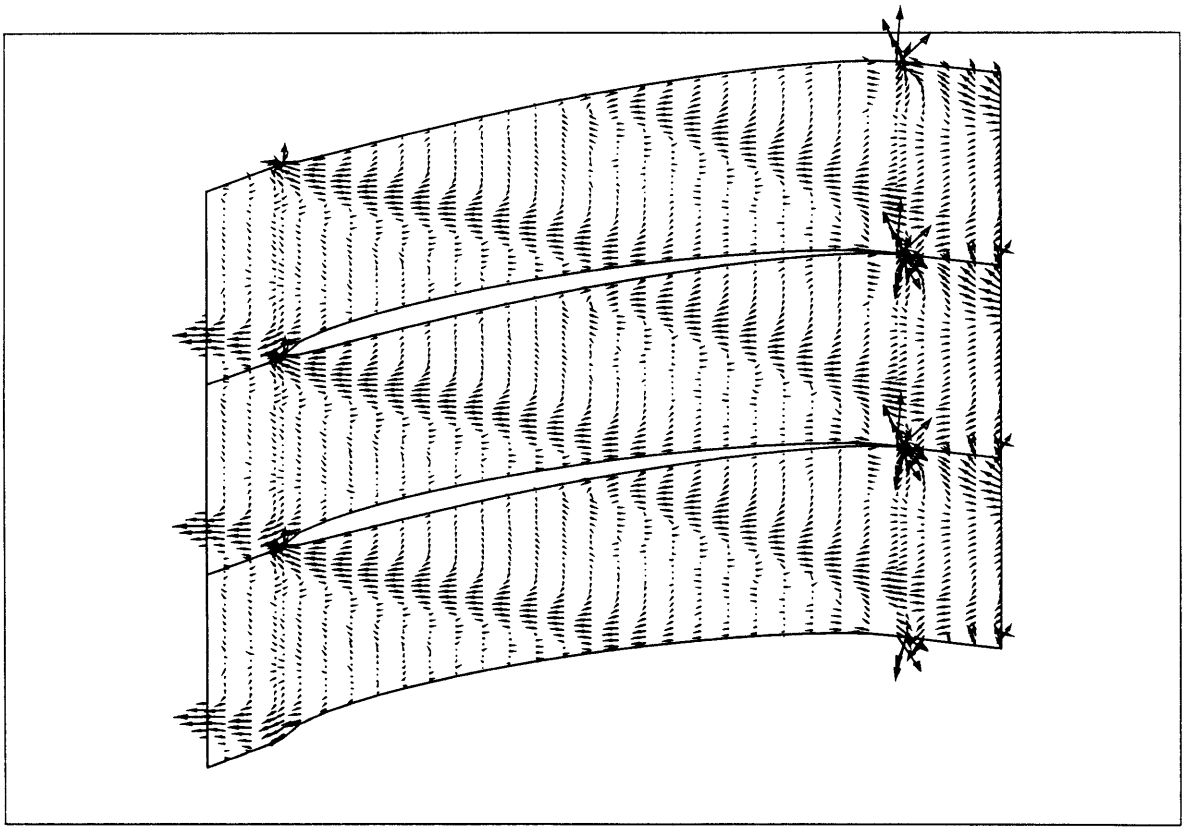

Figure 12a: Disturbance velocity vectors at time t

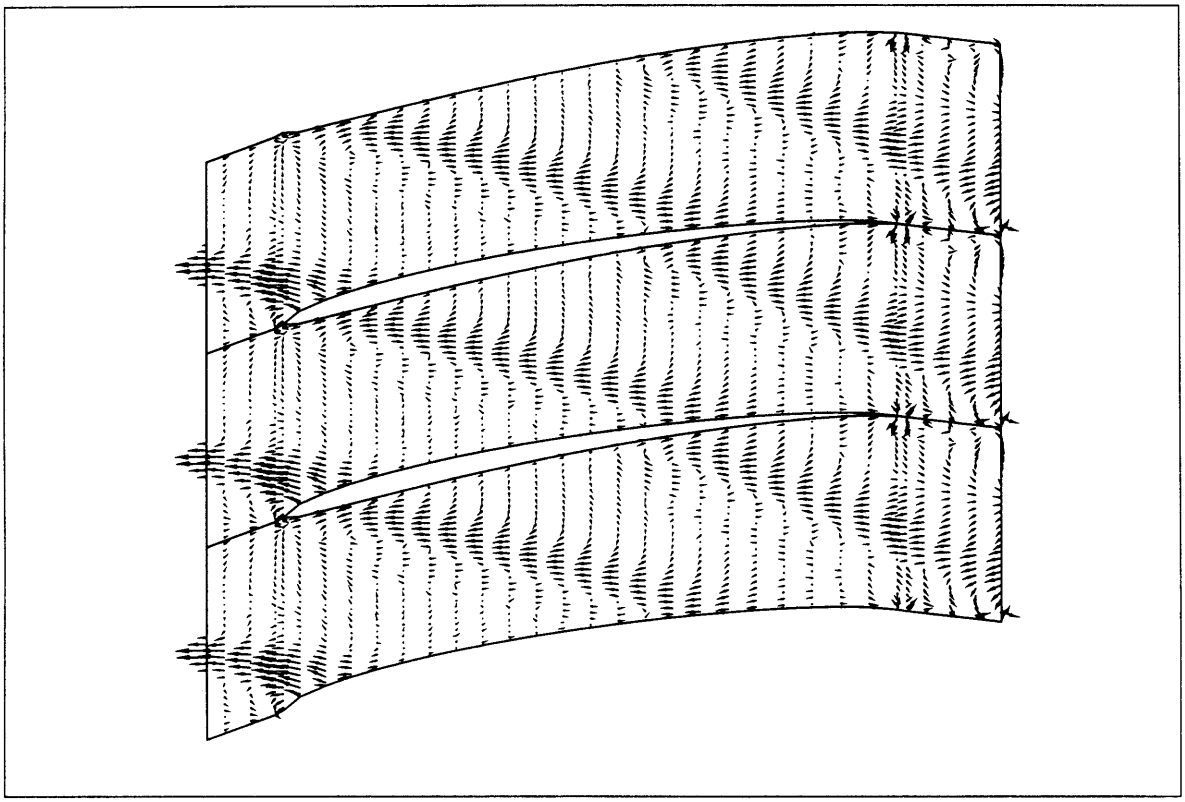

Figure 12b: Disturbance velocity vectors at time T + 0.2To

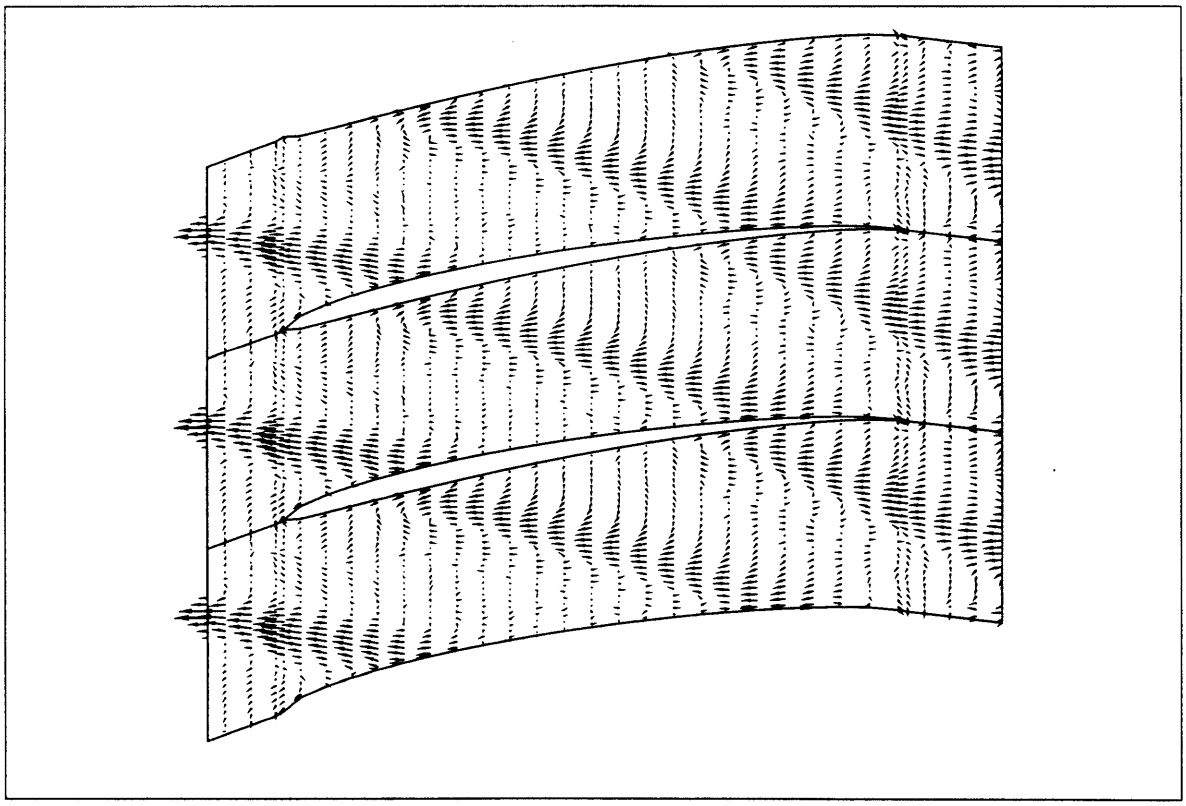

Figure 12c: Disturbance velocity vectors at time T + 0.4To

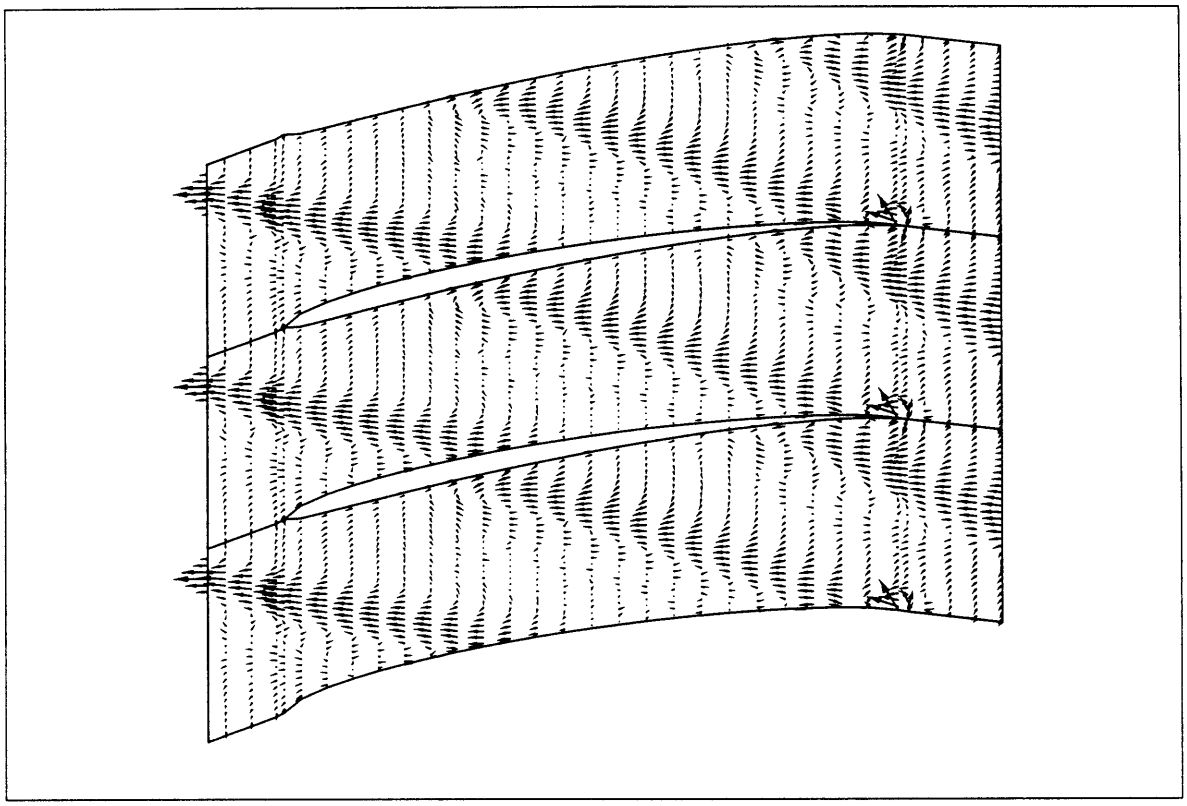

Figure 12d: Disturbance velocity vectors at time T + 0.6To

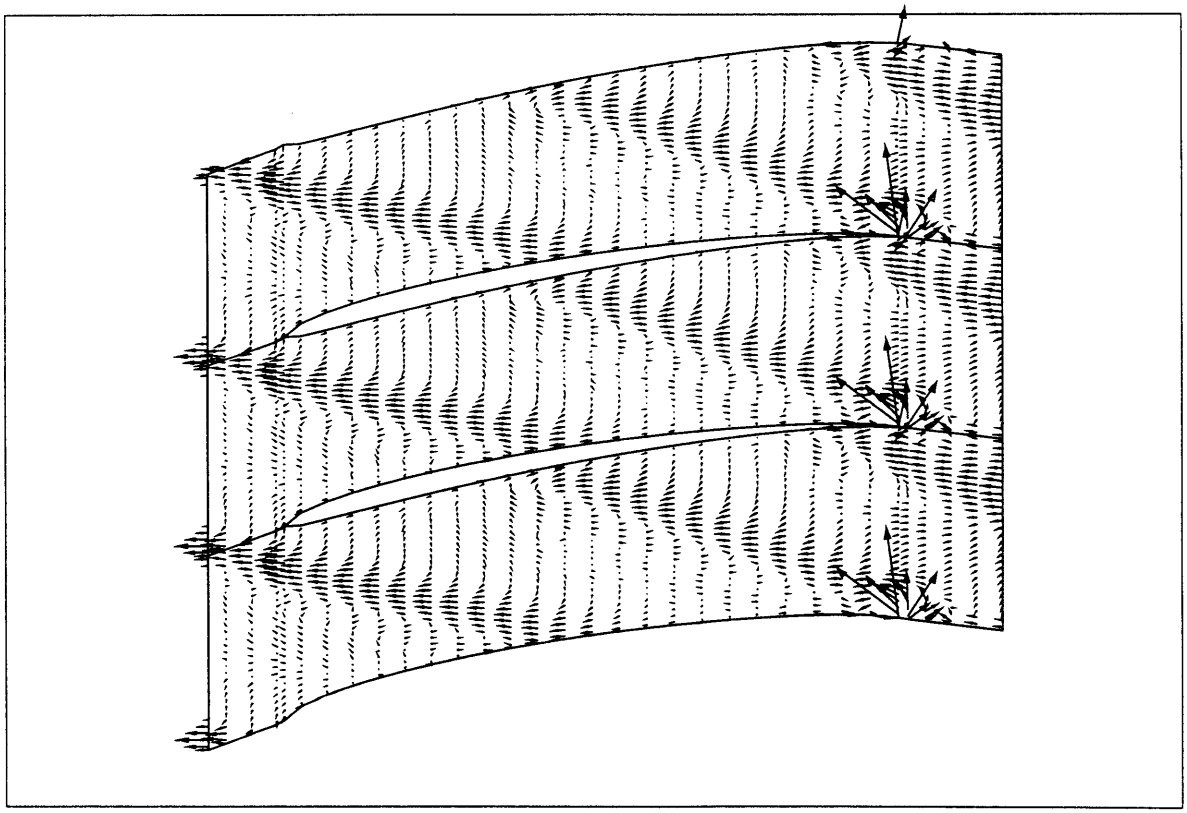

Figure 12e: Disturbance velocity vectors at time T + 0.8To

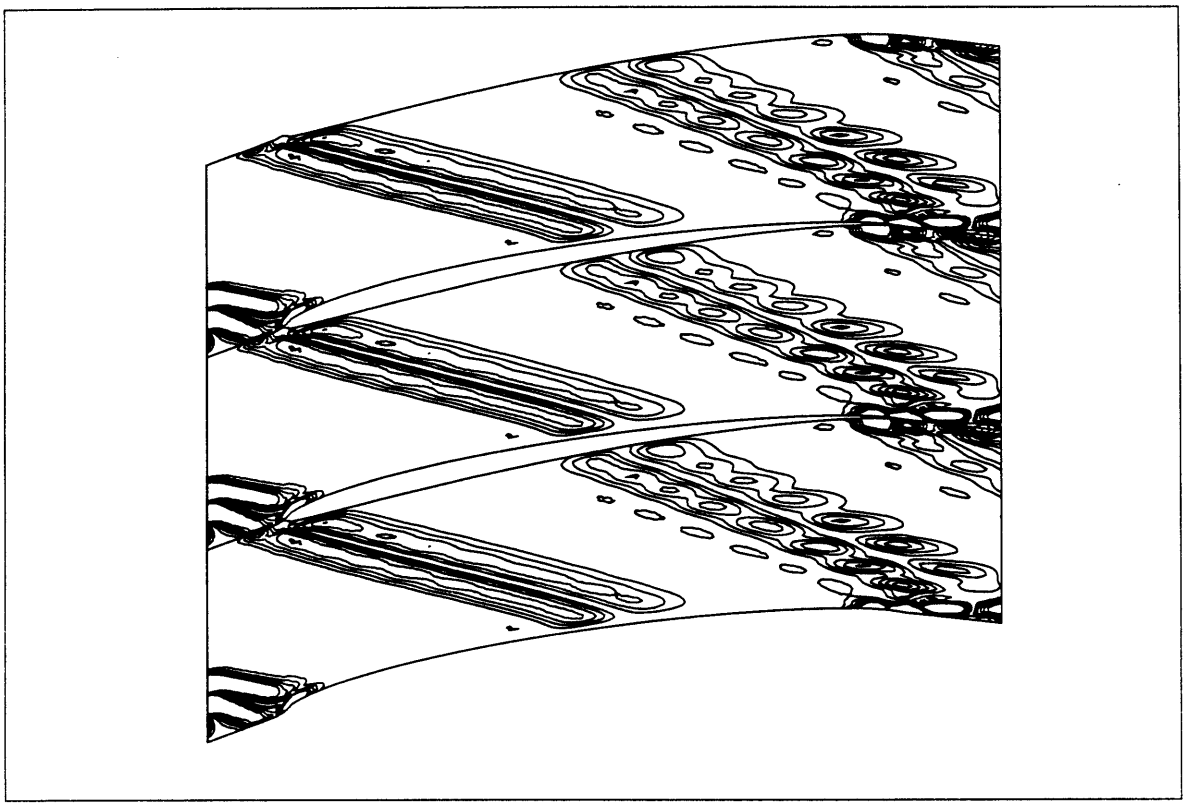

Figure 13a: Disturbance vorticity contours at time T

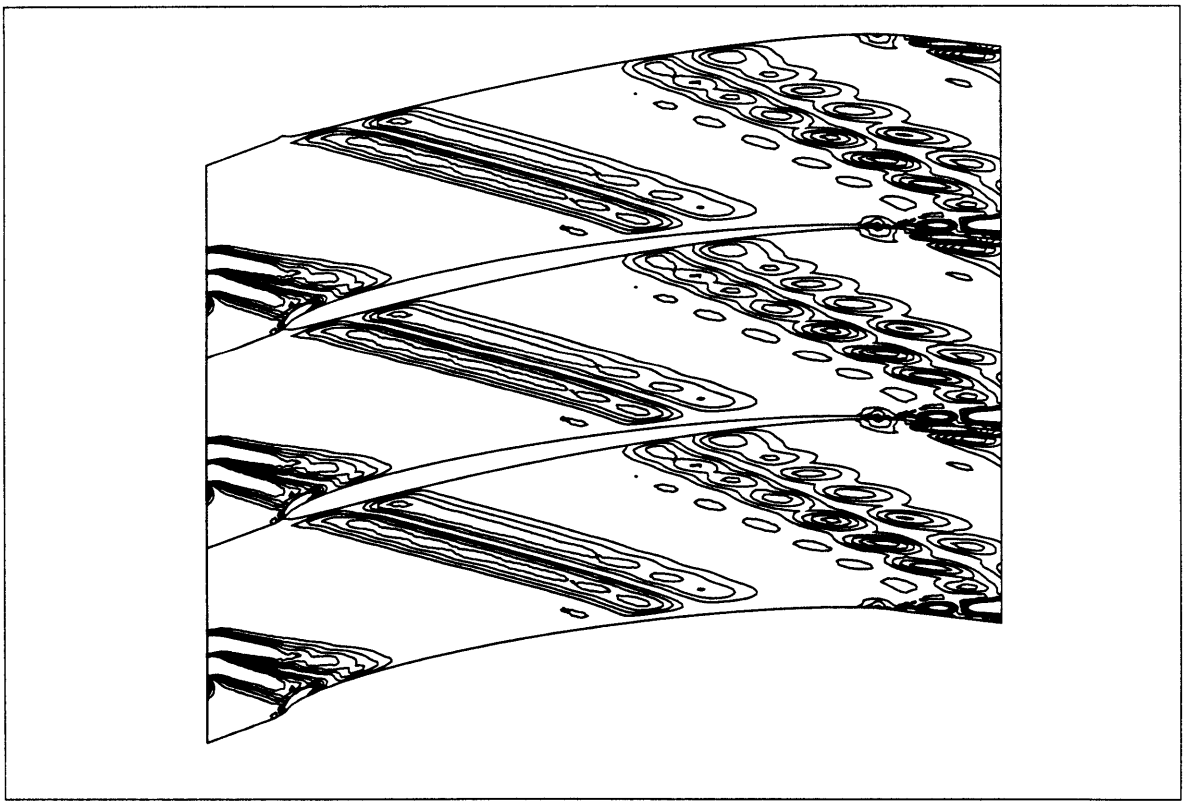

Figure 13b: Disturbance vorticity contours at time T + 0.2To

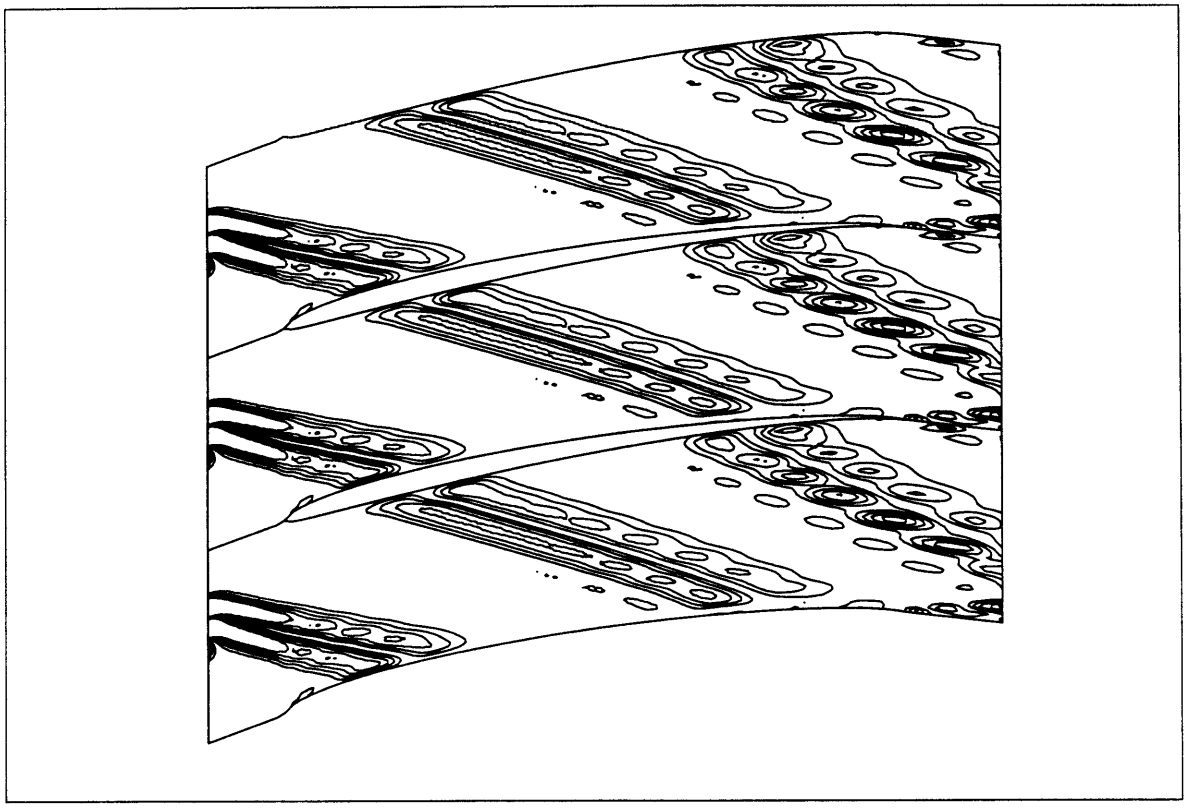

Figure 13c: Disturbance vorticity contours at time T + 0.4To

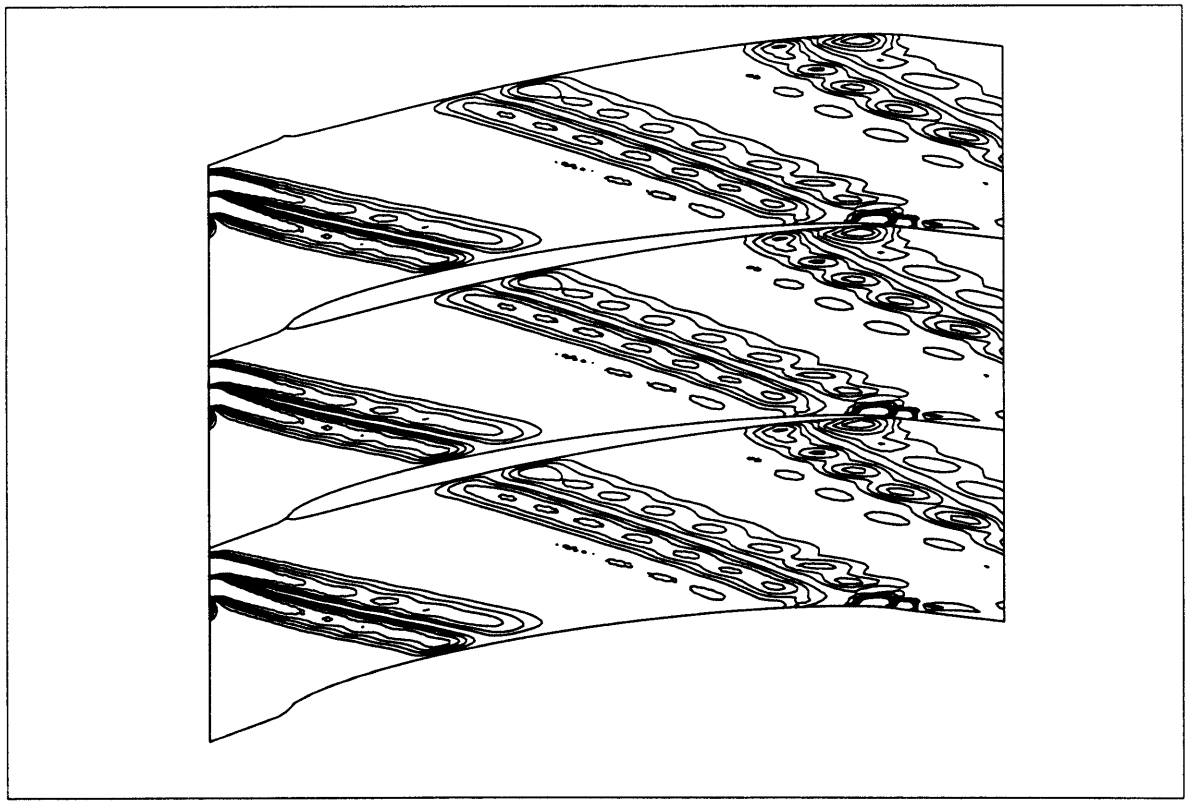

Figure 13d: Disturbance vorticity contours at time T + 0.6To

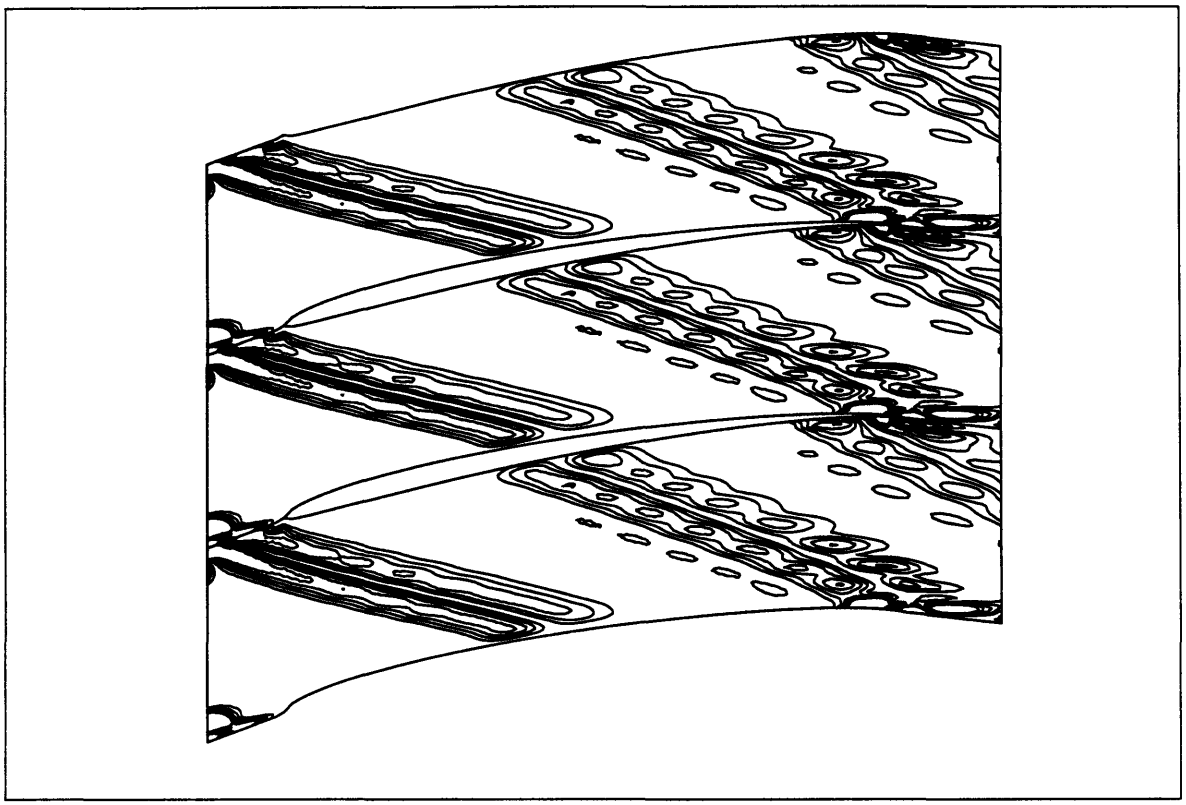

Figure 13e: Disturbance vorticity contours at time T + 0.8To

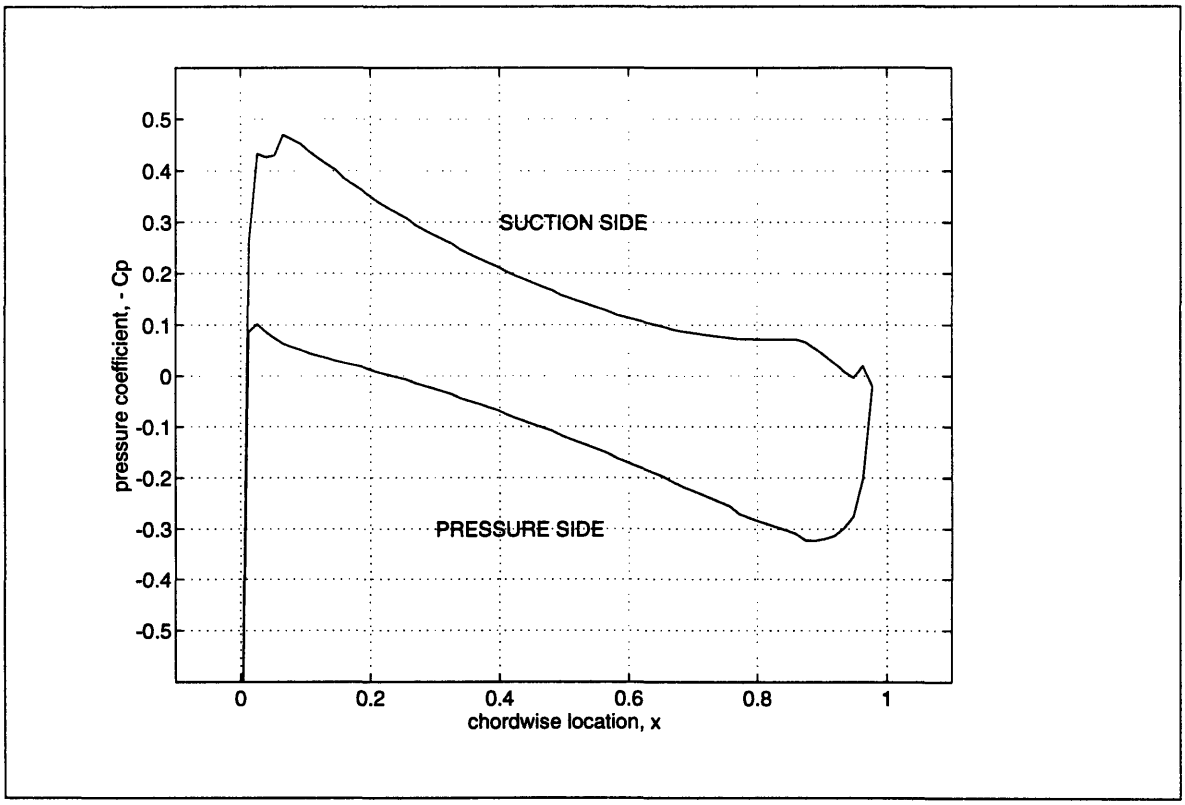

Figure 14: Steady static pressure

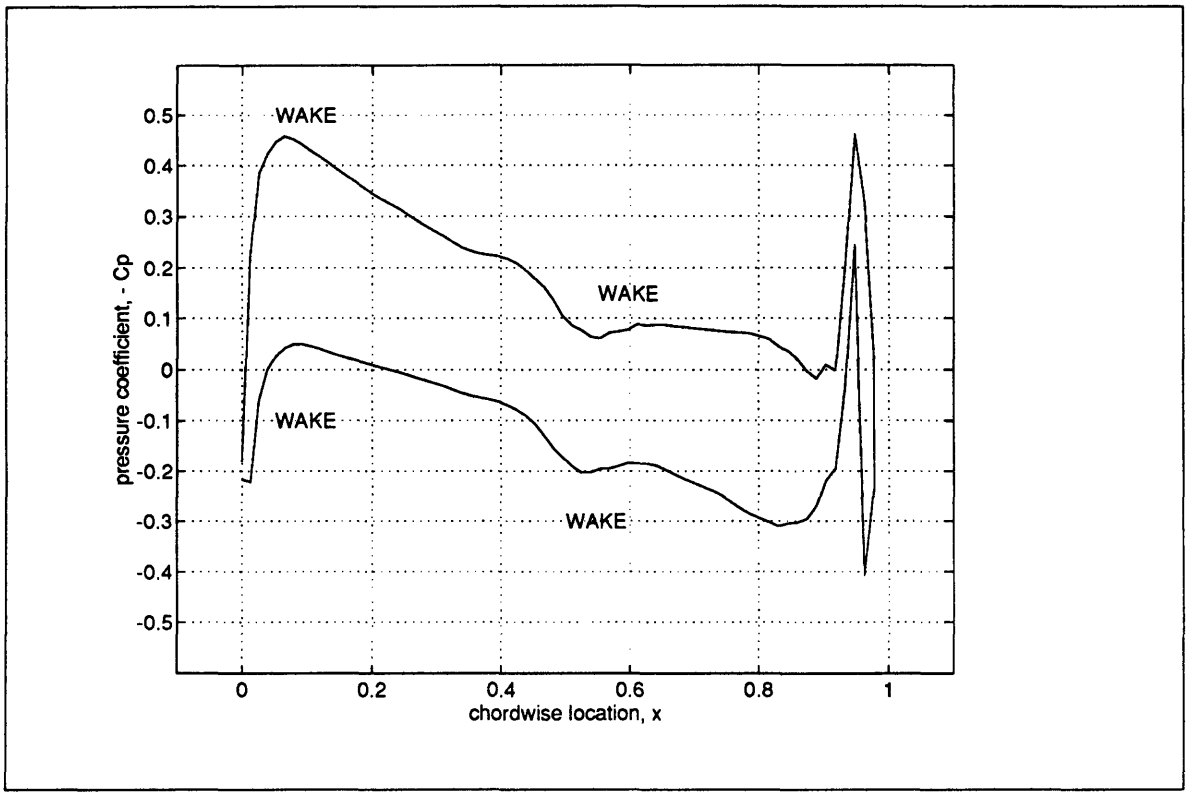

Figure 15a: Unsteady static pressure at time T

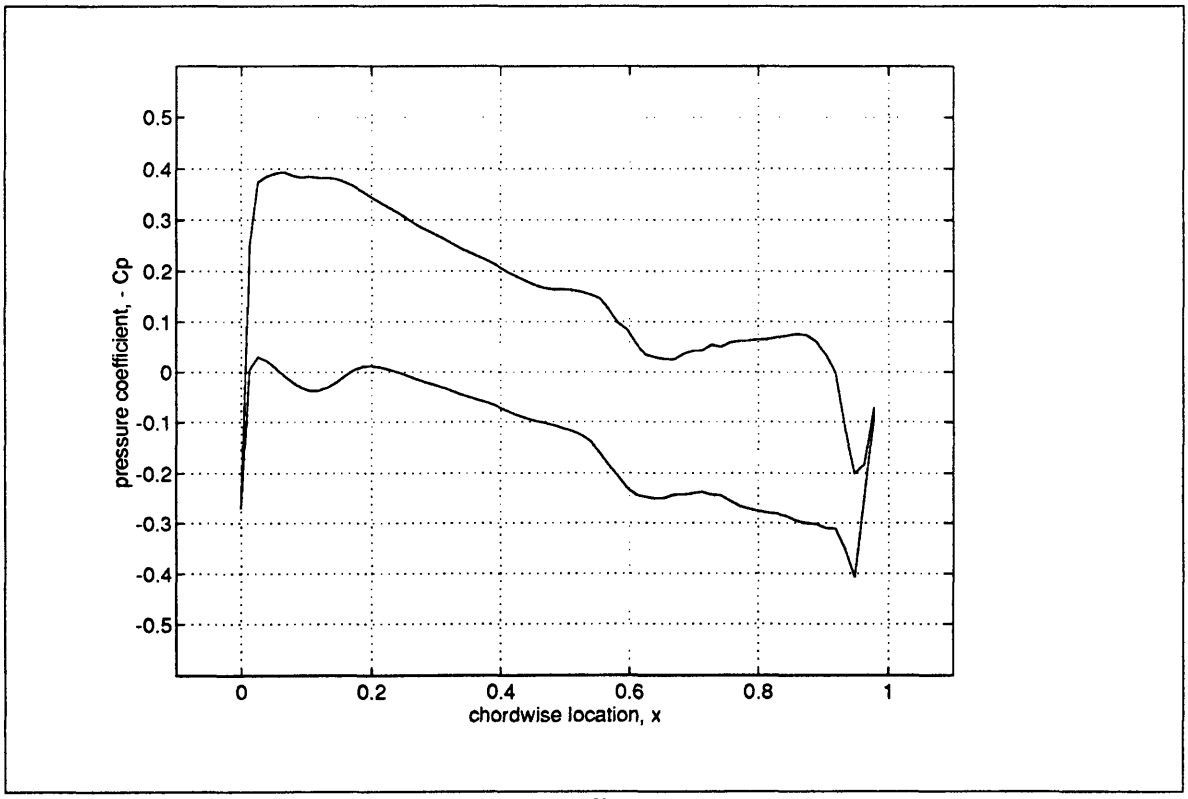

Figure 15b: Unsteady static pressure at time T + 0.2To

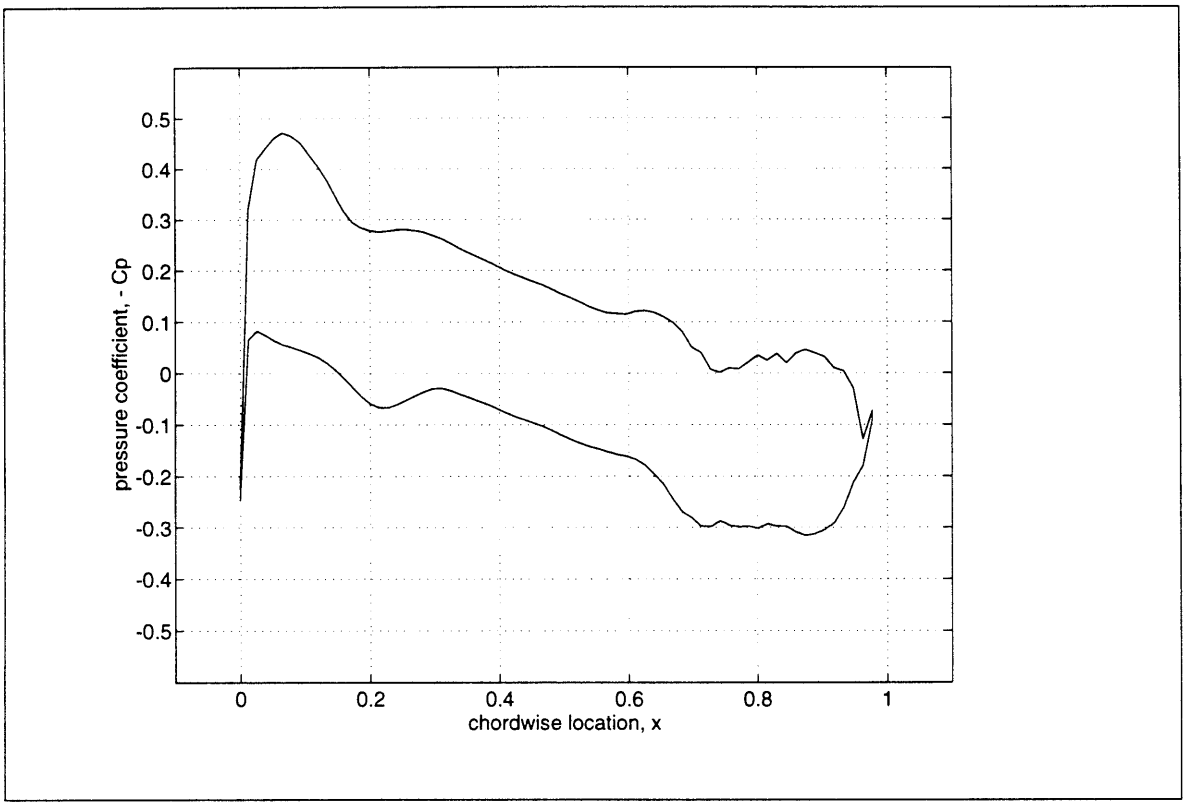

Figure 15c: Unsteady static pressure at time T + 0.4To

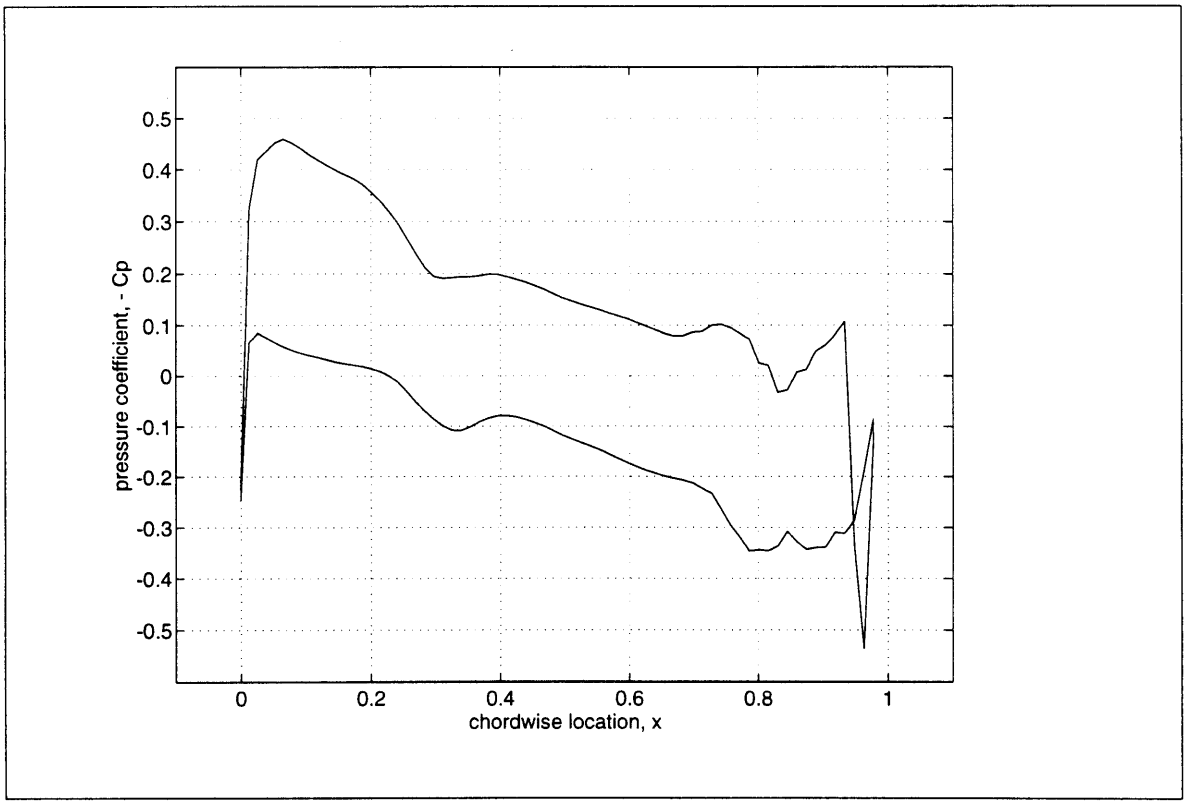

Figure 15d: Unsteady static pressure at time T + 0.6To

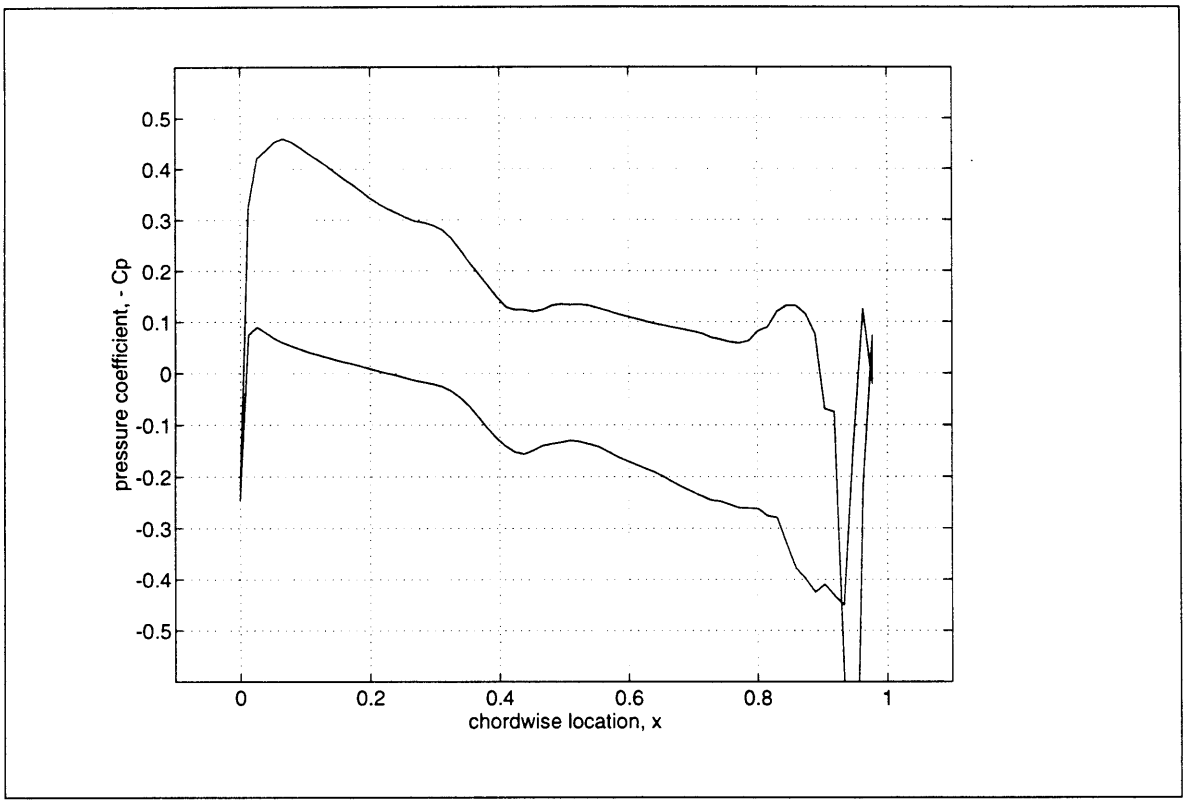

Figure 15e: Unsteady static pressure at time T + 0.8To

(SPACE LEFT BLANK)

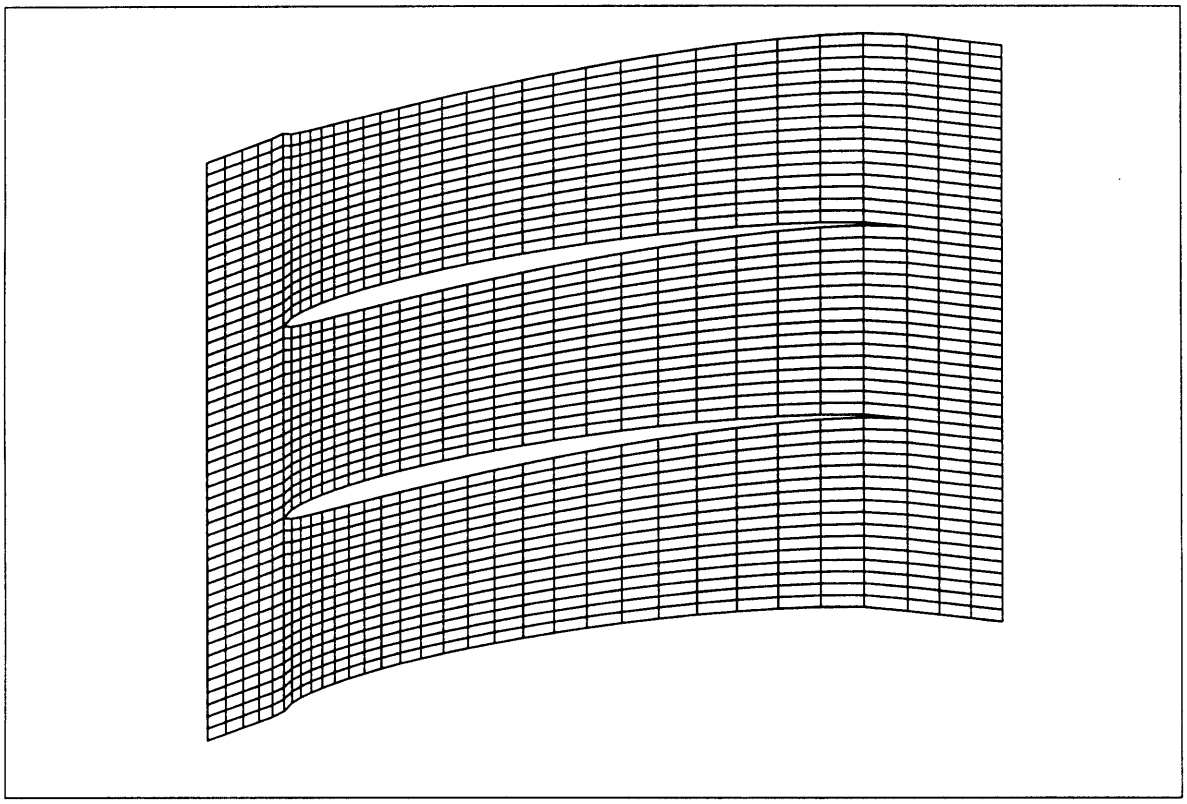

Figure 16: Eppler blade passages in X-Y cross-section

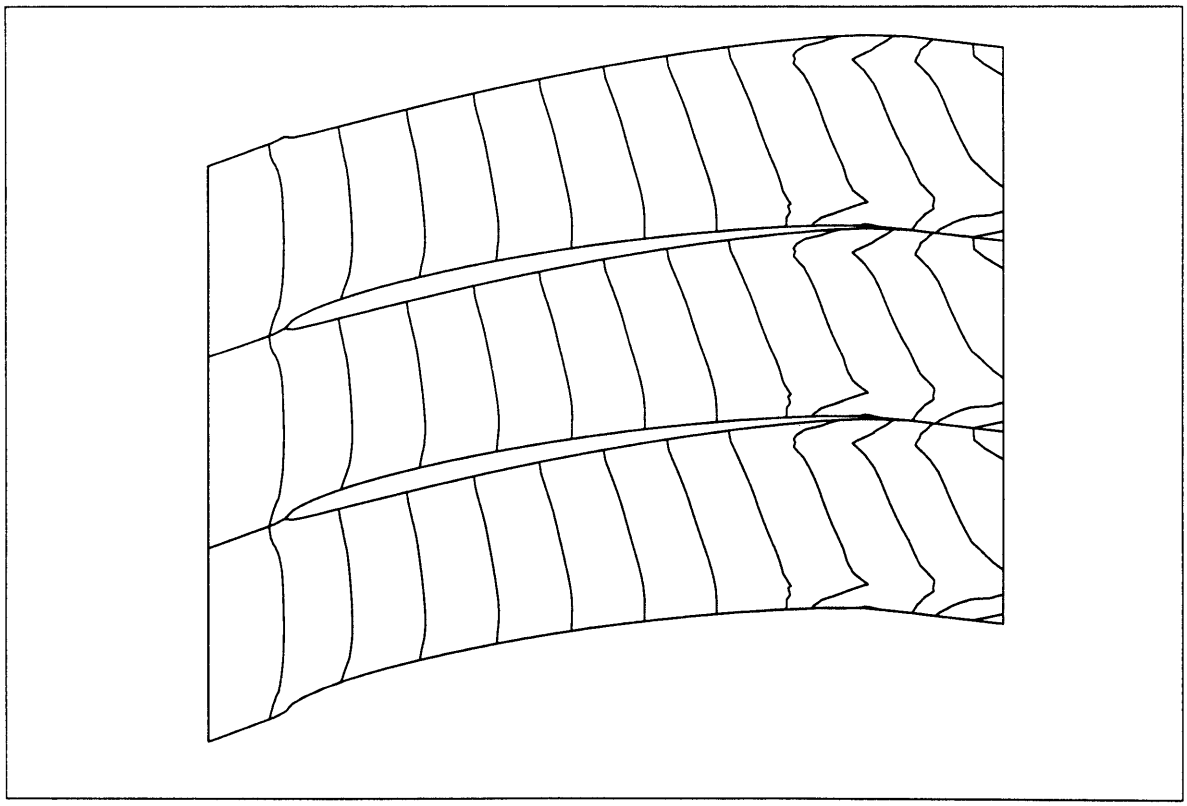

Figure 17: Drift times in X-Y plane

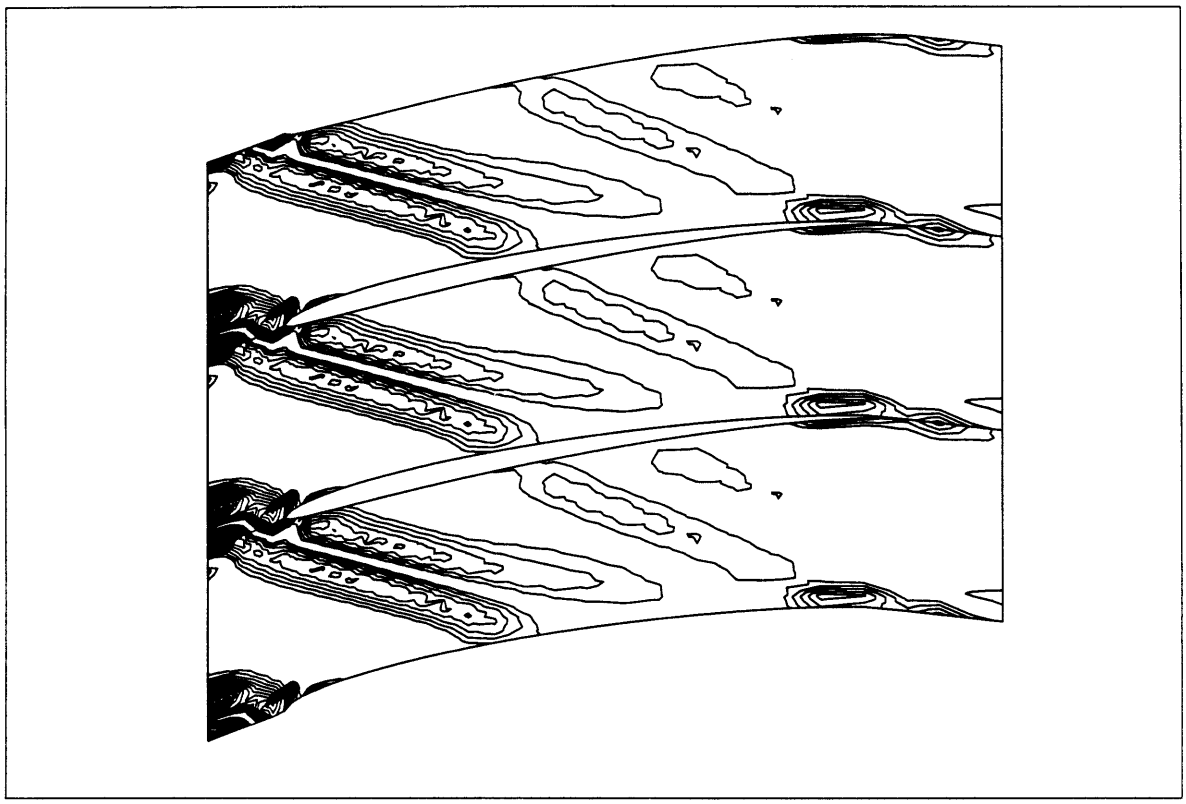

Figure 18a: Disturbance Z-vorticity contours in X-Y plane at z=0, time T

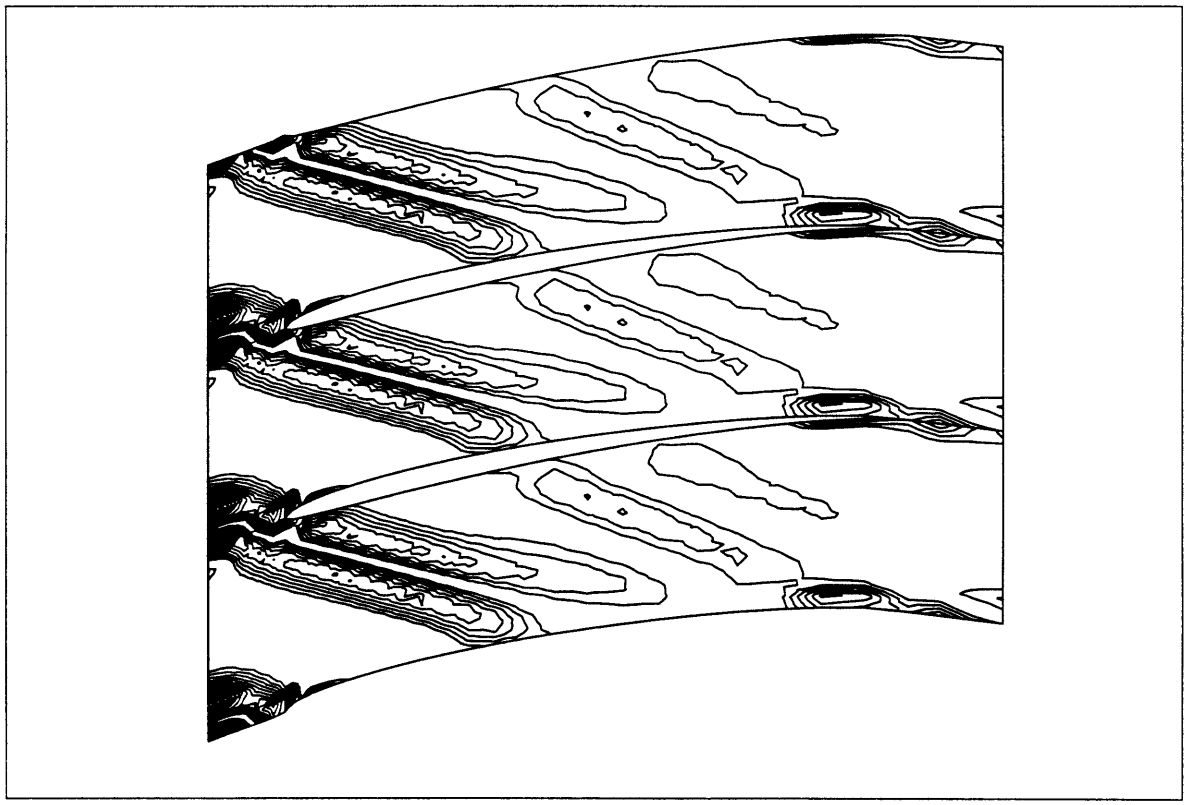

Figure 18b: Disturbance Z-vorticity contours in X-Y plane at z=0.25 L, time T

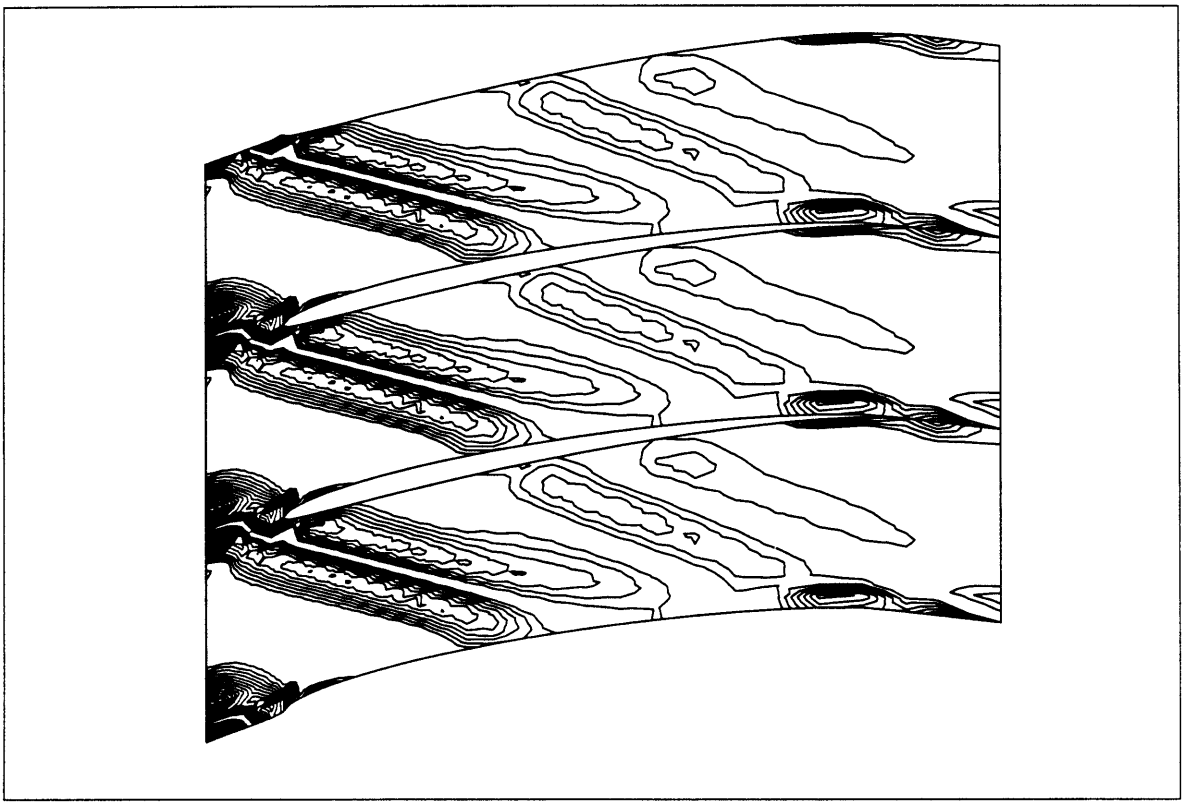

Figure 18c: Disturbance Z-vorticity contours in X-Y plane at z=0.50 L, time T

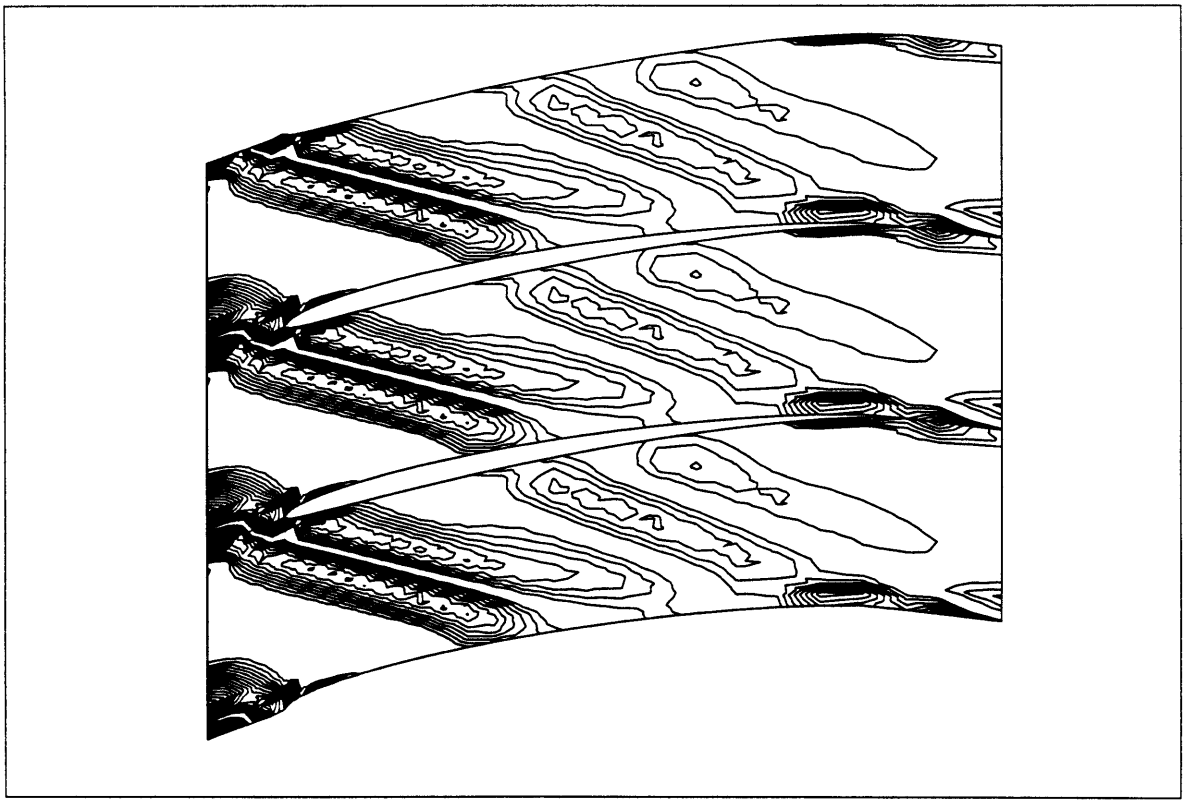

Figure 18d: Disturbance Z-vorticity contours in X-Y plane at z=0.75 L, time T

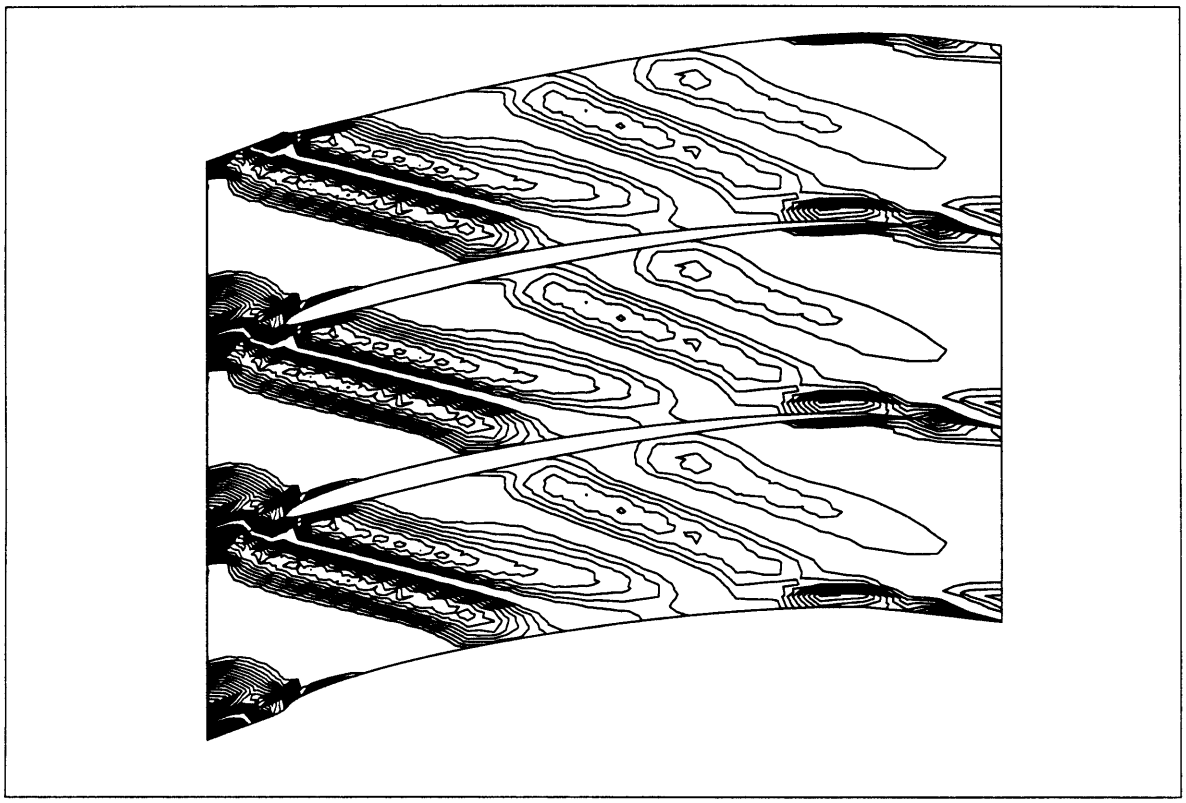

Figure 18e: Disturbance Z-vorticity contours in X-Y plane at z=L, time T

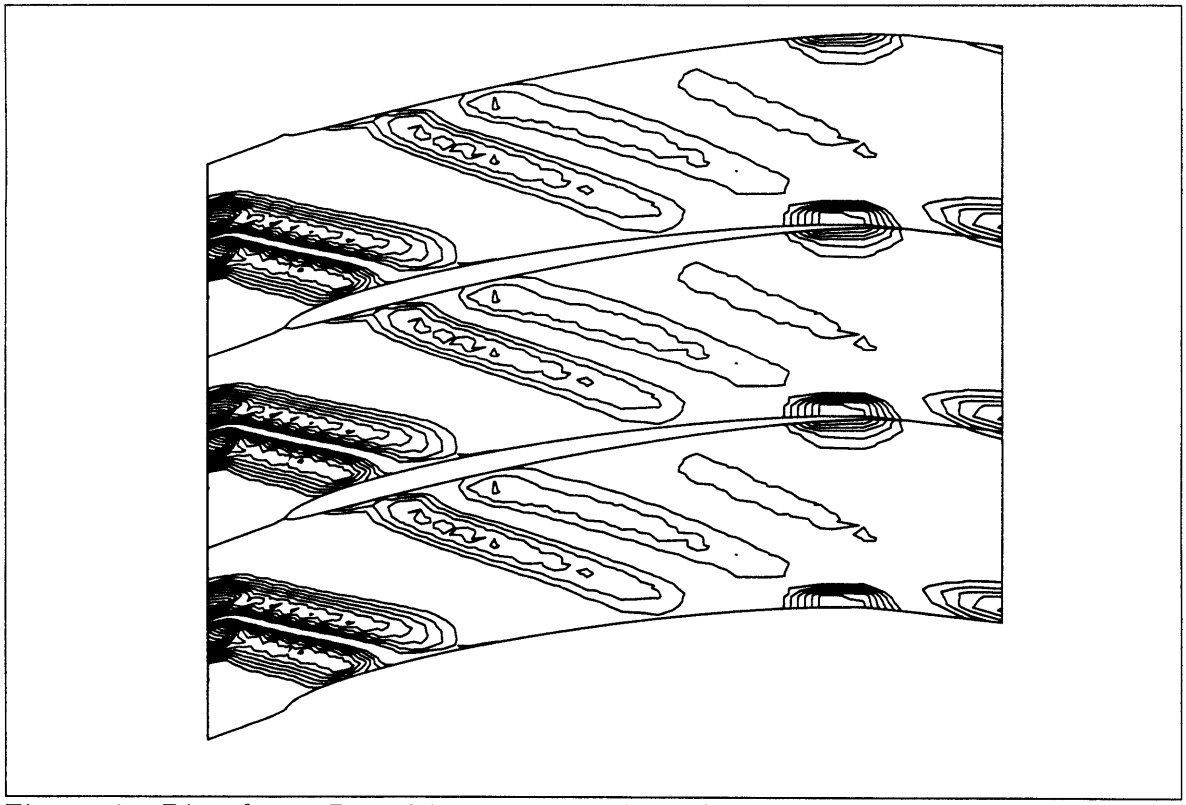

Figure 19a: Disturbance Z-vorticity contours in X-Y plane at z=0, time T + 0.5To

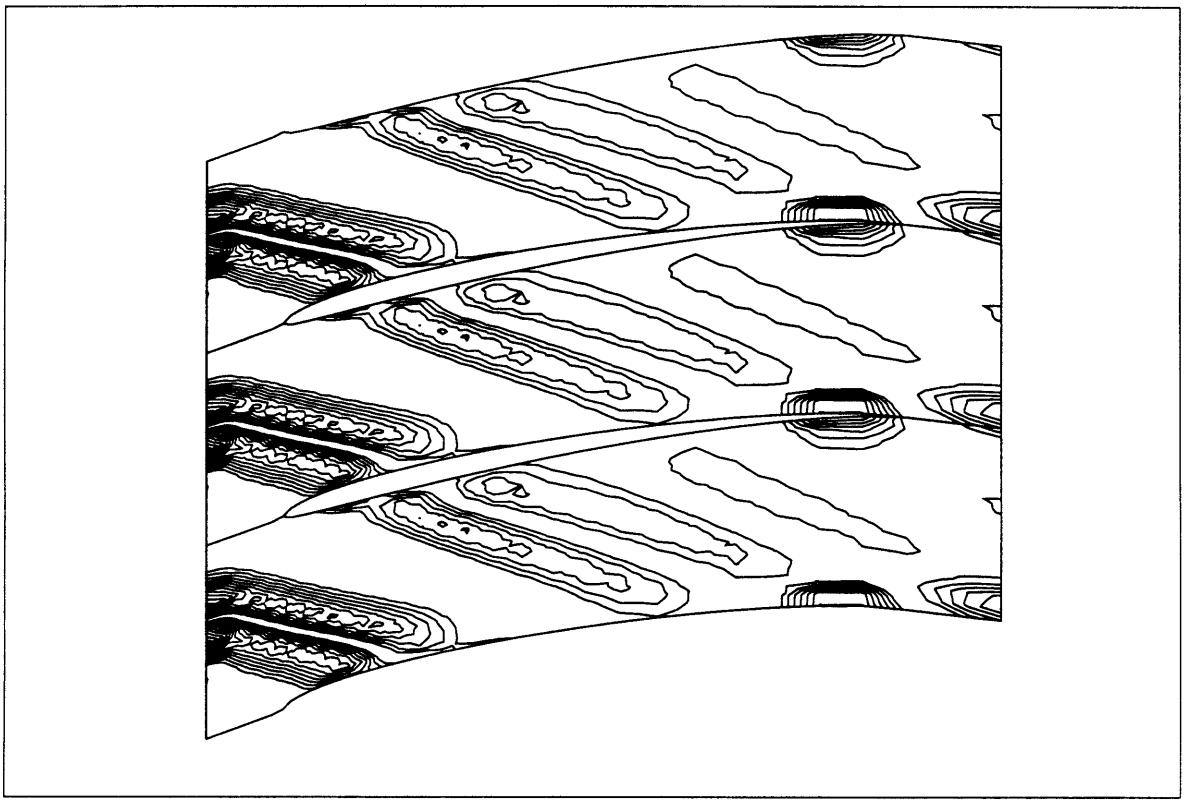

Figure 19b: Disturbance Z-vorticity contours in X-Y plane at z=0.25 L, time T + 0.5To

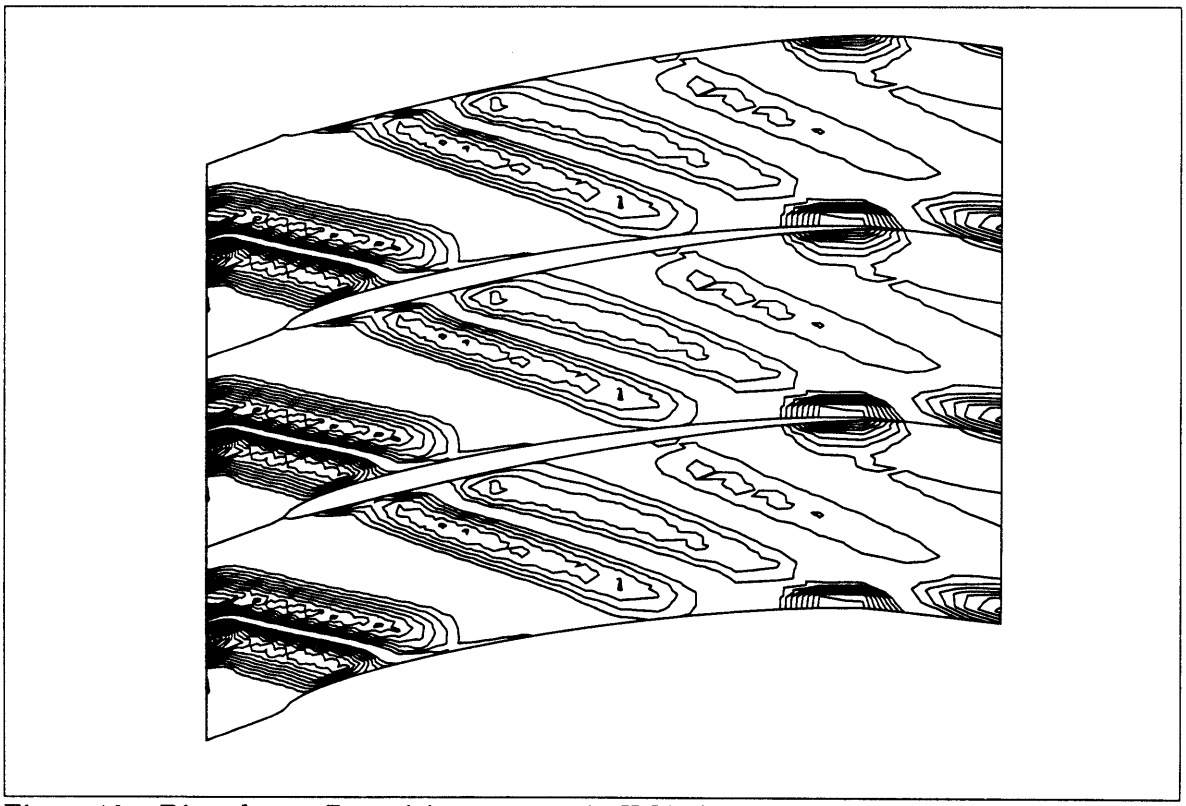

Figure 19c: Disturbance Z-vorticity contours in X-Y plane at z=0.50 L, time T + 0.5To

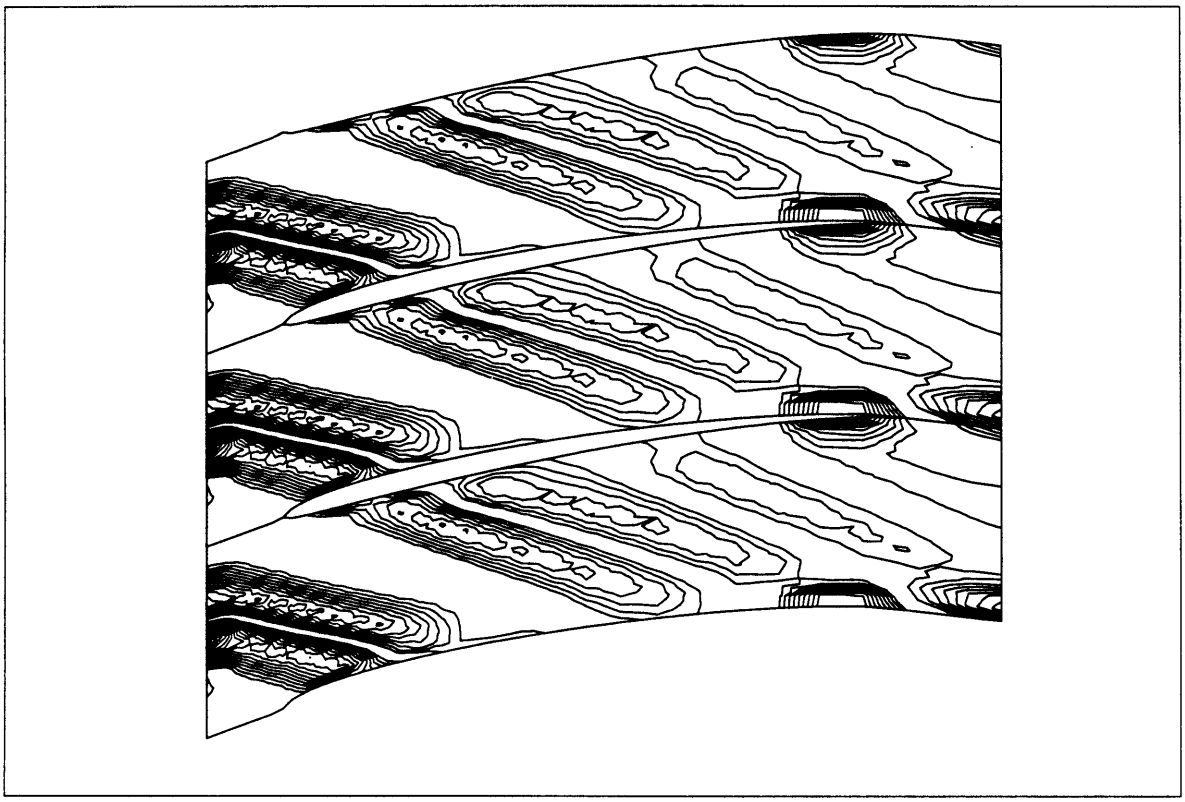

Figure 19d: Disturbance Z-vorticity contours in X-Y plane at z=0.75 L, time T + 0.5To

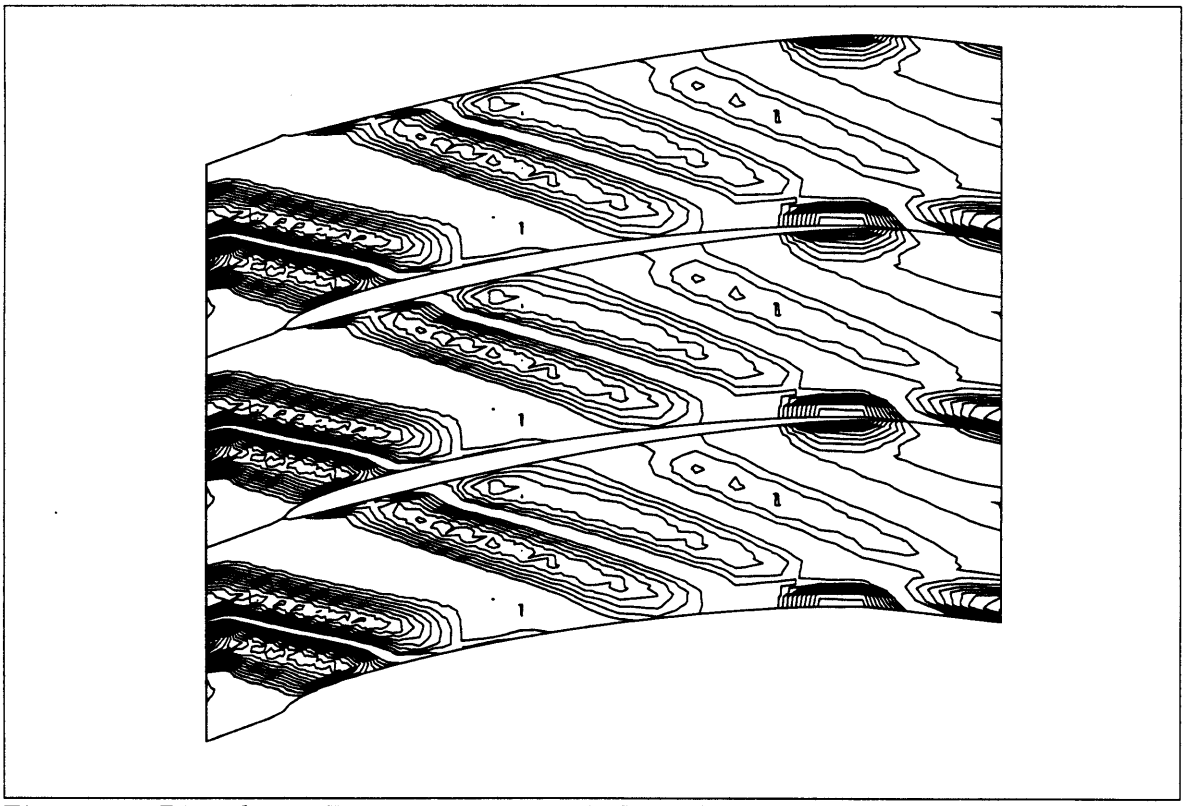

Figure 19e: Disturbance Z-vorticity contours in X-Y plane at z=L, time T + 0.5To

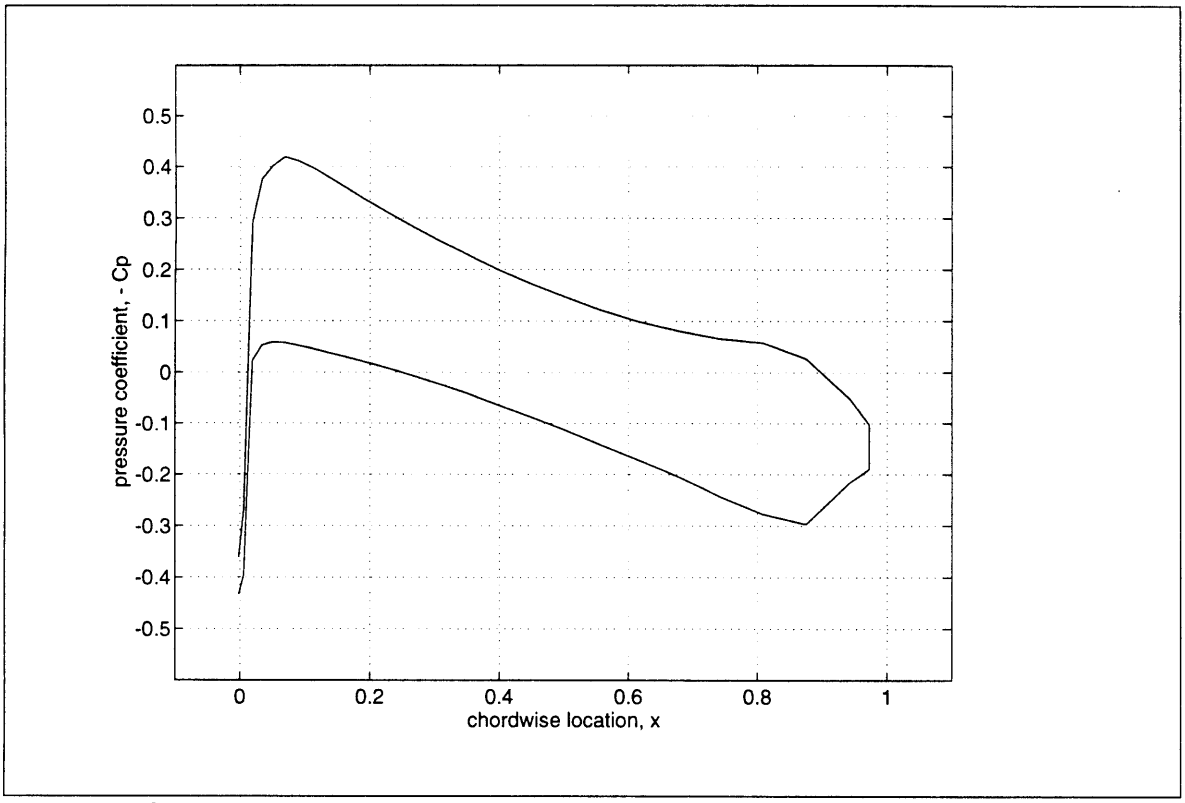

Figure 20: Steady static pressure

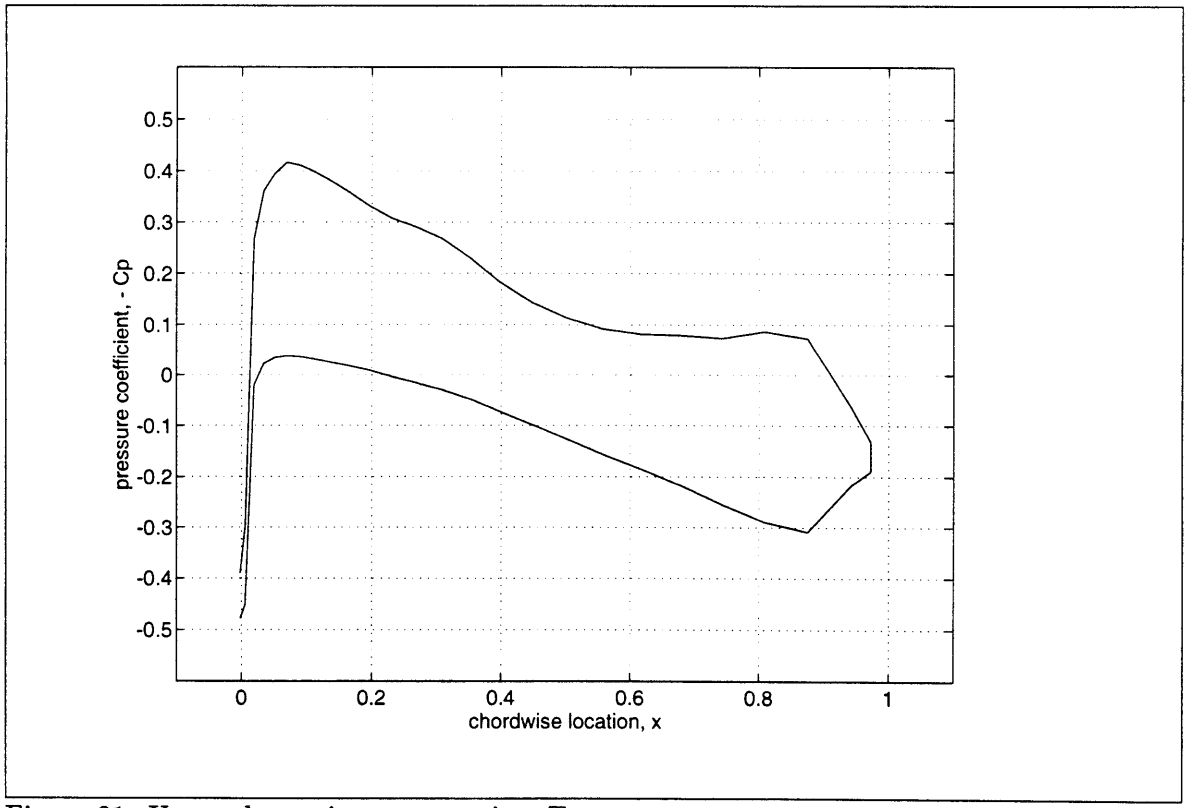

Figure 21: Unsteady static pressure, time T

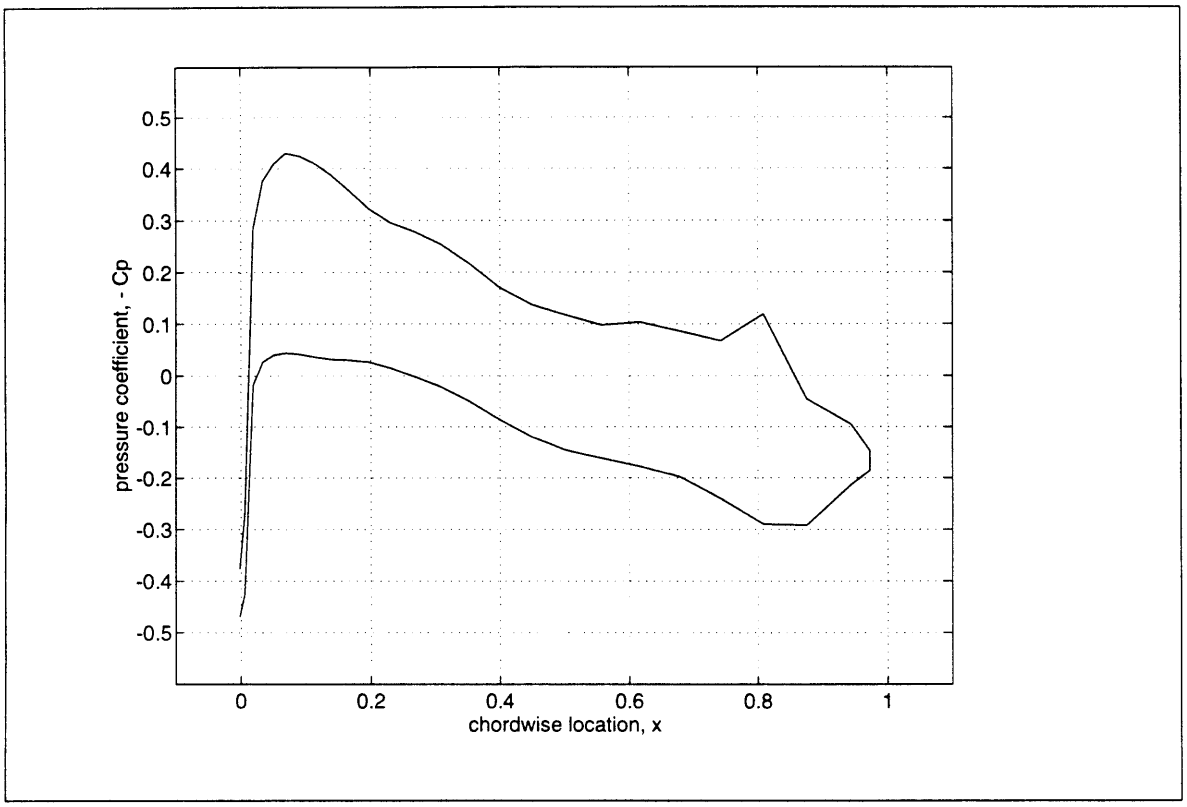

Figure 22: Unsteady static pressure, time T + 0.5To

(SPACE LEFT BLANK)